

FOR THE MONTH OF

DOE/BC/10331-9

**DISPLACEMENT OF OIL BY CARBON DIOXIDE**  
**Second Annual Report, October 1981-September 1982**

Work Performed for the Department of Energy  
Under Contract No. DE-AS19-80BC10331

Date Published—June 1983

New Mexico Institute of Mining and Technology  
Socorro, New Mexico



**U. S. DEPARTMENT OF ENERGY**

## DISCLAIMER

This report was prepared as an account of work sponsored by an agency of the United States Government. Neither the United States Government nor any agency thereof, nor any of their employees, makes any warranty, express or implied, or assumes any legal liability or responsibility for the accuracy, completeness, or usefulness of any information, apparatus, product, or process disclosed, or represents that its use would not infringe privately owned rights. Reference herein to any specific commercial product, process, or service by trade name, trademark, manufacturer, or otherwise, does not necessarily constitute or imply its endorsement, recommendation, or favoring by the United States Government or any agency thereof. The views and opinions of authors expressed herein do not necessarily state or reflect those of the United States Government or any agency thereof.

Printed in the United States of America. Available from:  
National Technical Information Service  
U.S. Department of Commerce  
5285 Port Royal Road  
Springfield, VA 22161

NTIS price codes  
Paper copy: \$13.00  
Microfiche copy: \$4.50

**DISPLACEMENT OF OIL BY CARBON DIOXIDE**  
**Second Annual Report, October 1981–September 1982**

*Contributors:*

R. E. Bretz  
B. T. Campbell  
K. K. Dai  
J. C. Franklin  
C. M. Jensen  
C. L. Lien  
M. P. Mayer  
M. T. Pelletier  
M. K. Silva  
R. M. Specter

F. M. Orr, Jr., and J. J. Taber, *Principal Investigators*  
New Mexico Petroleum Recovery Research Center  
New Mexico Institute of Mining and Technology  
Socorro, New Mexico 87801

L. A. Noll, *Technical Project Officer*  
Bartlesville Energy Technology Center  
P.O. Box 1398  
Bartlesville, Oklahoma 74005

Work Performed for the Department of Energy  
Under Contract No. DE-AS19-80BC10331

Date Published—June 1983

TABLE OF CONTENTS

	<u>PAGE NO.</u>
LIST OF TABLES . . . . .	iv
LIST OF FIGURES . . . . .	v
ABSTRACT . . . . .	x
1. Introduction . . . . .	1
2. Displacement Experiments . . . . .	2
2.1 Background . . . . .	2
2.2 Results of Flow Visualization Experiments . . . . .	4
Apparatus . . . . .	4
Secondary Displacements . . . . .	7
Tertiary Displacements . . . . .	12
2.3 Results of Single Phase Displacement Experiments . . . . .	19
Apparatus and Procedures . . . . .	19
Results and Discussion . . . . .	22
2.4 Results of Two-Phase, Steady-State Miscible Displacements . . . . .	34
Apparatus and Procedures . . . . .	34
Results and Discussion . . . . .	39
2.5 Conclusions . . . . .	43
3. Supporting Measurements: Phase Behavior and Fluid Properties of CO <sub>2</sub> -Crude Oil Mixtures . . . . .	45
3.1 Interpretation of Single Contact PVT Experiments . . . . .	45
Discussion . . . . .	52
3.2 Development of the Continuous Multiple Contact Experiment . . . . .	57
Equipment Modifications . . . . .	57
Measurement of Viscosities with an Oscillating Quartz Crystal . . . . .	63

	PAGE <u>NO.</u>
3.3 Results of Phase Composition Measurements . . . . .	66
3.4 Conclusions . . . . .	79
4. One-Dimensional Simulation of CO <sub>2</sub> Displacements . . . . .	80
4.1 Quantitative Prediction of Slim Tube Displacement Performance . . . . .	80
4.2 Effect of a Trapped Oil Saturation on One-Dimensional Displacement Performance . . . . .	94
Sample Calculations . . . . .	95
4.3 Conclusions . . . . .	101
5. Summary . . . . .	103
Acknowledgement . . . . .	104
References . . . . .	105

LIST OF TABLES

	<u>PAGE NO.</u>
Table 2.1 Summary of Miscible Displacement Experiments . . . . .	25
Table 3.1 Compositions of Gas, Oil and Recombined Fluids . . . . .	46
Table 3.2 Comparison of Oil Properties and Run Conditions for Continuous Multiple Contact Experiments for Maljamar and Rock Creek Crude Oils . . . . .	73
Table 3.3 Composition of Mixture of Aromatic Hydro- carbons Added to Rock Creek Crude Oil . . . . .	73
Table 3.4 Composition of Rock Creek Crude Oil Mixed with Selected Aromatic Hydrocarbons . . . . .	73
Table 4.1 Component Properties for Simulations of Slim Tube Displacements . . . . .	88

LIST OF FIGURES

	<u>PAGE</u> <u>NO.</u>
Figure 2.1 High pressure flow visualization apparatus . . . . .	5
Figure 2.2 Sample pore network. Dark areas are open to flow . . . . .	6
Figure 2.3 Secondary displacement of red-dyed soltrol by blue-dyed soltrol . . . . .	8
Figure 2.4 Secondary displacement of red-dyed soltrol by CO <sub>2</sub> at 1200 psia, 25°C . . . . .	9
Figure 2.5 Displacement of Maljamar crude oil by CO <sub>2</sub> at 1200 psia, 25°C . . . . .	10
Figure 2.6 Appearance of CO <sub>2</sub> -rich and oil-rich phases in the neighborhood of the CO <sub>2</sub> front in a secondary displacement of Maljamar crude oil by CO <sub>2</sub> at 1200 psia and 25°C . . . . .	11
Figure 2.7 Locations of oil left behind by a secondary CO <sub>2</sub> displacement of Maljamar crude oil . . . . .	13
Figure 2.8 Ideal tertiary displacement of oil by a miscible solvent . . . . .	14
Figure 2.9 Dendritic and isolated oil ganglia . . . . .	15
Figure 2.10 Distribution of oil, CO <sub>2</sub> and water at CO <sub>2</sub> breakthrough (0.037 PV) in a tertiary displacement of red soltrol by CO <sub>2</sub> at 1200 psia, 25°C . . . . .	17
Figure 2.11 Swelling of a trapped oil droplet by CO <sub>2</sub> diffusing through water . . . . .	18
Figure 2.12 Apparatus for single-phase miscible displacements . . . . .	20
Figure 2.13 Effect of a nonideal pulse on effluent concentrations for a displacement in a Berea sandstone core (Run 2) . . . . .	21

Figure 2.14	Concentration histories for miscible displacements in Berea sandstone (B-1). The brine data were obtained using a conductivity cell. The oil data were obtained by gas chromatography (Runs 2 and 3) . . . . .	23
Figure 2.15	End cap design . . . . .	24
Figure 2.16	Comparison of measured (Runs 2 and 3) and calculated effluent concentration histories for miscible displacements in a Berea sandstone core . . . . .	26
Figure 2.17	Comparison of measured and calculated effluent concentration histories for a miscible displacement with a step input in a Berea sandstone core (Run 1) . . . . .	28
Figure 2.18	Effluent concentration histories for miscible displacements in carbonate core H-1 . . . . .	29
Figure 2.19	Comparison of measured effluent concentrations from a San Andres carbonate core (Run 1) with those calculated using the convection-dispersion model . . . . .	30
Figure 2.20	Comparison of measured effluent concentrations from a San Andres carbonate core (Run 9) with those calculated using Deans' model . . . . .	33
Figure 2.21	Apparatus used to establish steady-state saturations of oil and water . . . . .	35
Figure 2.22	Two-phase displacement apparatus . . . . .	37
Figure 2.23	Schematic of the oil-water separator . . . . .	38
Figure 2.24	Effluent oil concentration histories at three oil fractional flows in a Berea sandstone core (B-1) . . . . .	40

	PAGE NO.
Figure 2.25 Comparison of a Berea sandstone oil fractional flow curve reported by Salter & Mohanty (1982) with that obtained here for core B-1 . . . . .	41
Figure 2.26 Effluent concentration history for the wetting (brine) phase during a two-phase, steady-state displacement in a Berea sandstone core (B-1) . . . . .	42
Figure 3.1 P-X diagrams for mixtures of CO <sub>2</sub> with Wasson oil . . . . .	47
Figure 3.2 P-X diagrams for mixtures of CO <sub>2</sub> with a recombined Wasson oil containing 312 SCF/BBL . . . . .	48
Figure 3.3 P-X diagrams for mixtures of CO <sub>2</sub> with a recombined Wasson oil containing 602 SCF/BBL . . . . .	49
Figure 3.4 Typical phase volume data for mixtures of CO <sub>2</sub> with Wasson oil at 90°F (32°C) . . . . .	51
Figure 3.5 Comparison of three-phase pressures for CO <sub>2</sub> -hexadecane mixtures with the vapor pressure of CO <sub>2</sub> . . . . .	53
Figure 3.6 Comparison of the extrapolated vapor pressure (solid line calculated with equation 3.1) of CO <sub>2</sub> with the pressure required to give a CO <sub>2</sub> density of 0.42 . . . . .	55
Figure 3.7 Comparison of extrapolated vapor pressure estimate of the minimum miscibility pressure with measured values reported by other investigators . . . . .	56
Figure 3.8 Comparison of extrapolated vapor pressure estimate of minimum miscibility with correlations offered by Yellig & Metcalfe (1980) and Holm & Josendal (1982) . . . . .	58
Figure 3.9 Continuous multiple contact apparatus . . . . .	59
Figure 3.10 Flowchart of data communications system . . . . .	61

	<u>PAGE NO.</u>
Figure 3.11 Axial view of a cylindrical crystal holder . . . . .	64
Figure 3.12 Crystal mounting schemes . . . . .	65
Figure 3.13 Quartz crystal resonance in air at 26 mm Hg . . . . .	67
Figure 3.14 Quartz crystal resonance in heptane . . . . .	68
Figure 3.15 Comparison of tie line slopes for a synthetic oil composed of C <sub>5</sub> , C <sub>10</sub> , C <sub>16</sub> , and C <sub>30</sub> paraffins and Maljamar crude oil . . . . .	69
Figure 3.16 Pseudo-ternary representation of phase compositions of mixtures of CO <sub>2</sub> with Maljamar separator oil at 1200 psia and 90°F . . . . .	71
Figure 3.17 Pseudo-ternary representation of phase compositions of mixtures of CO <sub>2</sub> with Rock Creek Separator Oil at 1300 psia and 75°F . . . . .	72
Figure 3.18 Comparison of component partitioning for Rock Creek separator oil and Maljamar separator oil . . . . .	74
Figure 3.19 Pseudo-ternary representation of phase compositions of mixtures of CO <sub>2</sub> with Rock Creek separator oil with aromatic spikes at 1300 psia and 75°F . . . . .	76
Figure 3.20 Comparison of component partitioning for Rock Creek separator oil and Rock Creek separator oil with aromatic spikes . . . . .	77
Figure 3.21 Comparison of weight fraction liquid for Rock Creek separator oil and Rock Creek separator oil with aromatic spikes . . . . .	78
Figure 4.1 Pseudo-ternary representation of phase compositions for mixtures of CO <sub>2</sub> with Maljamar separator oil at 5520 kPa and 32°C . . . . .	83
Figure 4.2 Pseudo-ternary representation of phase compositions for mixtures of CO <sub>2</sub> with Maljamar separator oil at 6890 kPa and 32°C . . . . .	84

Figure 4.3 Pseudo-ternary representation of phase compositions for mixtures of CO<sub>2</sub> with Maljamar separator oil at 8270 kPa and 32°C . . . . . 85

Figure 4.4 Pseudo-ternary representation of phase compositions for mixtures of CO<sub>2</sub> with Maljamar separator oil at 9650 kPa and 32°C . . . . . 87

Figure 4.5 Comparison of calculated (line) and experimental (symbols) oil recovery in slim tube displacements of Maljamar separator oil by CO<sub>2</sub> at 32°C . . . . . 89

Figure 4.6 Calculated saturation and composition profiles at 0.8 pore volumes CO<sub>2</sub> injected . . . . . 91

Figure 4.7 Secondary oil ( $S_{wi} = 0.312$ ) recovered by simultaneous injection of CO<sub>2</sub> and water . . . . . 97

Figure 4.8 Secondary oil ( $S_{wi} = 0.312$ ) recovered by alternate injection of CO<sub>2</sub> and water . . . . . 98

Figure 4.9 Tertiary oil ( $S_{wi} = 0.814$ ) recovered by simultaneous injection of CO<sub>2</sub> and water . . . . . 99

Figure 4.10 Tertiary oil ( $S_{wi} = 0.814$ ) recovered by alternate injection of CO<sub>2</sub> and water . . . . . 100

## ABSTRACT

Results of a comprehensive research effort to investigate and quantify factors which affect the performance of CO<sub>2</sub> flood processes in reservoir rocks are presented.

An apparatus is described in which displacement of oil from pore networks etched in glass by CO<sub>2</sub> at high pressure can be observed visually. Results of a series of secondary and tertiary, first contact and multiple contact miscible displacements are reported. Equipment for on-line measurements of mixing in one- and two-phase displacements is described. A new device designed to separate oil and water continuously in a chamber of very low dead volume is also described. Results of one- and two-phase displacements which validate the experimental techniques are reported.

Results of a series of PVT experiments to study the effects of changing both the amount of dissolved gas in a crude oil and the system temperature are given. Those results suggest strongly that the extrapolated vapor pressure of CO<sub>2</sub> is a good estimate of the minimum miscibility pressure if the temperature is below about 140°F. Modifications and improvements to the design of the continuous multiple contact apparatus are described, as are preliminary tests of the use of an oscillating quartz crystal to measure viscosities. Results of a series of phase composition measurements to study effects of oil composition on component partitioning in CO<sub>2</sub>-crude oil systems are reported.

The theory of the effect of CO<sub>2</sub>-crude oil phase behavior on displacements in an ideal porous medium is tested by predicting the performance of slim tube displacements from independently measured phase behavior and fluid property data obtained with the continuous multiple contact experiment. The quantitative agreement between prediction and experiment is good enough to suggest that the essentials of CO<sub>2</sub>-crude oil phase behavior can be modeled with a small number of pseudo-components. Finally, modifications to the one-dimensional process simulator to model effects of oil isolated by water are discussed and results of sample calculations are reported.

## 1. INTRODUCTION

The performance of a field-scale tertiary CO<sub>2</sub> flood is the result of a competition between a variety of physical effects. It is by now well established that under ideal flow conditions, CO<sub>2</sub> can displace crude oil very efficiently if the pressure is high enough that CO<sub>2</sub> is a good solvent for some of the hydrocarbons present in the crude oil (Holm & Josendal 1982; Gardner, Orr & Patel 1981; Orr, Yu & Lien 1981; Orr, Silva & Lien 1983). While ideal flow conditions can be obtained routinely in a slim tube packed with sand or glass beads, it is not likely that these conditions will occur in an oil reservoir where the porous medium is not uniform, instabilities driven by viscous and gravity forces have free rein, and enough brine is present to alter the time and spatial scales of mixing between CO<sub>2</sub> and oil.

The research effort described in this report is aimed at building quantitative understanding of how the nonidealities of flow in a reservoir setting alter the picture developed for simple displacements. In §2 we report on two sets of displacement experiments. Results of visual observations of secondary and tertiary CO<sub>2</sub> floods in two-dimensional pore networks are described. The displacements in the simple pore structures etched in glass clearly illustrate differences between secondary and tertiary CO<sub>2</sub> floods. Also in §2, we describe results of displacements in reservoir core samples. Those displacements are designed to provide information about the effects of pore structure heterogeneity and the presence of brine saturations on mixing of injected fluid with oil and water in place in the core. In §3 we report results of experimental investigations of the role of crude oil composition in determining the effectiveness of extraction of hydrocarbons by a CO<sub>2</sub>-rich phase. In addition, improvements and modifications to the continuous multiple contact experiment are described, as is progress in development of a technique for measurement of phase viscosities. An analysis of pressure-composition phase diagrams is given along with a simple way to estimate minimum miscibility pressure for low temperature reservoirs. Finally in §4, we report results of a quantitative test of understanding of the effects of phase behavior and volume change on mixing in displacement experiments. In that test, results of simulations of slim tube tests are compared with experimental results. The simulations were based on results of continuous multiple contact experiments in which phase compositions and densities were measured. The agreement suggests that the essentials of phase behavior of CO<sub>2</sub>-crude oil systems can be represented in terms of a small number of pseudo-components.

## 2. DISPLACEMENT EXPERIMENTS

### 2.1 Background

When CO<sub>2</sub> displaces oil in an ideal flow setting, one in which viscous fingering is eliminated, water is absent, and the porous medium is uniform, the amount of oil recovered is determined by the phase behavior of the CO<sub>2</sub>-crude oil mixtures which occur during the displacement process (see §4 for results of calculations which confirm this statement). Indeed, Helfferich (1981) proved for one-dimensional flows what had long been understood qualitatively (Hutchinson & Braun 1961; Rathwell, Stalkup & Hassinger 1971): if extraction of hydrocarbons by CO<sub>2</sub> is efficient enough, mixtures which form during the displacement will avoid the two-phase region, and the displacement will recover all of the oil in place, just as would a first-contact miscible displacement. Helfferich's proof requires two assumptions, however: the phases present at any point in the porous medium are assumed to be in chemical equilibrium, and there is no dispersive mixing or viscous fingering, either of which would invalidate an assumption of strictly local mixing. It has been shown that the effect of dispersion is to produce a small residual oil saturation to CO<sub>2</sub> (Gardner, Orr & Patel 1981). Thus, it has been established that if the pressure is high enough so that phase behavior is favorable, and if viscous fingering is eliminated, CO<sub>2</sub> can displace nearly all of the oil with which it can mix during flow through a uniform porous medium. In field scale CO<sub>2</sub> floods, however, none of those assumptions is satisfied. The reservoir rocks are not uniform, viscous flow instability is usually a problem and the presence of high water saturations may alter appreciably the space and time scales over which mixing occurs. Thus, it is important to consider how these complications alter the picture of CO<sub>2</sub> flooding which arises out of the simple flow theory.

The experiments described in this section are designed to provide independent information about the effect of high water saturations on mixing in oil and water phases flowing in reservoir rocks. In any CO<sub>2</sub> flood, even on a laboratory core scale, several flow mechanisms interact (Orr et al 1981). Phase compositions determine phase properties (see §3) which, along with phase saturations, determine flow rates under an imposed pressure gradient. Unless precautions are taken, viscous fingering will affect recovery. Thus, it can be difficult to unravel the effects of mixing from those of other factors operating in the displacement.

Two types of experiments are being performed:

- (1) Flow visualization studies with both well-characterized oils and crude oils in simple two-dimensional pore networks etched in glass, and
- (2) Core displacement experiments with well-characterized oils in actual reservoir core samples.

The flow visualization experiments investigate the physical behavior of complex fluids flowing in a simple porous medium, while the core floods use simple fluids to study the effects of the complex structure of the rocks themselves. Results of the flow visualization studies are presented in §2.2. They provide direct visual evidence concerning the interactions of phase behavior with mixing when water is present and illustrate clearly the difficulties of tertiary oil recovery and the beneficial properties which enable CO<sub>2</sub> to recover oil that remains after a waterflood.

To isolate the effects of rock pore structure and the distribution property variations, a sequence of displacement experiments with well-characterized fluids is being performed for a variety of reservoir core samples. The sequence for a given reservoir core is:

- (1) Saturate the core with one fluid and displace it by another with matched density and viscosity.
- (2) Displace oil and brine into the core at fixed flow rates until steady state is reached. Then start injection of new oil and new brine, each with density and viscosity matched to the old oil and brine. Repeat at a variety of water saturations.

In both sets of displacements, the compositions of produced fluid samples are measured. Under an appropriate set of assumptions, the produced fluid compositions can then be interpreted to give information about mixing of injected fluids with those present in the core. A review of models used to interpret such displacement experiments has been given by Orr & Taber (1982).

The single-phase displacements (1), results of which are given in §2.3, are designed to yield information about the effect of rock pore structure on mixing in an ideal miscible displacement. Such experiments provide direct evidence of heterogeneity: displacements in a uniform porous medium will produce effluent composition data which are modeled accurately by a convection-diffusion equation with a single parameter, the Peclet number; while effluent compositions from a heterogeneous core show significant asymmetry which requires a more complex model of the flow (Deans 1963; Coats & Smith 1964; Orr & Taber 1982).

The two-phase displacements, discussed in §2.4, are designed to answer three questions for a given core at a specific water saturation:

- (1) What fractions of the wetting and nonwetting phases are displaced directly by injected fluid?
- (2) What fractions of the wetting and nonwetting phases can be contacted but are recovered slowly, presumably by diffusion from stagnant areas into a flowing stream?
- (3) What fractions of the wetting and nonwetting phases are isolated (trapped) from contact with injected wetting and nonwetting fluid?

Salter and Mohanty (1982) reported results of extensive measurements of this type for a Berea sandstone core, but no results of measurements for cores from reservoirs to be CO<sub>2</sub> flooded have been published.

## 2.2 Results of Flow Visualization Experiments

### Apparatus

Fig. 2.1 is a schematic of the apparatus used to observe the flow of CO<sub>2</sub>-crude oil-brine mixtures in two-dimensional pore networks. A pressure cell with polycarbonate windows houses a glass model in which a pore network has been etched. Details of the cell and window design are reported by Campbell (1983). The model is surrounded by glycerine which is pressurized to the displacement pressure by the injected CO<sub>2</sub>. Thus, the glass model is subjected to an overburden pressure equal to that of the fluids being displaced through the model. After the model has been filled with oil or oil and water, the pressure in the CO<sub>2</sub> injection pump is balanced against the pressure in a nitrogen vessel at the downstream end of the apparatus, and the pump is started to establish flow through the bypass loop. The entire flow system is allowed to stabilize at the flow rate selected. Because the pressure drop needed to move fluid through the model is very small, careful balancing of the CO<sub>2</sub> and N<sub>2</sub> pressure is required to prevent rapid flow from one of the vessels caused by expansion of either the CO<sub>2</sub> or the nitrogen. When the flow through the bypass is stable, the bypass valve is closed and the model inlet valve opened, and CO<sub>2</sub> is forced through the model. The displacement is observed on a color television monitor and is recorded on videotape.

Displacements are being performed for a variety of pore network models. In this section we compare results of several displacements in one model, a drawing of which appears as Fig. 2.2. Pore networks are prepared by etching mirror images of the network into two glass plates, which are then placed face to face and annealed. Additional details of the photographic process used to etch the models have been reported by Chatzis (1981) and Campbell (1983). The model shown in Fig. 2.2 is approximately 6.3 cm by 4.2 cm, contains around 1700 pores with average diameter of .035 cm and has a total pore volume of 0.2825 cm<sup>3</sup>. Unless otherwise stated, the flow rate was .014 cm<sup>3</sup>/min, which corresponds to about 1/20 pore volume per minute. That model was used in the following sequence of displacements:

### Secondary

- (1) Displacement of red-dyed Soltrol by blue-dyed Soltrol.
- (2) Displacement of red-dyed Soltrol by CO<sub>2</sub>.
- (3) Displacement of Maljamar crude oil by CO<sub>2</sub>.

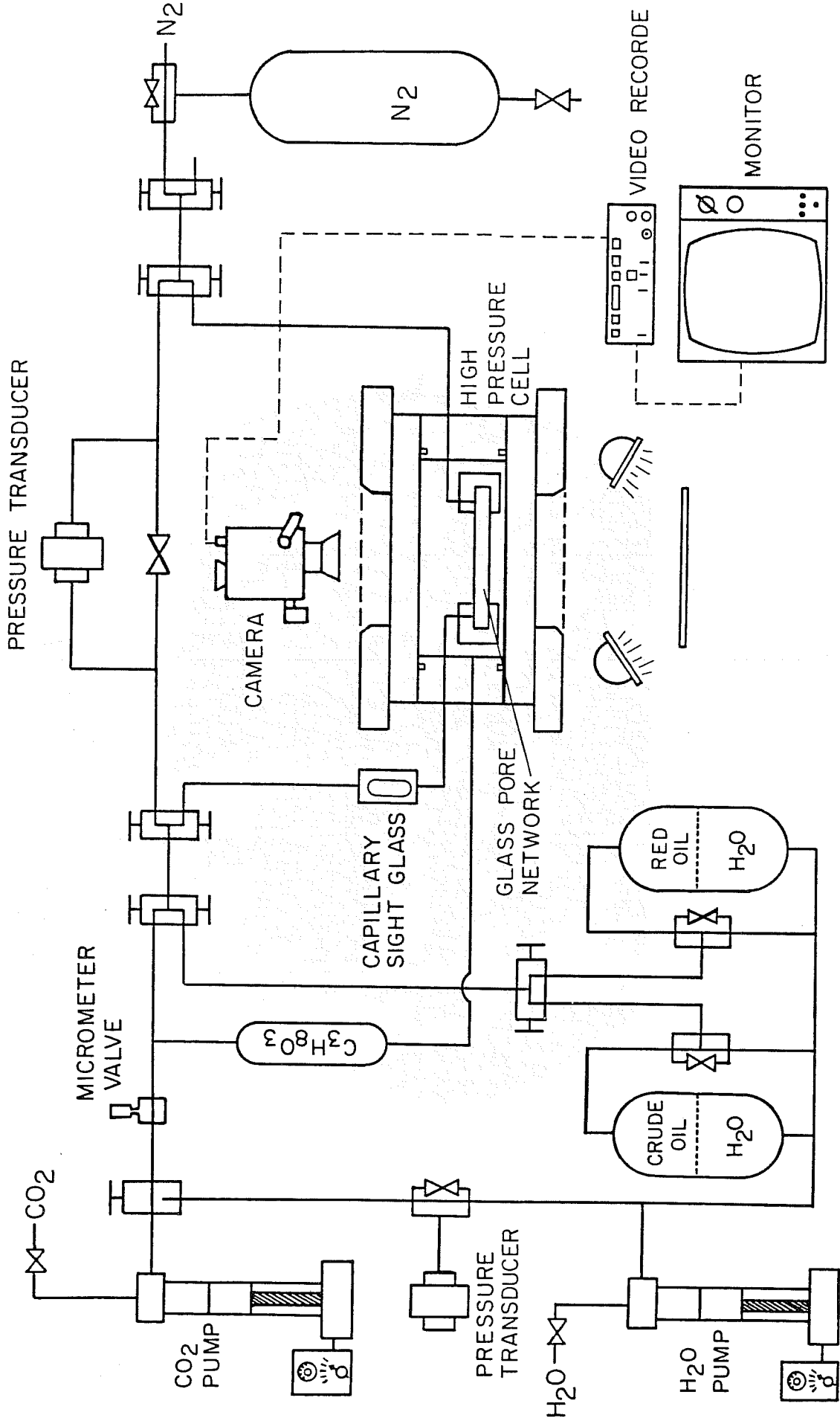


Fig. 2.1 High pressure flow visualization apparatus.

CO2-83-002

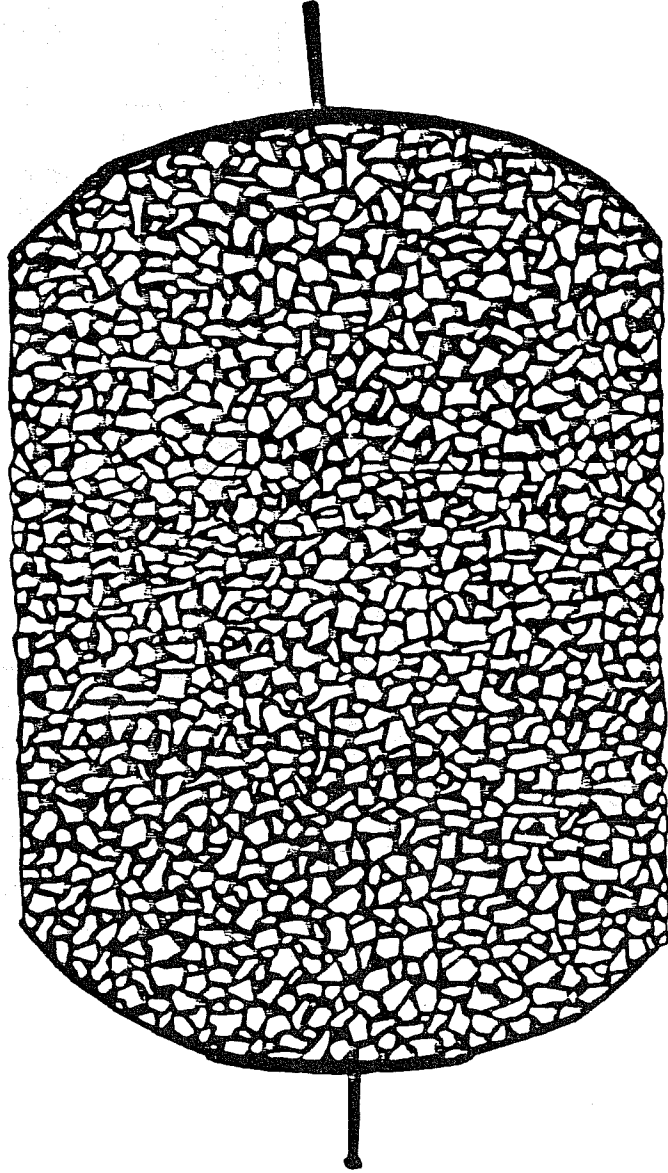


Fig. 2.2 Sample pore network. Dark areas are open to flow.

### Tertiary

- (4) Displacement of red-dyed Soltrol by water, followed by injection of blue-dyed Soltrol.
- (5) Displacement of red-dyed Soltrol by water, followed by injection of CO<sub>2</sub>.
- (6) Displacement of Maljamar crude oil by water, followed by injection of CO<sub>2</sub>.

### Secondary Displacements

Displacement (1) was intended to identify any preferential flow paths in the model. Fig. 2.3 shows approximate locations of the displacement front as a function of pore volumes injected. While some irregularity of the front can be seen, the flow pattern is close to what would be expected for a displacement with a favorable mobility ratio in a uniform pore network. The central portion of the model is swept more rapidly, because it lies on the central streamline from the injection port to the outlet port, along which the flow velocity is highest. Flow near the corners of the model is slower. Essentially all of the red Soltrol was displaced by the time 1.15 PV had been injected.

Results of displacement (2) are summarized in Fig. 2.4, which shows approximate displacement front locations for the unstable displacement of red Soltrol by CO<sub>2</sub> at 25°C and 1200 psia. The viscosity of the Soltrol was 1.74 cp while the viscosity of CO<sub>2</sub> was about .05 cp (Michels, Botzen & Schuurman 1957). Even in this small model, the displacement fronts show clearly the development of fingers as a result of the viscous instability. At the displacement conditions, CO<sub>2</sub> was first-contact miscible with the Soltrol, a mixture of branched C<sub>9</sub> - C<sub>13</sub> paraffins. All of the Soltrol was recovered, but it took 1.31 PV to complete the displacement.

Fig. 2.5 shows the positions of displacement fronts for the flood (3), in which CO<sub>2</sub> displaced Maljamar crude oil at 25°C and 1200 psia. The pressure was above the vapor pressure of CO<sub>2</sub> (944 psia at 25°C), so that the injected CO<sub>2</sub> was a liquid. Hence, the displacement was "miscible" in the multiple contact sense (see §3.1 and Orr & Jensen 1982). Detailed results of phase composition measurements for that crude oil have been reported previously (Orr & Taber 1981; Orr & Taber 1982; Orr, Yu & Lien 1981; Orr, Silva, Lien & Pelletier 1981; Orr, Silva & Lien 1983). Computations reported by Gardner, Orr & Patel (1981), Orr, Yu & Lien (1981) and Orr, Silva & Lien (1983) indicate that a small amount of a second phase should appear as the CO<sub>2</sub> front passes. Fig. 2.6 is a sketch of the appearance of the two liquid phases in pores in the neighborhood of the CO<sub>2</sub> front at 0.70 PV injected. The shapes of the interfaces between the CO<sub>2</sub>-rich and oil-rich phases were quite different from those observed between oil and water or CO<sub>2</sub> and water. The long, gently curved surfaces, which moved easily through very tight constrictions, suggest that the interfacial tensions between the two phases were substantially lower than typical oil-water tensions (Rosman & Zana 1977). It seems likely,

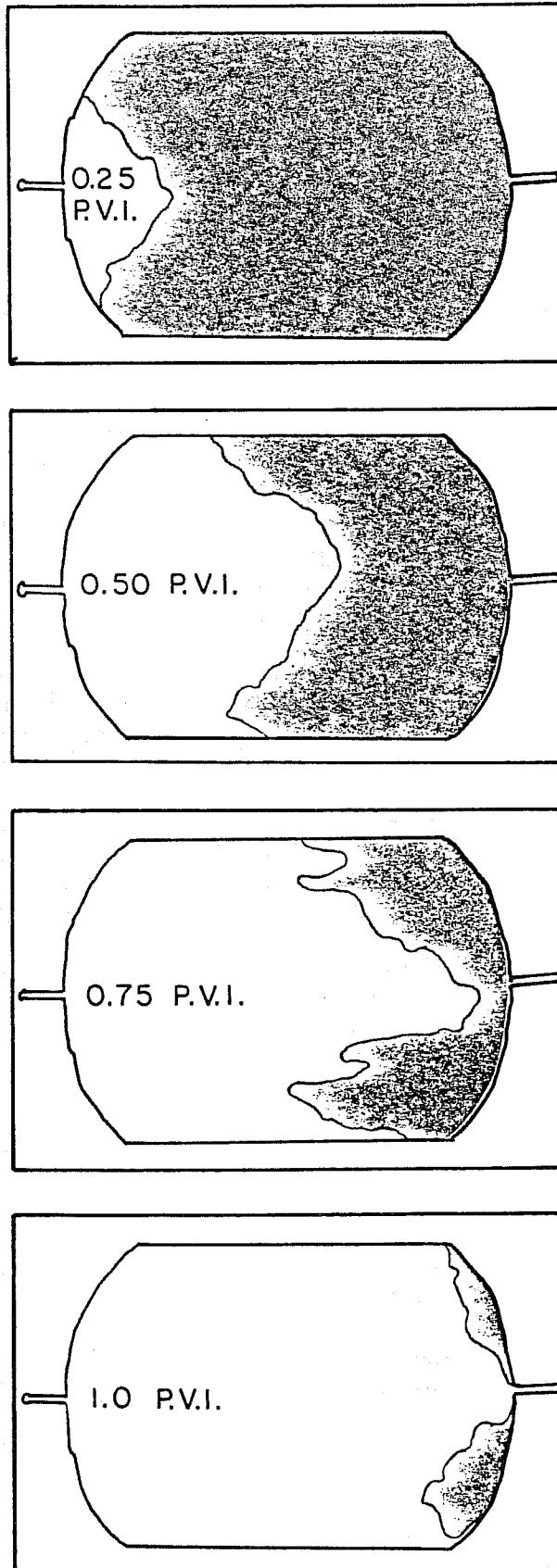


Fig. 2.3 Secondary displacement of red-dyed soltrol by blue-dyed soltrol.

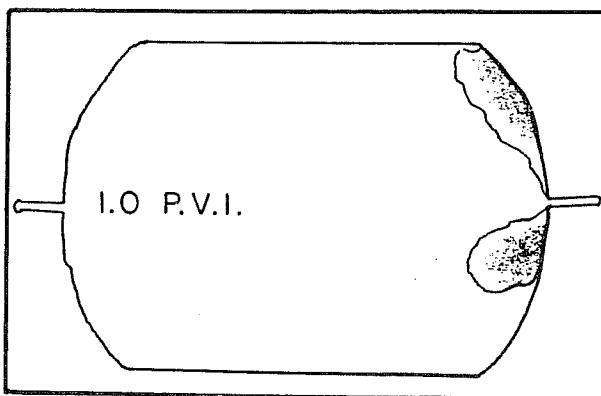
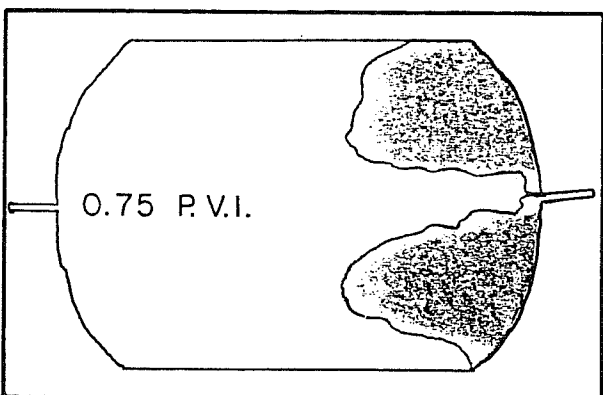
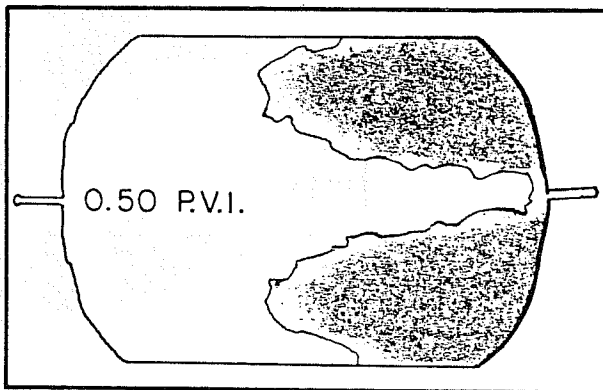
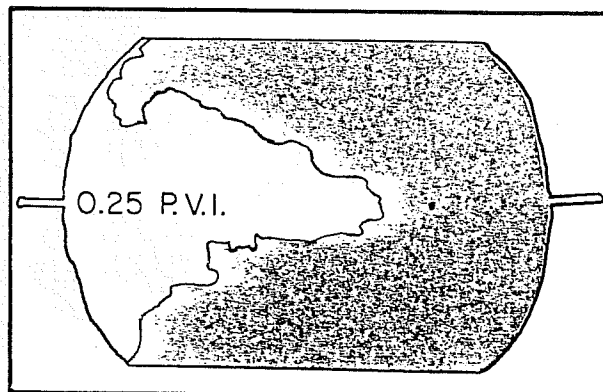


Fig. 2.4 Secondary displacement of red-dyed soltrol by CO<sub>2</sub> at 1200 psia, 25°C.

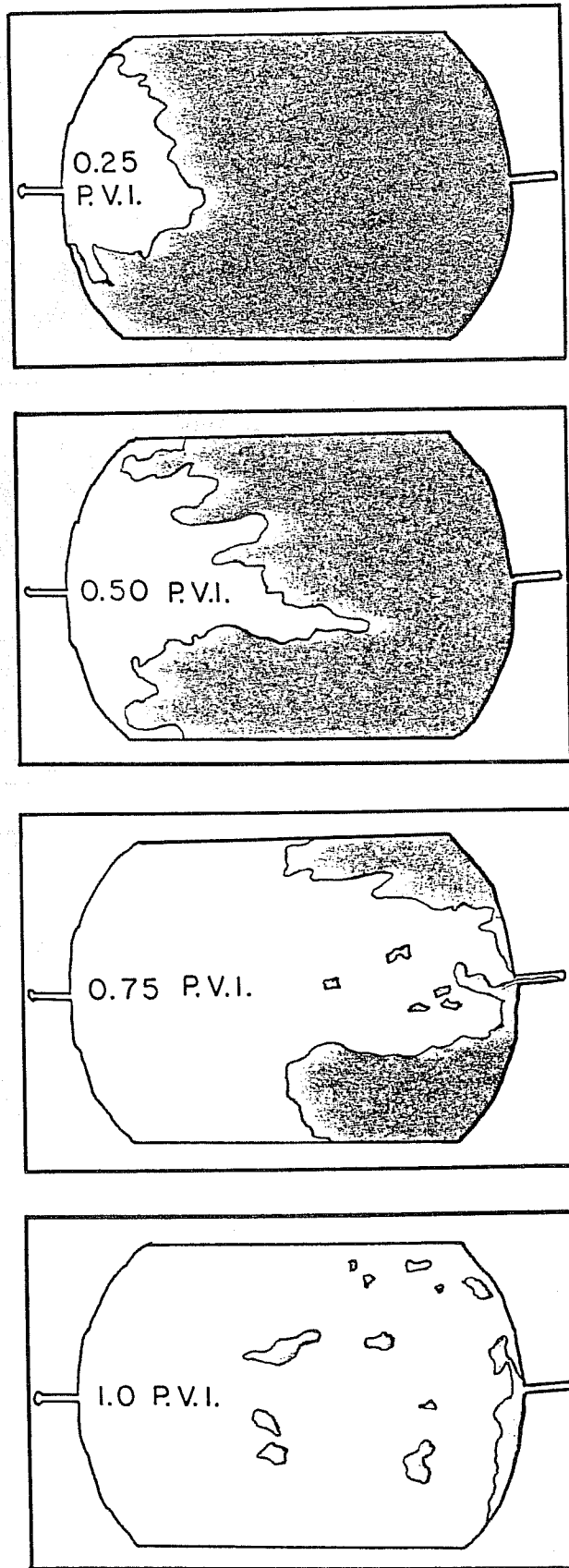


Fig. 2.5 Displacement of Maljamar crude oil by CO<sub>2</sub> at 1200 psia, 25°C.

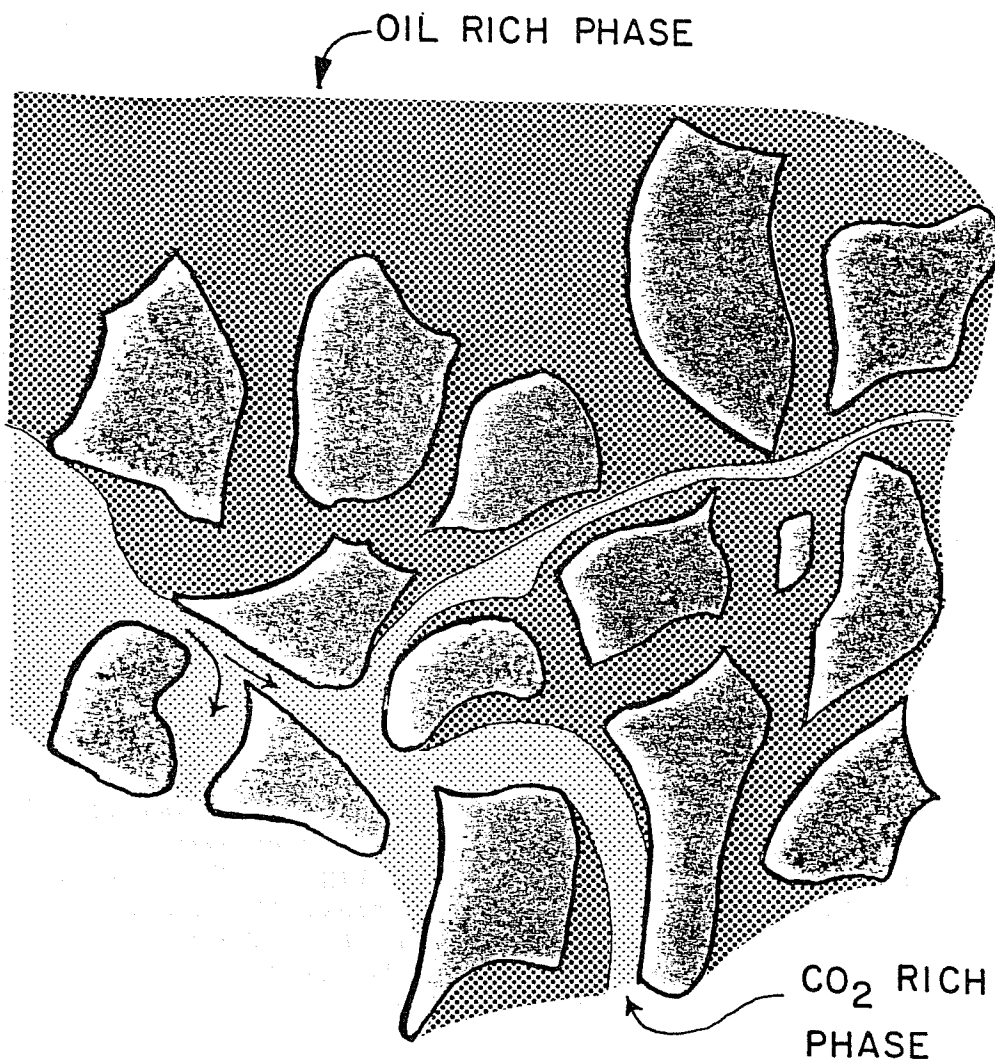


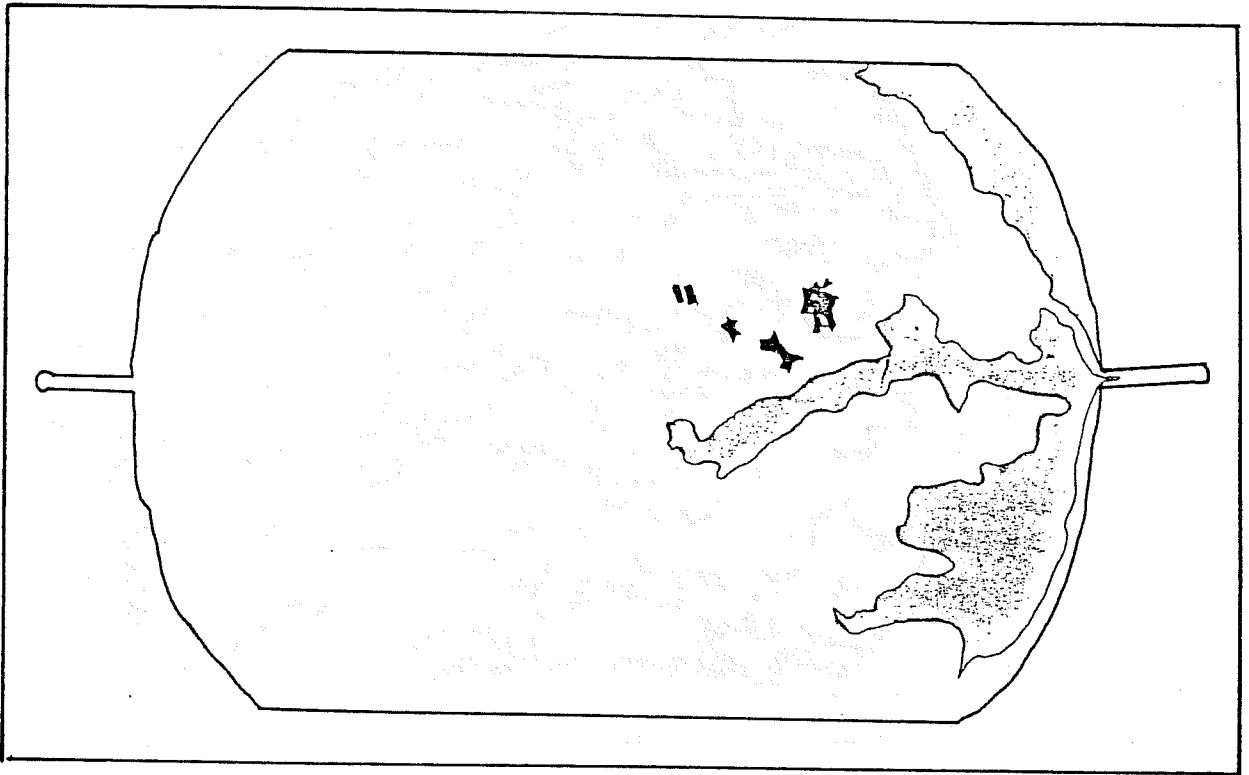
Fig. 2.6 Appearance of CO<sub>2</sub>-rich and oil-rich phases in the neighborhood of the CO<sub>2</sub> front in a secondary displacement of Maljamar crude oil by CO<sub>2</sub> at 1200 psia and 25°C.

however, that low interfacial tensions do not play a major role in the recovery of oil in secondary floods such as this because the saturation of the second phase is always very low. There is simply not very much oil left to be recovered by two-phase flow allowed by low interfacial tensions. Most of the oil has already been removed by the favorable effects of phase behavior.

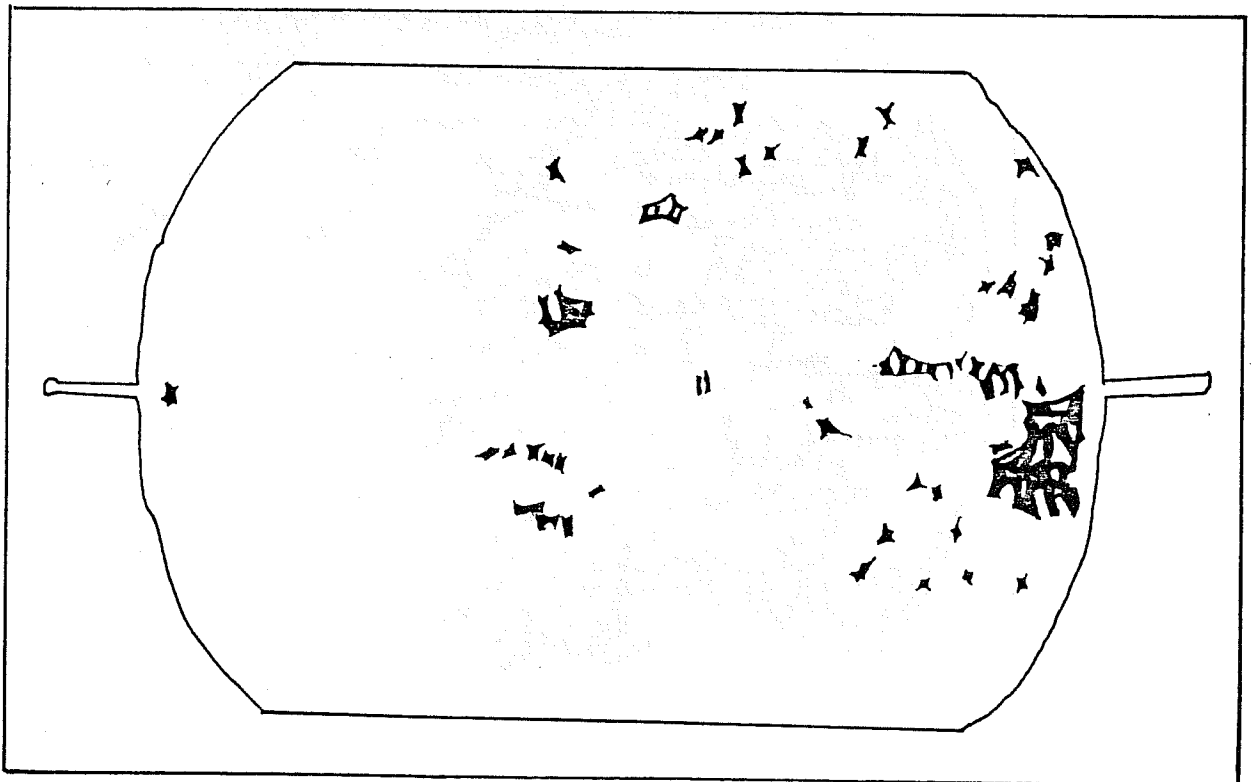
The appearance of the secondary displacement of crude oil in this model was consistent with the idea that the length required to "develop" miscibility was very short, much less than the length of the model. As Helfferich (1981) proved for one-dimensional displacements, the length required is infinitesimal, if only strictly local mixing is allowed. Dispersion or viscous fingering can lead to some finite length, but it is probably measured in pore lengths, the size of the cells in which mixing occurs in the model. It is the interaction between phase behavior and dispersive mixing which accounts for the presence of the second phase (Orr & Taber 1981). Gardner & Ypma (1982) showed that there is a similar interaction between viscous instability and phase behavior. They reported results of two-dimensional computations which indicated that the oil saturation after a CO<sub>2</sub> flood was higher in zones swept first by a viscous finger. Observations of the CO<sub>2</sub>-crude oil displacement in the two-dimensional network confirm that prediction. Shown in Fig. 2.7a is the location of the CO<sub>2</sub> front at 0.85 PV. It is clear that there is more oil left behind in the central finger than elsewhere in the model. Fig. 2.7b shows the approximate distribution of residual oil after a CO<sub>2</sub> flood (to 1.1 PV).

### Tertiary Displacements

Recovery of oil from a pore network which has been waterflooded to completion is by its nature far more difficult than secondary recovery, even if effects of viscous instability are absent. Fig. 2.8 illustrates the difficulties faced in any tertiary flood. It shows the locations of red Soltrol (oil), blue Soltrol (solvent) and water at breakthrough of injected fluid (blue Soltrol), which occurred at 0.15 PV injected in displacement (4). As comparison of the distributions of oil, solvent and water shown in Fig. 2.8a and b indicates, much of the injected solvent simply resaturated areas occupied previously by water. Significant portions of the red oil were reconnected with injected solvent, but very little oil was driven ahead of the solvent as an oil bank. It should be emphasized that the viscosity ratio for the solvent water displacement was favorable. The Soltrols (red and blue) had a viscosity of 1.74 cp while the water viscosity was 0.9 cp. Despite the favorable viscosity ratio, however, most of the recovery of red oil was by diffusion into the flowing stream of blue oil from dendritic or dead-end oil ganglia which were open to the flowing stream, but which were prevented by capillary forces from being displaced directly. Fig. 2.9 is a photograph of an actual dendritic ganglion which occurred during displacement (4). The red oil at the feet of the dendritic ganglion was displaced from its original position after the waterflood by injected blue oil. Eventually, however, those feet entered pores from which there was no exit which could be traversed at the capillary pressure available to the blob. At that point, then, the blob ceased to move, but the red oil in it continued to diffuse slowly into the flowing stream of blue oil to which it was connected. Thus, the

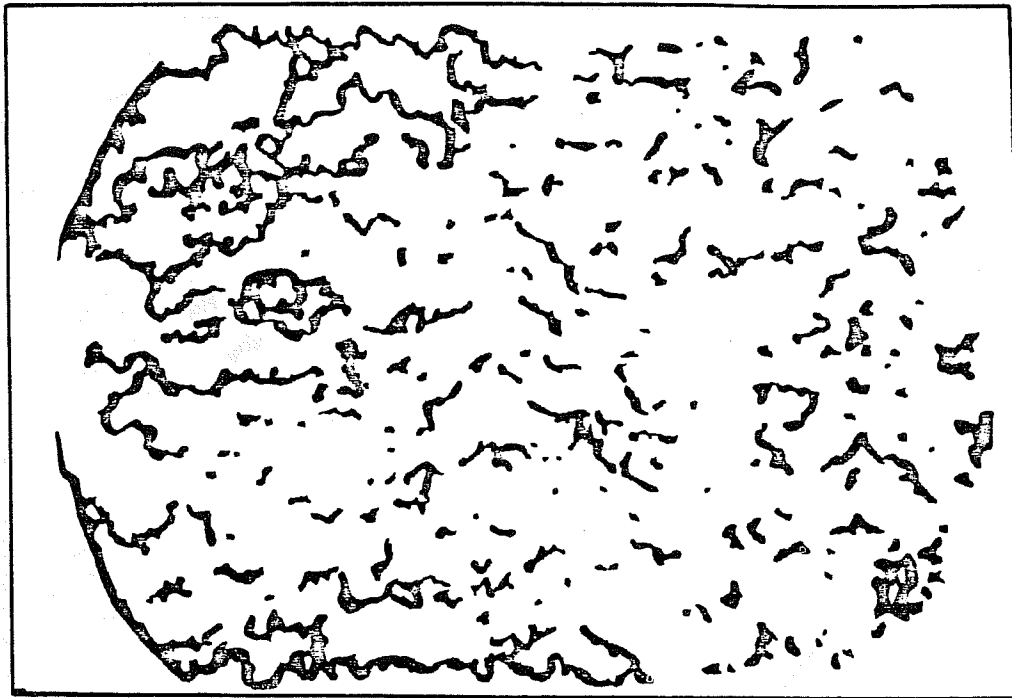


a. Distribution of residual oil at 0.85 PV



b. Distribution of residual oil at 1.1 PV

Fig. 2.7 Locations of oil left behind by a secondary CO<sub>2</sub> displacement of Maljamar crude oil.



a. Residual red oil (dark ganglia) to a waterflood (water is clear)



b. Distribution of red oil (dark areas), solvent (blue soltrol, outlined areas) and water (clear) at solvent breakthrough (0.15 PV)

Fig. 2.8 Ideal tertiary displacement of oil by a miscible solvent.

CO<sub>2</sub>-83-009

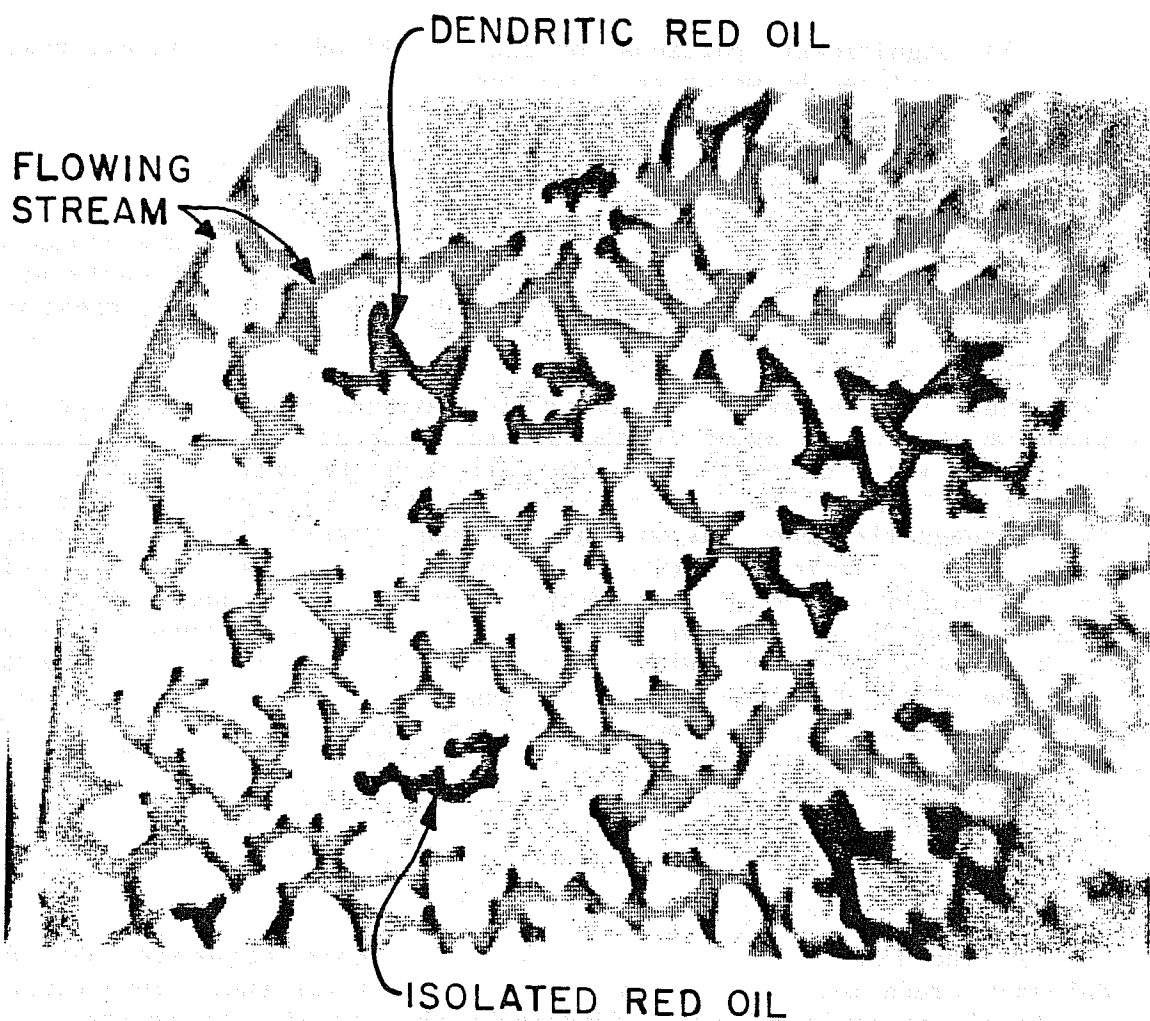


Fig. 2.9 Dendritic and isolated oil ganglia.

observations of the two-dimensional, favorable mobility ratio, tertiary miscible displacement clearly indicated that:

- (1) Oil production and solvent breakthrough occurred almost simultaneously.
- (2) Much of the oil recovered was by diffusion, a slower process than displacement, from dendritic ganglia, even though the pore network contained no dead-end pores.
- (3) Significant portions of the waterflood residual oil remained isolated by water and inaccessible to flowing solvent.

Fig. 2.10 shows distributions of red oil,  $\text{CO}_2$  and water at  $\text{CO}_2$  breakthrough in displacement (5). Because  $\text{CO}_2$  was much less viscous than the water or Soltrol, it did a poor job of moving water and hence contacted little of the oil directly. Consequently, breakthrough occurred early at 0.037 PV injected. Thus, the initial performance of the tertiary  $\text{CO}_2$  flood was poorer than that of the corresponding tertiary Soltrol flood.

There was, however, one important favorable effect present in the  $\text{CO}_2$  flood which did not occur in the Soltrol displacement.  $\text{CO}_2$  is sufficiently soluble in water that it can diffuse through the water to reach trapped oil droplets. To study qualitatively the effects of diffusion through the water, flow through the model was stopped, though pressure was maintained, and the model left overnight. After 21 hours, there was clear evidence of redistribution of the oil and water phases, as must happen if  $\text{CO}_2$  diffuses into and swells an isolated oil droplet. Then, flow through the model was started again, and individual isolated ganglia close to the flowing  $\text{CO}_2$  stream were observed. Fig. 2.11 shows the change in size of one ganglion as time passed. Eventually, that ganglion swelled enough to break a water interface separating it from the flowing stream. In addition, after a full day of flow, a second flow channel formed near the top of the model. Thus, though the time scales for such behavior are different in reservoir rocks, it is clear that  $\text{CO}_2$  can reach isolated droplets which would be inaccessible to an injected solvent such as Soltrol.

In the final tertiary displacement in this sequence,  $\text{CO}_2$  displaced Maljamar crude oil. For reasons which are still under investigation,  $\text{CO}_2$  displaced the crude oil more effectively than it did the Soltrol. A greater percentage of the model was swept at  $\text{CO}_2$  breakthrough, and additional flow channels developed as the run progressed. Whether the improved performance was due to changes in wetting behavior of the crude oil or the presence of numerous interfaces between  $\text{CO}_2$  and oil-rich phases in the swept zone is not yet known. It is clear, however, that  $\text{CO}_2$  can displace crude oil effectively even when the water saturation is high, though it is also clear that the presence of water alters the mixing of  $\text{CO}_2$  and oil. The effect of that change in mixing on composition paths and hence local recovery efficiency is also not yet known. It is apparent that in actual reservoir rocks, the way in which residual oil is distributed in the rock pore space, the distribution of sizes of oil ganglia and the average distance between flowing  $\text{CO}_2$  channels will all act to influence the reconnection and recovery of residual oil.

CO<sub>2</sub>-83-010

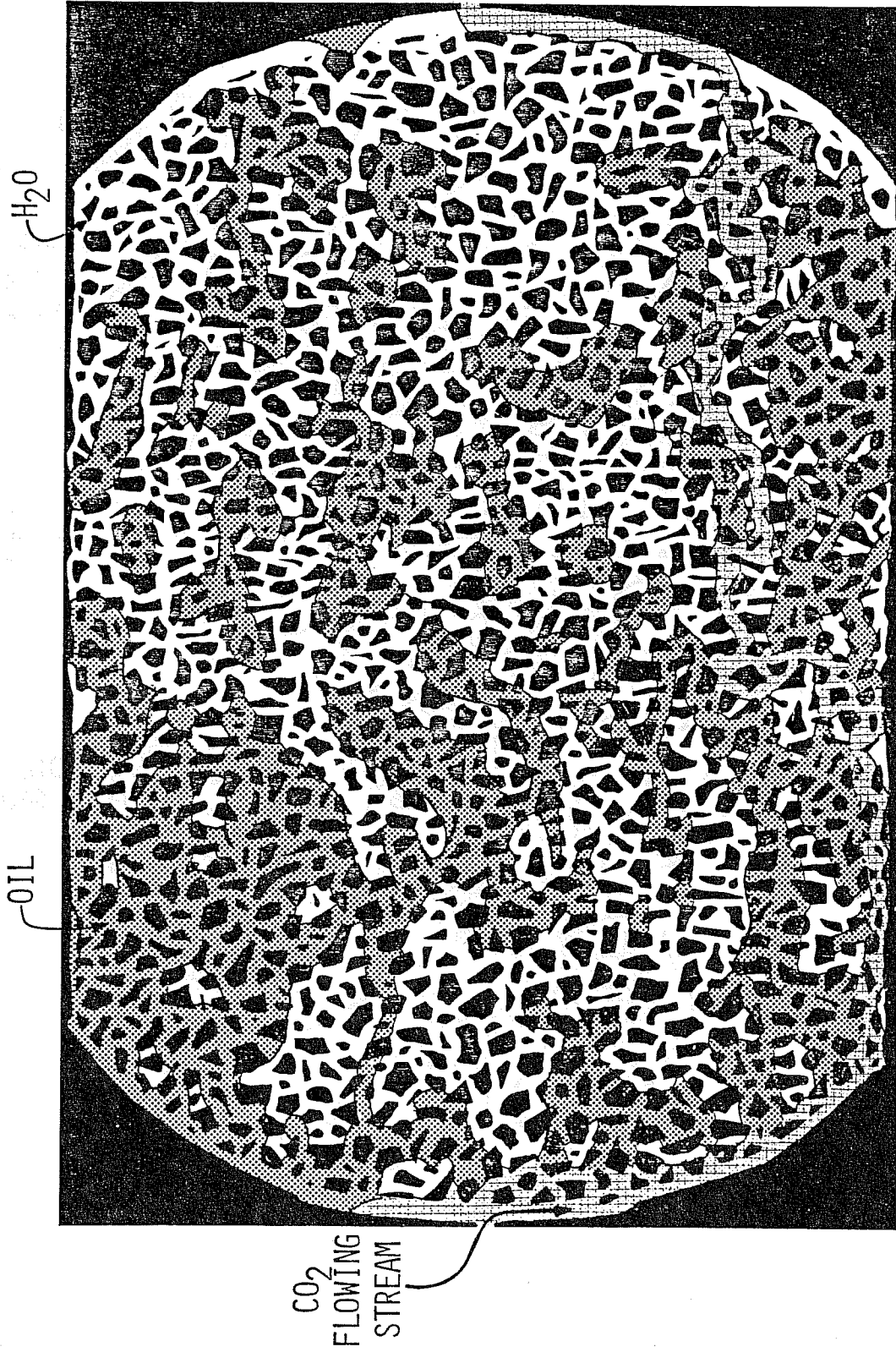


Fig. 2.10 Distribution of oil, CO<sub>2</sub> and water at CO<sub>2</sub> breakthrough (0.037 PV) in a tertiary displacement of red soltrol by CO<sub>2</sub> at 1200 psia, 25°C.

CO<sub>2</sub>-83-011

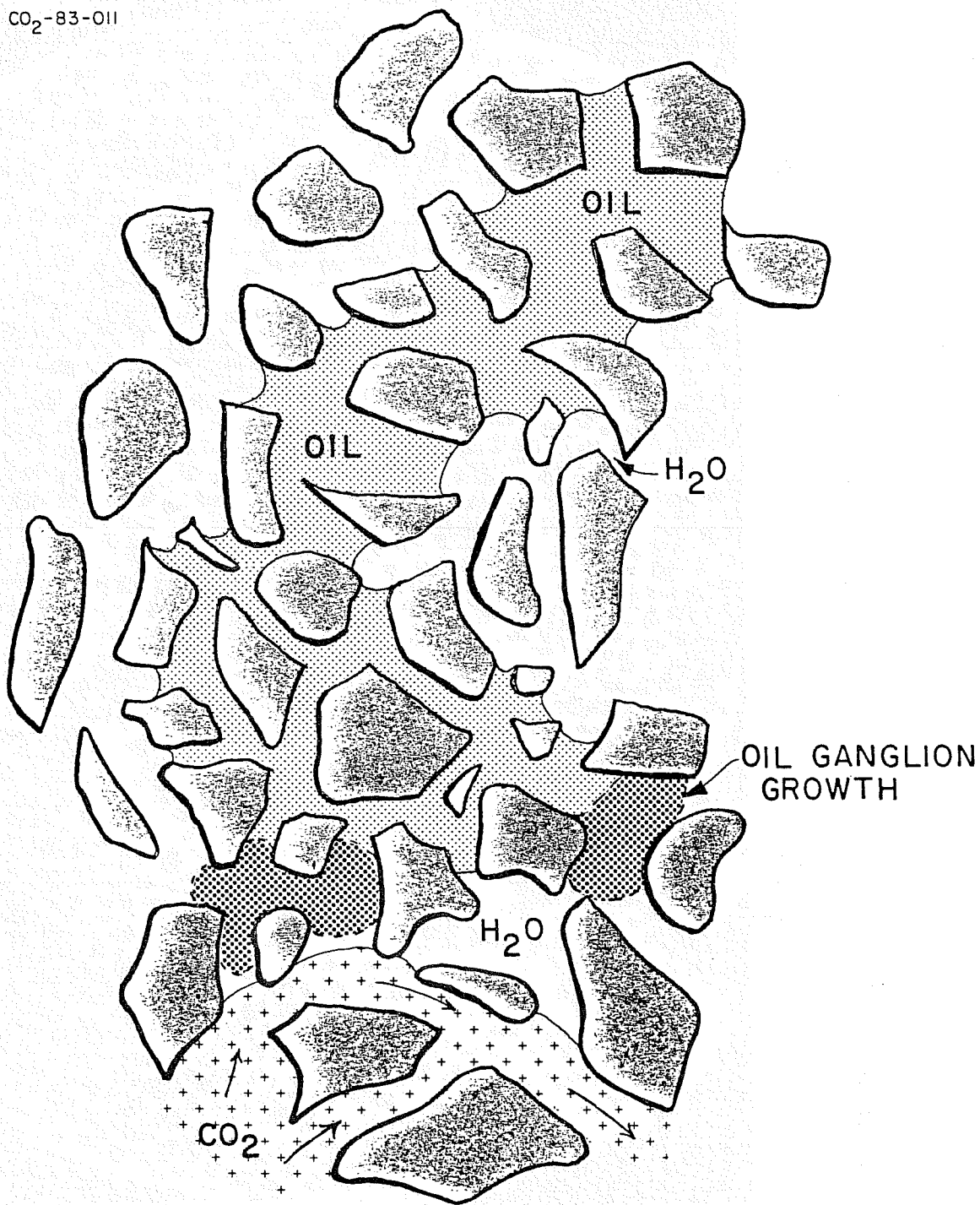


Fig. 2.11 Swelling of a trapped oil droplet by CO<sub>2</sub> diffusing through water.

It should be noted that the time and space scales over which diffusional and convective mixing take place in the pore networks used here are not the same as those which would occur in a reservoir rock. The pores in a rock are much smaller, and typical flow velocities are much lower in field scale displacements. Thus, diffusion of CO<sub>2</sub> into trapped oil droplets should be more effective in reservoir rocks than in the model displacements described here. Nevertheless, the pore network displacements illustrate clearly the variety of mechanisms which operate when CO<sub>2</sub> displaces oil whenever the water saturation is high. The challenge which remains is to quantify the relationships between heterogeneity, diffusion, dead-end pores, phase behavior, and viscous instability and to understand the importance of each in determining field-scale displacement performance.

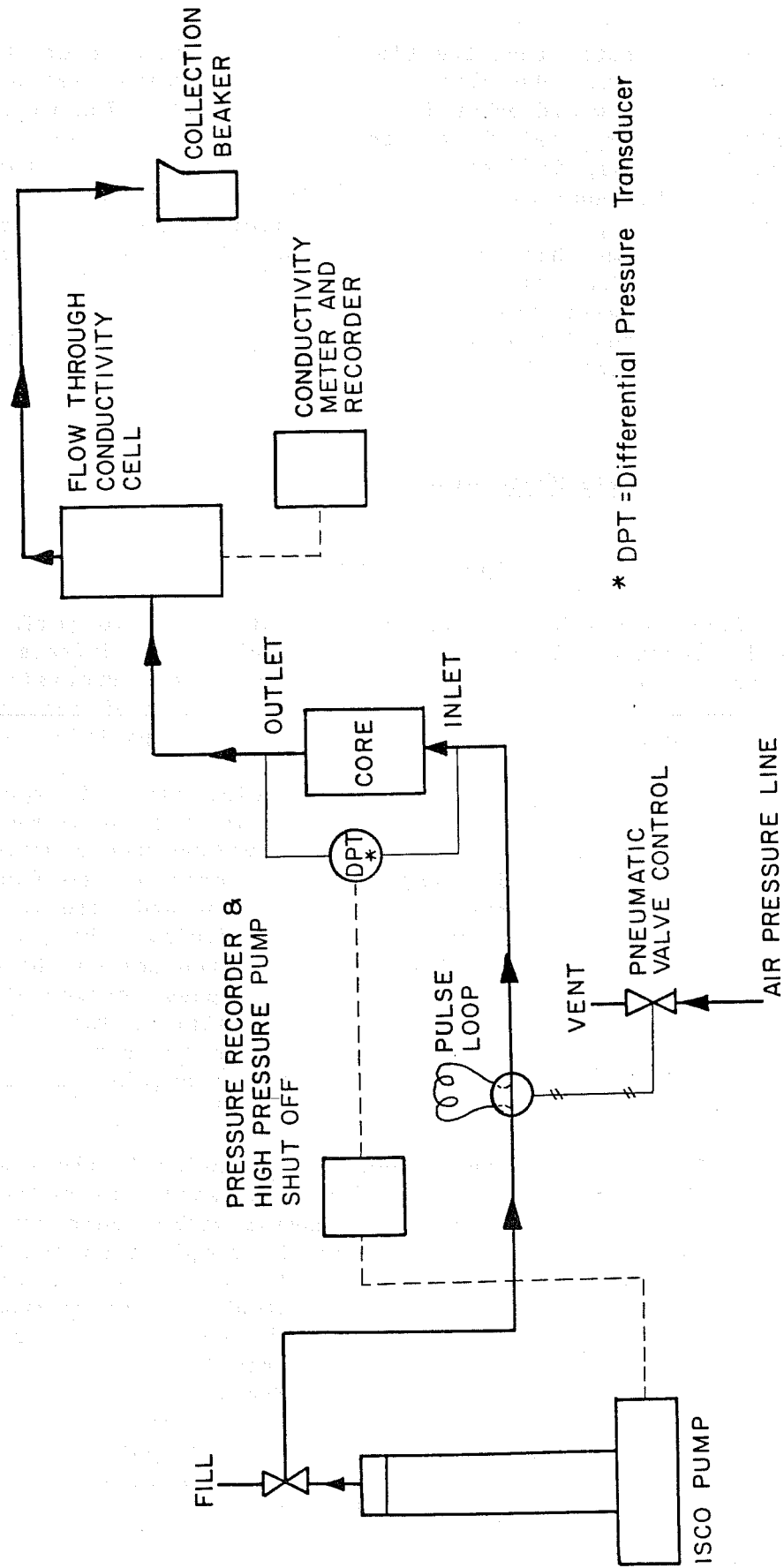
### 2.3 Results of Single Phase Displacement Experiments

#### Apparatus and Procedures

Fig. 2.12 is a schematic of the apparatus used to perform single phase miscible displacements in reservoir core samples. It differs from the design reported previously (Orr & Taber 1982) in two ways. Provision has been made for injection of a slug of displacing fluid in place of continuous injection, and an on-line detector for measurement of brine compositions has been added.

Injection of a slug (pulse) of displacing fluid is accomplished by a pulse loop similar to those used for the injection of samples in gas and liquid chromatography. The loop of known volume was constructed from two pneumatically operated slider valves and a coil of teflon tubing. The experiment is performed by first filling the pump and core with one fluid and then loading the sample loop with a matching fluid. The pump is started at the proper displacement rate and the pressure drop across the core allowed to stabilize while the sample loop is in the by-pass configuration. Then the slider valves are switched to the "sample" position, which directs the flow from the pump through the loop before flowing to the core. The volume of the sample loop may be varied by using different lengths of tubing. So far nominal volumes of 5 cc and 15 cc have been used.

Fig. 2.13 demonstrates the effect of dispersion in the sample loop on the concentration history at the outlet of a Berea sandstone core. The corrected concentration history represents the behavior which would have been observed if an ideal pulse (without dispersion in the sample loop and the dead volume upstream) were used. To obtain this corrected concentration history, the actual concentration history and the concentration history from a sample loop displacement (which is the input wave form seen by the core) at the same velocity were transformed from the time domain to the frequency domain via a fast Fourier transform (FFT) algorithm. The transformed core concentration history was then divided by the transformed actual input waveform. The resulting transfer function is equivalent to the impulse response function in the time domain, and describes the system response to an impulse input. The transfer function was then multiplied by the transformed ideal pulse input.



\* DPT =Differential Pressure Transducer

Fig. 2.12 Apparatus for single-phase miscible displacements.

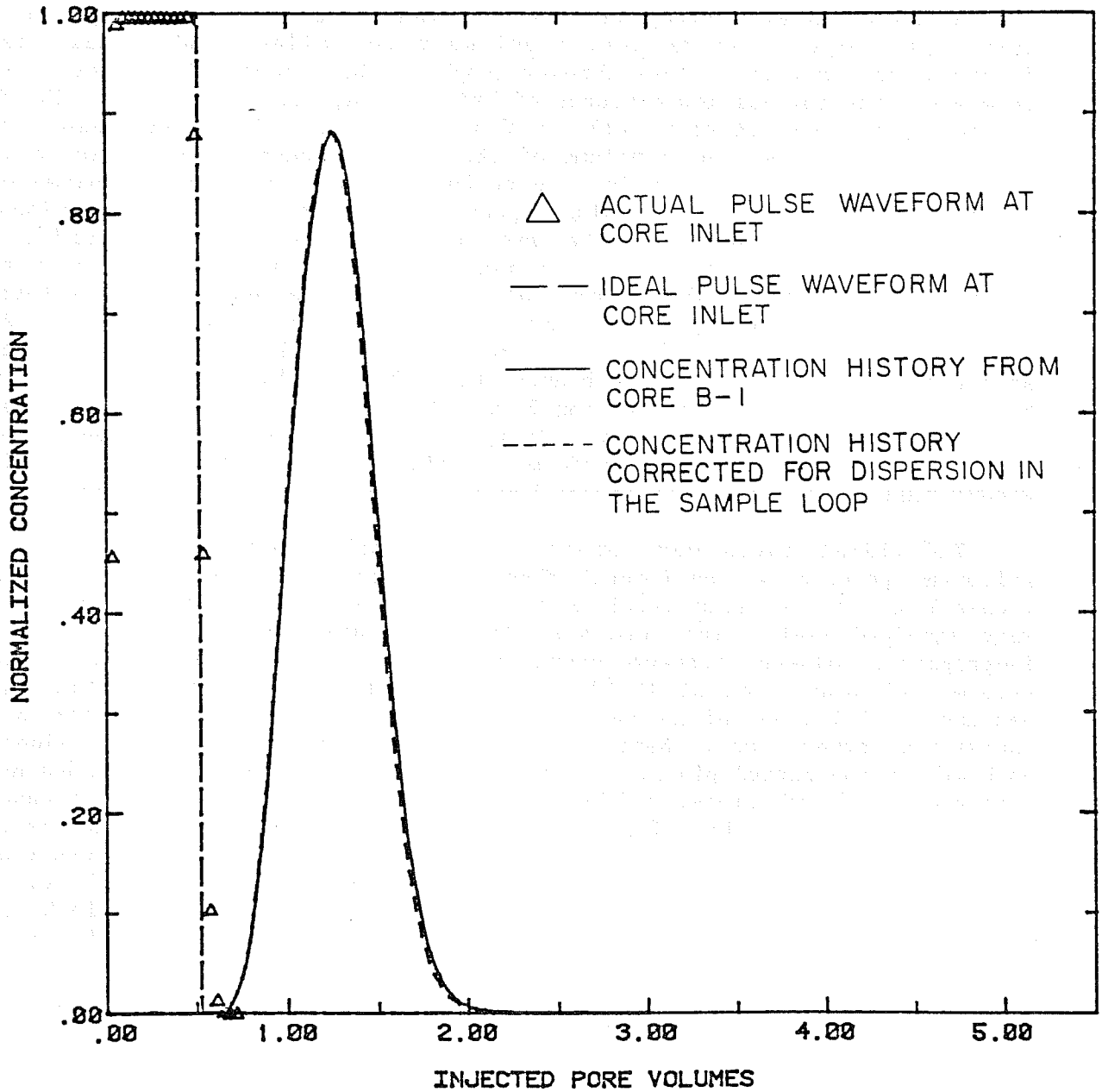


Fig. 2.13 Effect of a nonideal pulse on effluent concentrations for a displacement in a Berea sandstone core (Run 2).

This multiplication is equivalent to convolution in the time domain. The product was then transformed via an inverse FFT to the time domain. Clearly the dispersion in the sample loop had little effect on the results of this experiment.

As shown in Fig. 2.12, an on-line conductivity meter has replaced the multiport sampling valve used previously to collect individual sample fractions for analysis by gas chromatography. The conductivity meter is used to measure the composition mixtures of brines of different salinity. The dead volume of the conductivity cell is about  $0.3 \text{ cm}^3$ . Thus, the composition averaging due to the finite volume of the cell is roughly comparable to that of measurements in which samples are collected since the minimum volume of a sample is about  $0.5 \text{ cm}^3$ . In single-phase displacements reported previously, ethyl benzene and ethyl butyrate were used as the miscible fluids, and compositions were determined by chromatography, a slower procedure than on-line measurements. The current procedure also leaves the core saturated with brine and therefore ready for two-phase displacements. Fig. 2.14 compares results of injection of a pulse of ethyl butyrate into a Berea sandstone core containing ethyl benzene with those of injection of 2 wt % NaCl brine into the same core containing 2 wt % NaCl brine. The two displacements clearly gave equivalent results. Thus, it appears that on-line conductivity measurements can be used to perform efficiently the single-phase miscible floods required to characterize the heterogeneity of a particular core.

Individual cores were prepared for displacement according to the following procedure. Horizontal plugs 1.5 inches in diameter and about 3 inches long were cut from vertical reservoir cores, and the ends of the cores were machined flat. The core was cleaned by displacing many volumes of isopropanol, toluene, tetrahydrofuran and acetone through it and dried under vacuum and in an oven at  $100^\circ\text{C}$ . After cleaning, air permeabilities were measured. Two core plugs were then butted together with filter paper sandwiched between them. Next, end caps, cast in epoxy resin, were added at each end of the butted plugs, the entire assembly placed inside the annulus of a section of 2 inch diameter fiber reinforced polyester pipe, and the annulus filled with epoxy. Fig. 2.15 illustrates the end cap design. Two central inlet (or outlet) tubes connect to separate spiral grooves which distribute oil and water over the core face. The inlet tubes used are 1/16 inch OD, .003 ID stainless steel. The spiral grooves are 1/16 inch wide by 1/32 inch deep. The resulting dead volume of the end cap with tubes was found to be  $0.2 \text{ cm}^3$ .

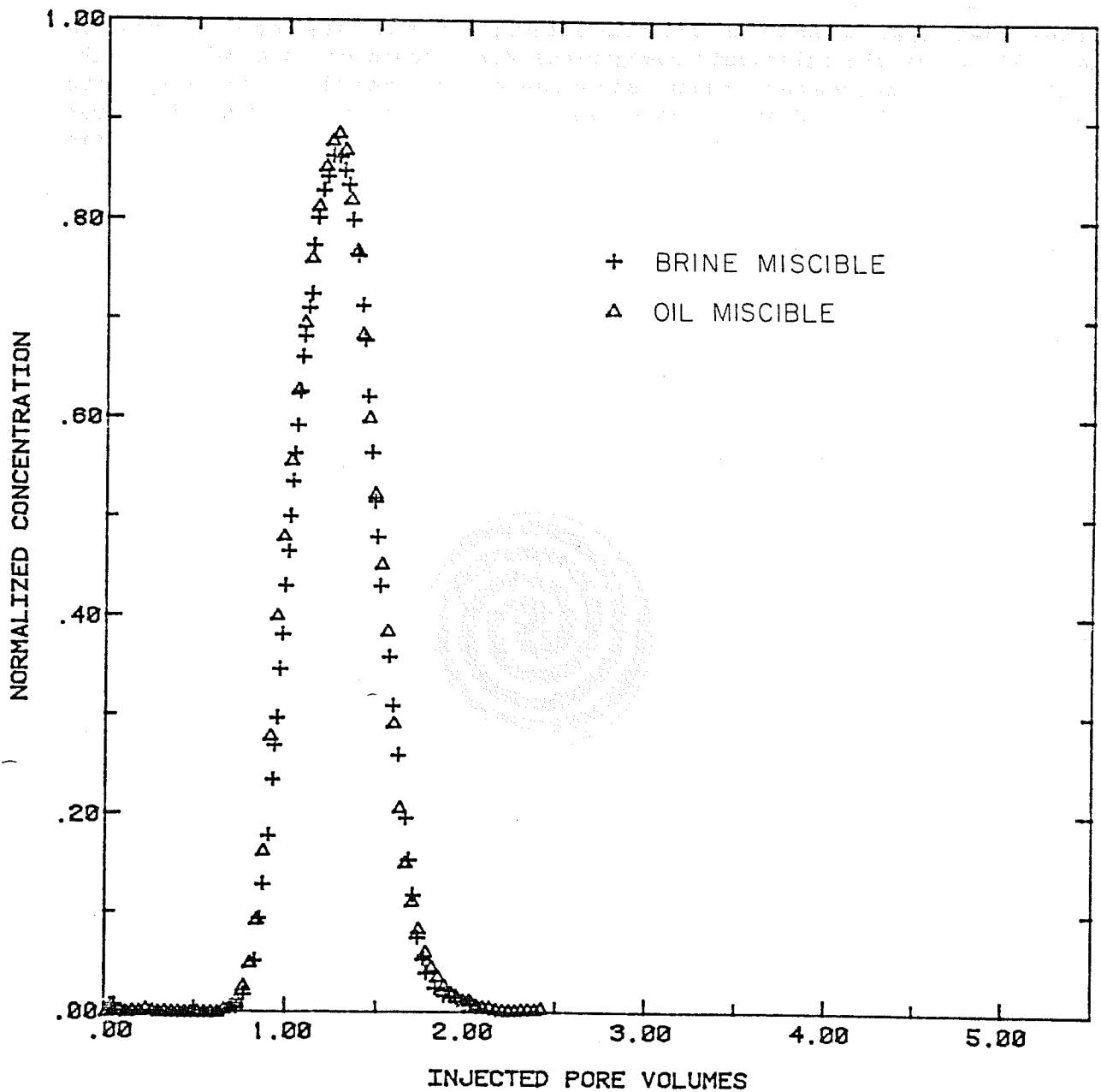


Fig. 2.14 Concentration histories for miscible displacements in Berea sandstone (B-1). The brine data were obtained using a conductivity cell. The oil data were obtained by gas chromatography (Runs 2 and 3).

## Results and Discussion

Miscible core displacements performed for two core samples are summarized in Table 2.1. Fig. 2.16 is a pair of concentration histories for miscible pulse displacements in a Berea sandstone, Core B-1, at a displacement velocity of approximately 12 ft/day ( $4.3 \times 10^{-3}$  cm<sup>2</sup>/sec). It has been repeatedly established that miscible displacements in the absence of viscous instabilities in the relatively homogeneous Berea sandstone are well described by the single parameter, dispersion-convection model. The dispersion coefficient for these displacements was determined by minimizing the square error to be  $7.7 \times 10^{-4}$  cm<sup>2</sup>/sec. The dispersion coefficient predicted using



Fig. 2.15 End cap design.

Table 2.1 Summary of Miscible Displacement Experiments

Run No.	Core I.D.	Rock Type	Type of Displacement	Type of Fluid	Rock Pore Volume cm <sup>3</sup>	Pulse Volume cm <sup>3</sup>	Air Permeability m Darcies	Porosity %	Length cm	Diameter cm	Displacement Velocity ft/day	Average Interstitial Velocity cm/sec
1	B-1	Berea sandstone	Step	Oil	28.9*	N/A	180	18.2	13.9*	3.81	--	$2.6 \times 10^{-3}$
2	B-1	"	Pulse	"	28.6*	14.3	"	"	13.6*	"	12	$4.3 \times 10^{-3}$
3	B-1	"	"	Brine	28.6	14.3	"	"	"	"	"	"
4	H-1	Dolomite	"	"	35.85	"	20	17.9	16.2	"	0.78	$2.7 \times 10^{-4}$
5	H-1	"	"	"	"	"	"	"	"	"	14	$4.4 \times 10^{-3}$
6	H-1	"	"	"	"	"	"	"	"	"	78	$2.7 \times 10^{-2}$
7	H-1	"	"	Oil	"	"	"	"	"	"	14	$4.4 \times 10^{-3}$
8	H-1	"	"	"	"	"	"	"	"	"	0.78	$2.7 \times 10^{-4}$
9	H-1	"	"	Brine	"	"	"	"	"	"	14	$4.4 \times 10^{-3}$

\*Differences due to shortening the rock during end cap replacement

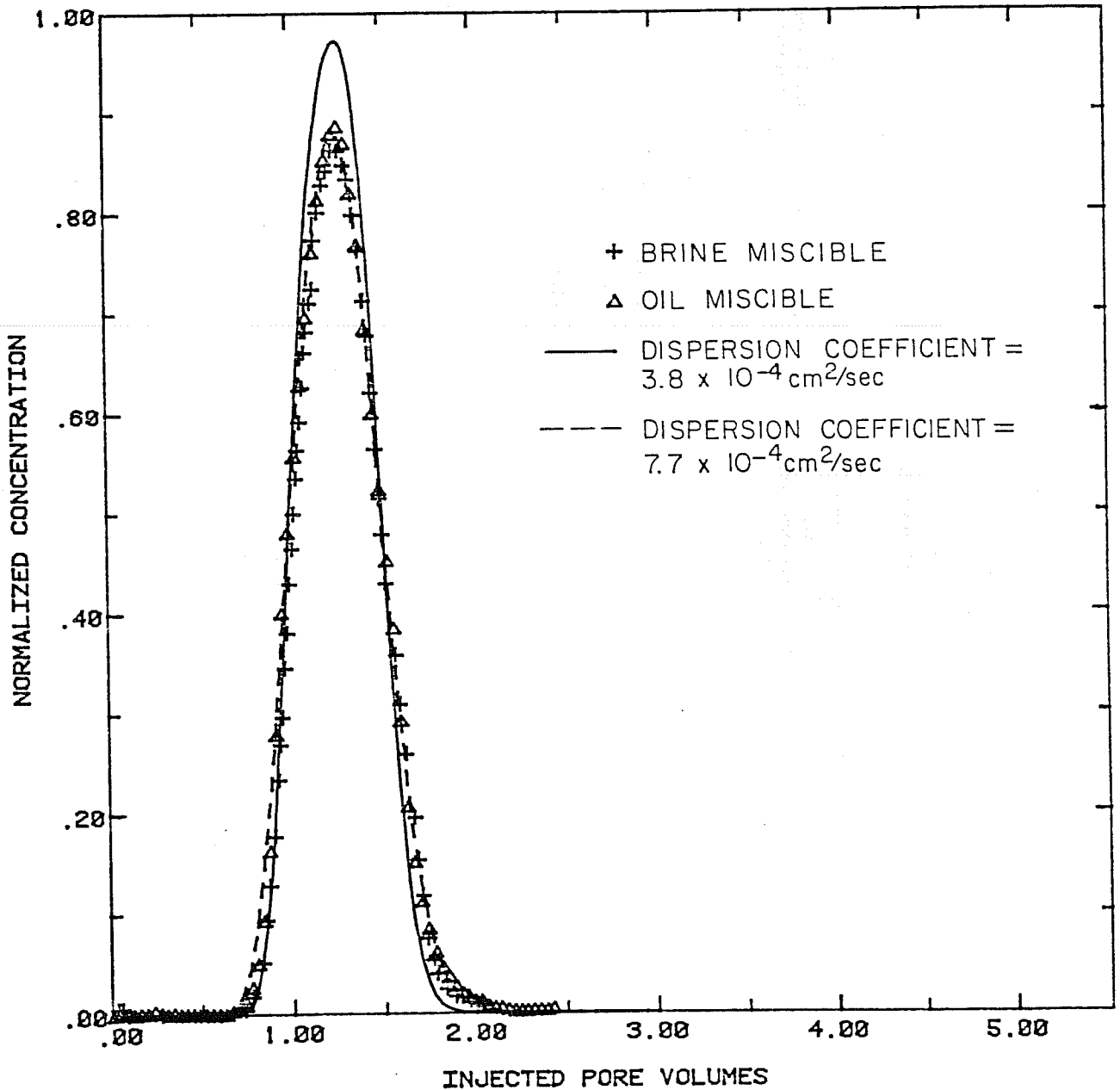


Fig. 2.16 Comparison of measured (Runs 2 and 3) and calculated effluent concentration histories for miscible displacements in a Berea sandstone core.

the correlation suggested by Salter & Mohanty, (1982) for another Berea sandstone core is somewhat lower ( $4.8 \times 10^{-4}$  cm<sup>2</sup>/sec) than the value determined here. Fig. 2.16 also shows effluent composition histories calculated using values of the dispersion coefficient of  $3.8 \times 10^{-4}$  and  $7.7 \times 10^{-4}$ . While the two calculated solutions differ only slightly in the leading and trailing edges of the pulse, there is an easily discernible difference in peak heights. Thus, the use of a pulse input rather than a step change in inlet concentration probably improves the sensitivity of the determination of the dispersion coefficient.

The concentration history for a step input displacement for the same core at a slightly lower interstitial velocity ( $2.6 \times 10^{-3}$  cm<sup>2</sup>/sec) is presented in Fig. 2.17. The dispersion coefficient obtained using a least squares fit of a straight line to effluent composition data plotted in arithmetic probability coordinates (Brigham, Reed & Dew 1961) was also somewhat higher for this core ( $4.8 \times 10^{-4}$  cm<sup>2</sup>/sec) than is predicted by Salter & Mohanty's (1982) correlation ( $2.7 \times 10^{-4}$  cm<sup>2</sup>/sec). Fig. 2.17 also shows calculated effluent composition histories for the dispersion coefficient obtained from the arithmetic probability plot and for values two times higher and lower. The value of  $4.8 \times 10^{-4}$  cm<sup>2</sup>/sec for the dispersion coefficient produces a calculated effluent composition which matches the experimental history well for concentrations below about 50 percent though it is slightly less accurate at the trailing edge. That value is also consistent with the one obtained in the pulse experiment. If the velocity exponent is estimated as 1.16 (Salter & Mohanty 1982), then the value of D at the lower velocity estimated from the dispersion coefficient determined in the pulse experiment is  $4.3 \times 10^{-4}$  cm<sup>2</sup>/sec. Thus, the pulse and step input experiments yield consistent results.

Fig. 2.18 compares results of six displacements in a west Texas reservoir core sample. The displacements were conducted at three rates, 0.78, 14 and 78 ft/day, using both oils and brines as the miscible fluids. The core sample, a San Andres dolomite, is by nature more heterogeneous than the Berea sandstone sample. In all of the displacements, breakthrough of injected fluid occurred at about 0.4 PV injected. One of the displacements (with brine at 0.78 ft/day) differed significantly from the others, though an oil displacement at the same rate was indistinguishable from the other displacements. Whether the difference was real or was due to experimental difficulties of some sort is not yet known. The other displacements were remarkably consistent.

The effluent compositions shown in Fig. 2.18 were not the result of dispersion alone. Fig. 2.19 compares typical effluent data with a composition history calculated, using the convection-dispersion model, with a dispersion coefficient chosen to give a peak height in approximate agreement with the experimental value. The injected pulse appears substantially earlier in the experiment and has a longer tail.

One interpretation of the results shown in Fig. 2.18 is that the pore space is composed of regions in which the average flow velocities differ markedly. Such flows can be modeled as flowing and stagnant volumes (Deans 1963; Coats & Smith 1964; Stalkup 1970; Baker 1977; Batycky, Maini & Fisher 1982; Spence & Watkins 1980; Salter & Mohanty 1982). The simplest model of such a pore system is that offered by Deans (1963). In his model the effect

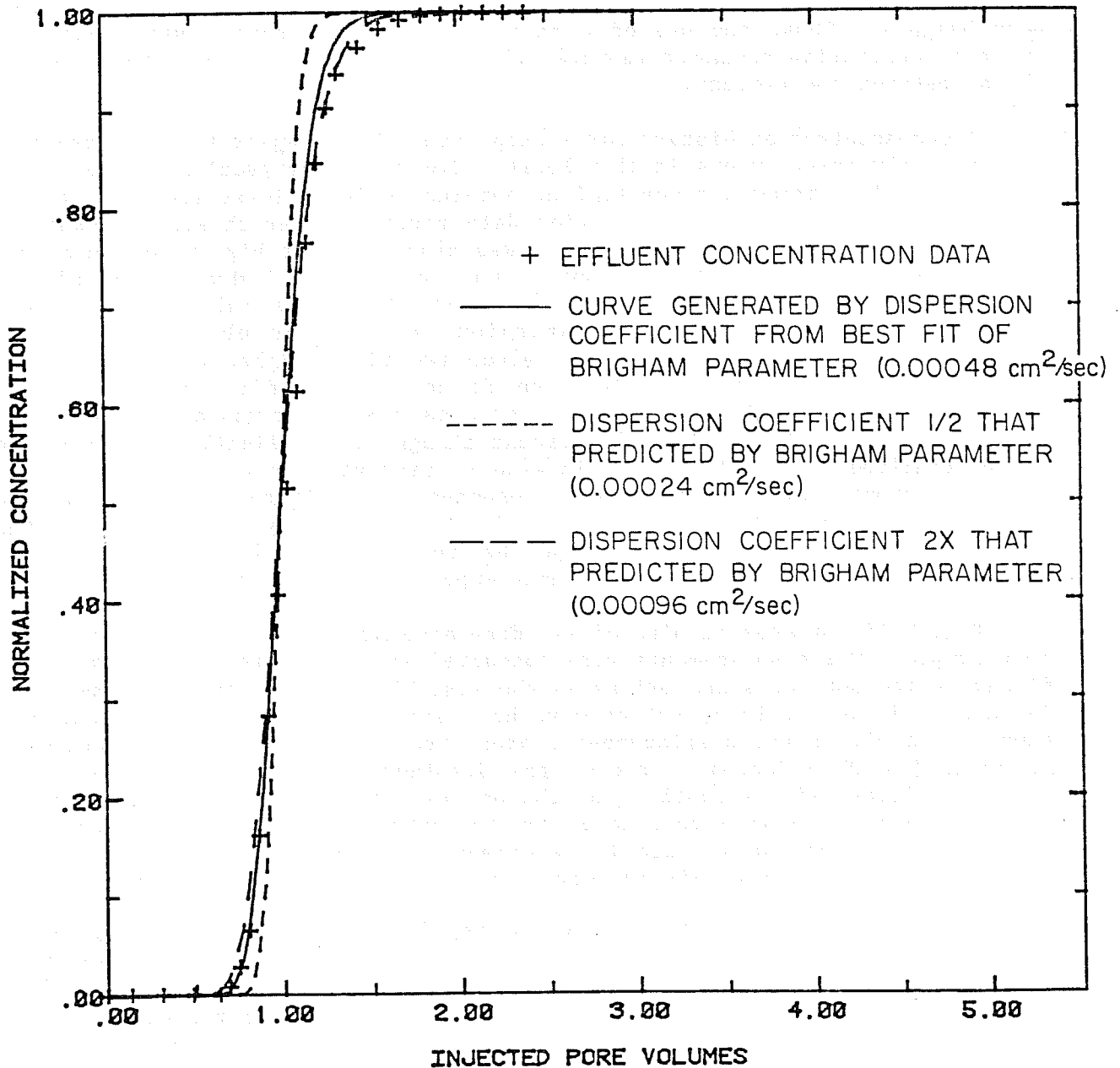


Fig. 2.17 Comparison of measured and calculated effluent concentration histories for a miscible displacement with a step input in a Berea sandstone core (Run 1).

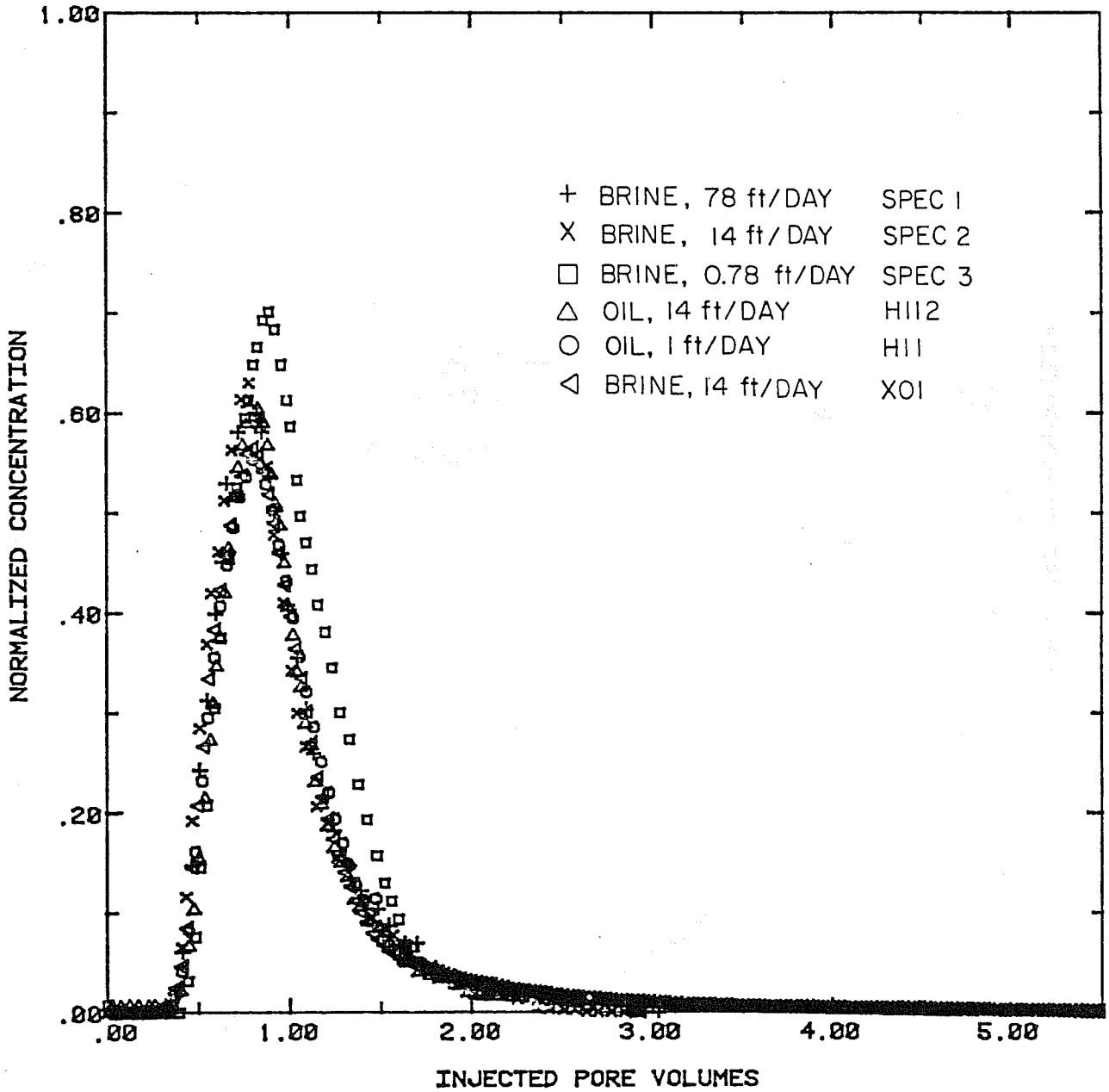


Fig. 2.18 Effluent concentration histories for miscible displacements in carbonate core H-1.

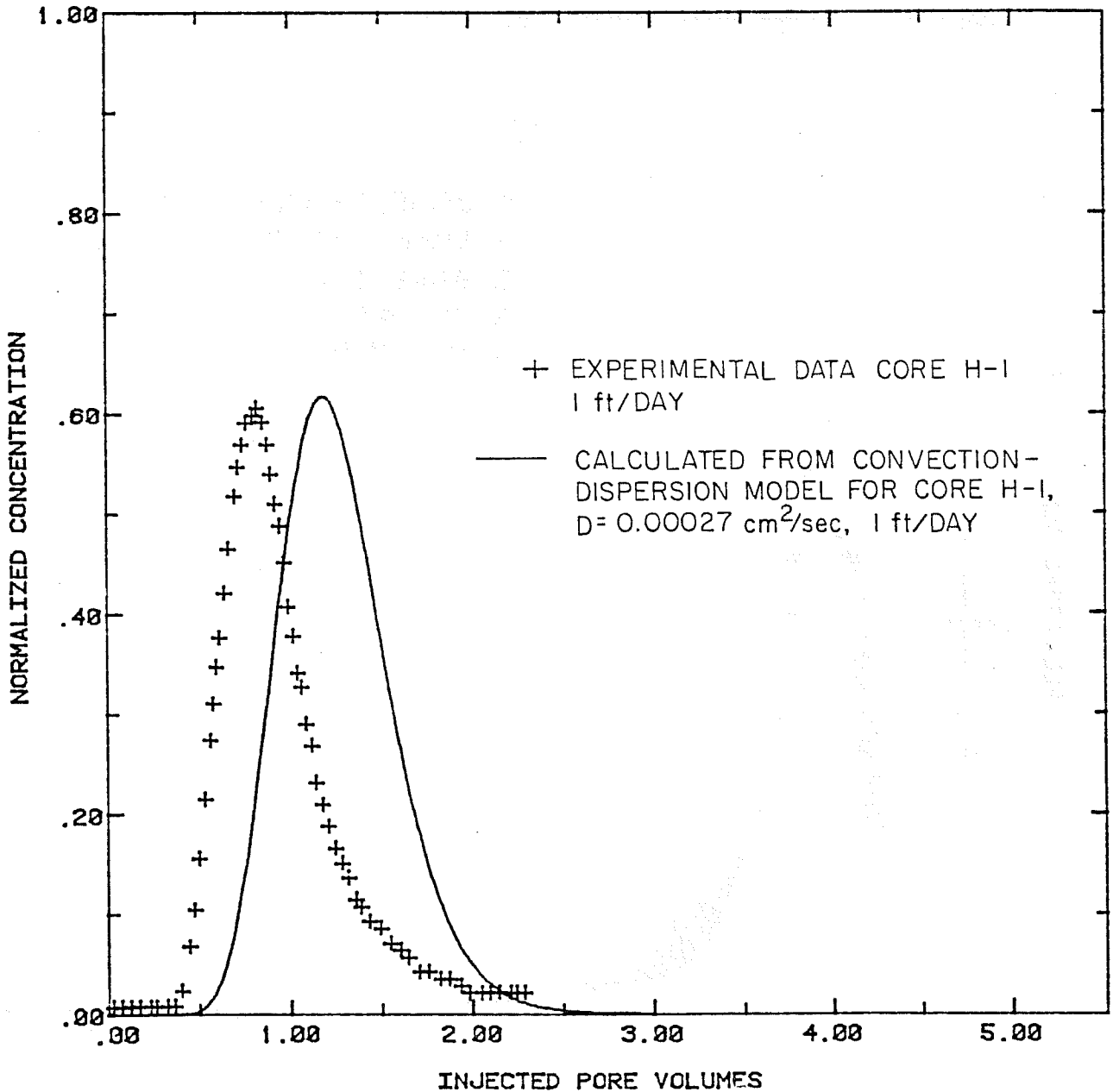


Fig. 2.19 Comparison of measured effluent concentrations from a San Andres carbonate core (Run 1) with those calculated using the convection-dispersion model.

of axial dispersion is ignored, but injected fluid can transfer to and from the stagnant volume. While Deans' model has the obvious limitation that it allows only plug flow, it illustrates clearly the difference in calculated composition history between convection-dispersion and mass transfer models. The model has the form

$$f \frac{\partial c}{\partial t} + v \frac{\partial c}{\partial x} + (1 - f) \frac{\partial c^*}{\partial t} = 0 \quad (2.1)$$

$$(1 - f) \frac{\partial c^*}{\partial t} = K (c - c^*)$$

where  $f$  is the flowing fraction,  $v$  the average interstitial velocity,  $c$  and  $c^*$  the volume fraction of injected fluid in the flowing and stagnant portions of the pore space,  $t$  the time, and  $K$  the mass transfer coefficient. With initial and boundary conditions

$$\begin{aligned} c &= c^* = 0 & t &= 0, \quad 0 \leq x \leq L \\ c &= 1, & 0 < t < \frac{\beta L}{v}, \quad x &= 0 \\ c &= 0, & t > \frac{\beta L}{v}, \quad x &= 0 \end{aligned} \quad (2.2)$$

where  $L$  is the length of the core and  $\beta$  is the size of the injected pulse in pore volumes, the solution is (Thomas 1944)

$$\begin{aligned} c &= 0 & z &< 0 \\ c &= 1 - e^{-z} \int_0^y e^{-t} I_0(2\sqrt{zt}) dt & 0 < z < z_0 \\ c &= e^{-(z-z_0)} \int_0^y e^{-t} I_0(2\sqrt{(z-z_0)t}) dt \dots \\ &\dots - e^{-z} \int_0^y e^{-t} I_0(2\sqrt{zt}) dt & z_0 < z \end{aligned} \quad (2.3)$$

where

$$z = \frac{af}{1-f} \left[ \frac{\tau}{f} - \frac{x}{L} \right]$$

$$y = \frac{ax}{L}$$

$$a = \frac{KL}{v}$$

$$\tau = \frac{vt}{L}$$

$$z_0 = \frac{a\beta}{1-f}$$

and  $I_0$  is a modified Bessel function of zero order.

Fig. 2.20 compares effluent compositions calculated for the carbonate core displacements with equation (2.3). The flowing fraction was arbitrarily chosen as  $f = 0.4$ , and the mass transfer coefficient ( $a = 0.8$ ) was selected to give a peak height close to that observed. It is apparent from Fig. 2.20 that Deans' two parameter ( $f, a$ ) model also fails to match accurately the shape of the effluent composition history. If the flowing fraction and mass transfer coefficient are adjusted to give an appropriate arrival time and height for the peak, the tail of the calculated peak is much too long. This occurs because the mass transfer coefficient is being used to adjust peak height. In the experiment, however, peak height is also influenced by dispersion. Thus, neglecting the effects of dispersion in the flowing stream leads to a choice of the mass transfer coefficient large enough to account partly for the effects of dispersion. That choice leads in turn to the exaggerated tail. Thus, it appears that a three parameter model (Coats & Smith 1964), which models dispersion in the flowing stream, is the least complex which has a chance to match the experimental observations. Indeed, the shapes of the effluent composition curves suggest a small mass transfer coefficient which would produce a long tail with low concentrations. Peak height would then be determined mainly by dispersion in the flowing stream, with the arrival time set by the flowing fraction.

In dimensionless form, the Coats-Smith model can be written

$$f \frac{\partial c}{\partial \tau} + (1-f) \frac{\partial c^*}{\partial \tau} + \frac{\partial c}{\partial \xi} - \frac{1}{Pe} \frac{\partial^2 c}{\partial \xi^2} = 0$$

(2.4)

$$(1-f) \frac{\partial c^*}{\partial \tau} = a(c - c^*)$$

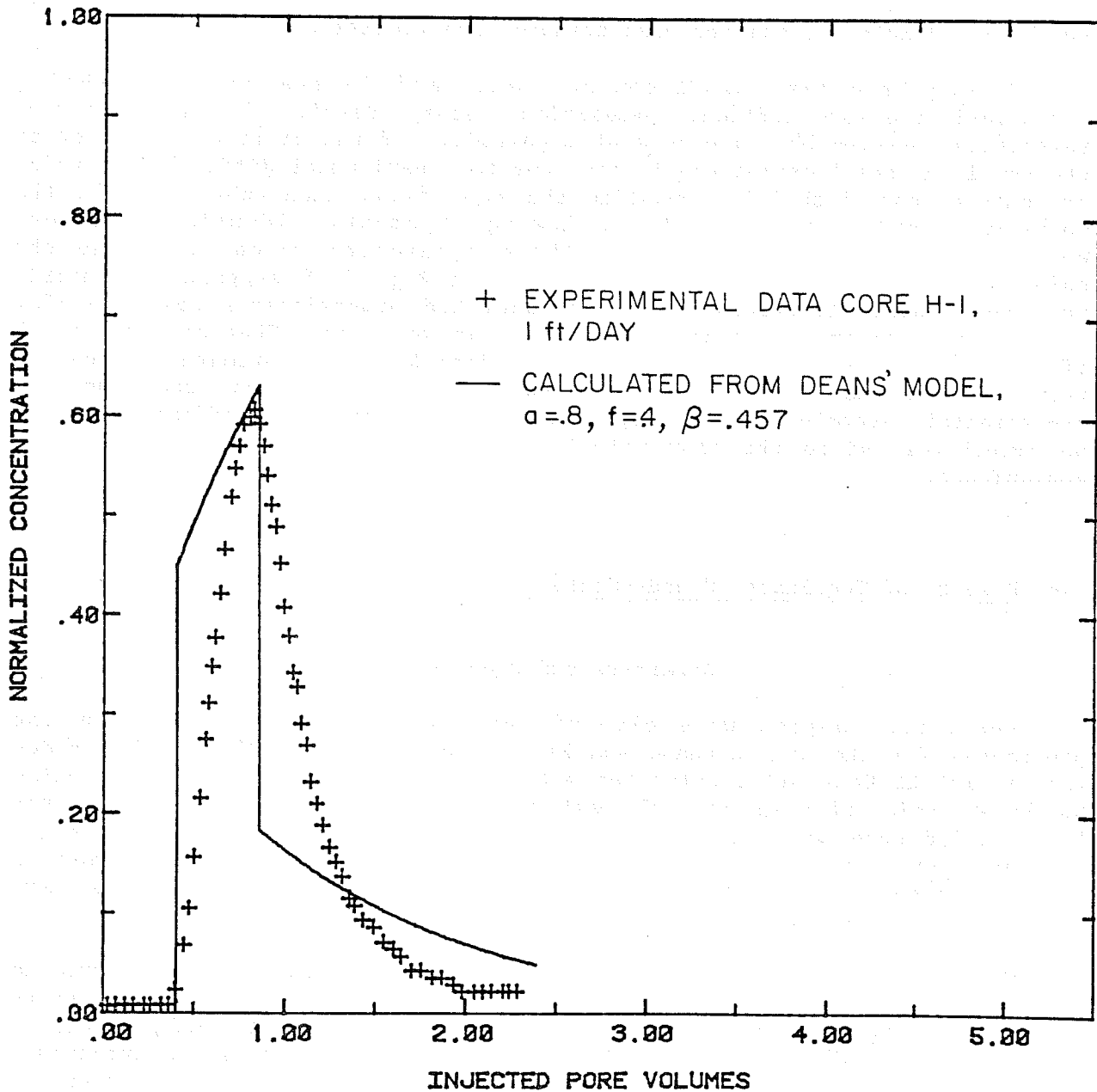


Fig. 2.20 Comparison of measured effluent concentrations from a San Andres carbonate core (Run 9) with those calculated using Deans' model.

where  $\xi = x/L$   
 $\tau = vt/L$   
 $a = KL/v$   
 $Pe = vL/D$

The three parameters which determine the solution are the flowing fraction  $f$ , the Peclet number  $Pe$ , and the mass transfer coefficient  $a$ .

Four of the five displacements performed in the H-1 core showed essentially the same effluent composition history, despite the fact that flow velocities differed by two orders of magnitude. If the different behavior of the remaining displacement was in fact due to experimental difficulties, which can only be established by repeating the experiment, then application of the Coats-Smith model leads to the following argument. Identical effluent compositions can only occur if the three parameters which determine the solution are the same. The results shown in Fig. 2.18 suggest, therefore, that the flowing fractions, Peclet numbers and dimensionless mass transfer coefficients remained constant with changes in velocity. That can only occur if the dispersion and mass transfer coefficient  $K$  are approximately linear in velocity. If such behavior were found to be true for most rock samples, experimental determination of dispersion and mass transfer coefficients would be simplified, since the flow velocity could be chosen for experimental convenience.

## 2.4 Results of Two-Phase, Steady-State Miscible Displacements

### Apparatus and Procedures

Reservoir samples were cleaned and prepared as described in the procedures for the single-phase samples. The cores were then filled under vacuum with 2% NaCl brine saturated with  $\text{CaSO}_4$  containing 0.01% sodium azide as an anti-microbial agent. To establish connate water saturation the brine-filled cores were then flooded with at least 100 pore volumes of ethyl benzene. Finally, the core was flooded with at least 100 pore volumes of brine to establish the residual oil saturation. All saturations were determined gravimetrically.

Once residual oil saturation was achieved, the cores were transferred to the core preparation apparatus to establish a secondary drainage, steady-state saturation. Fig. 2.21 is a schematic of that apparatus. Oil (ethyl benzene) and water (2% NaCl brine) are pumped simultaneously at constant fractional flow through the core. When the pressure drop across the core remains constant for an appropriate time period (usually 24 hours), steady-state saturation is assumed to have been reached.

The oil-water separator and reservoir (see Fig. 2.21) allows both fluids to be repeatedly circulated through the core without interrupting the operation or requiring large volumes of oil and brine. The 50 cc graduated cylinders allow the flow rate to be measured directly. The pulse dampening

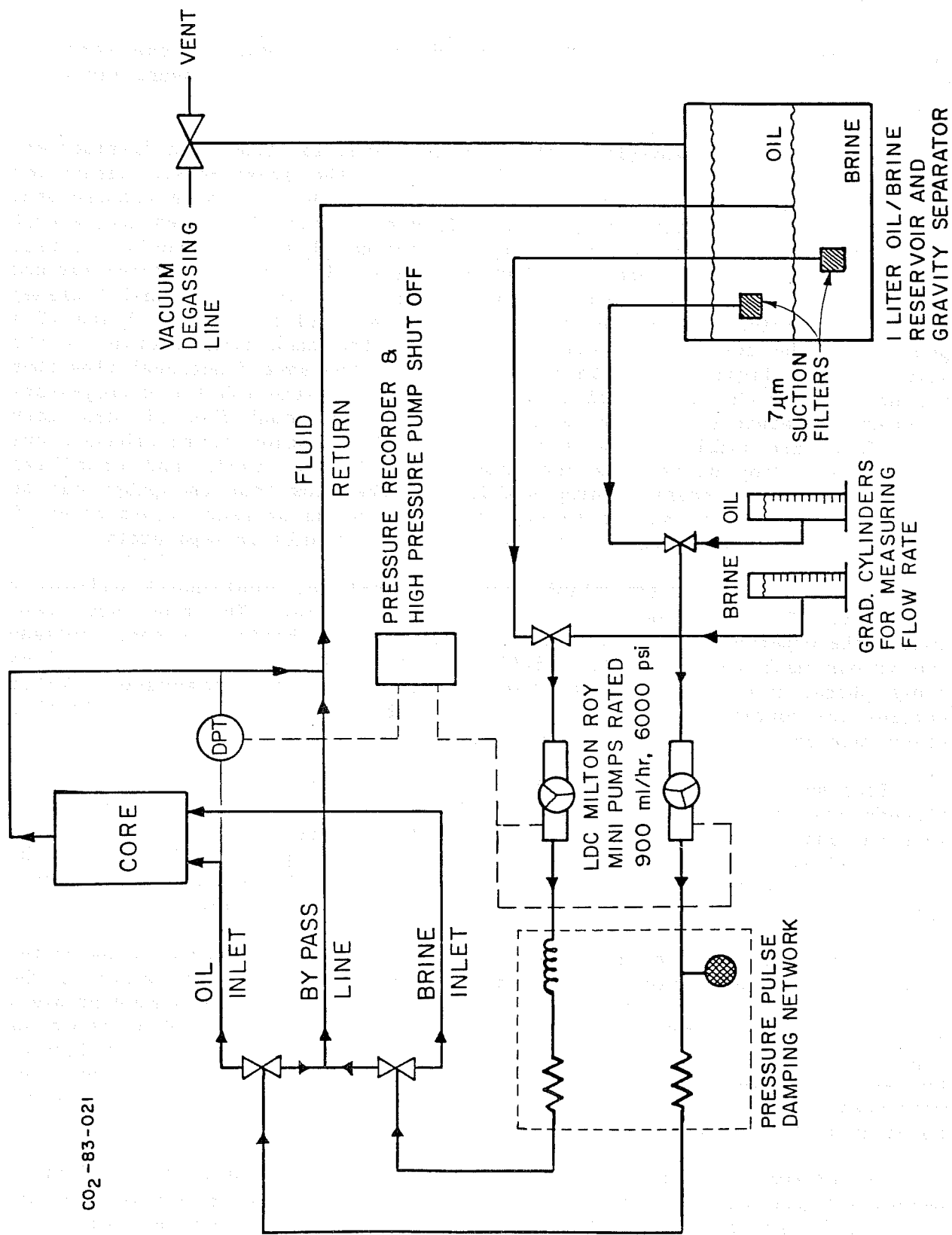


Fig. 2.21 Apparatus used to establish steady-state saturations of oil and water.

network limits the size of the pulse to the core due to the positive displacement pumps. At a 300 psi core inlet pressure, the pressure ripple is less than 5 psi.

Fig. 2.22 is a schematic of the apparatus used for two-phase displacement experiments with reservoir core samples. After the steady-state saturation has been established, the core is transferred to the two-phase displacement apparatus, which is similar to that used in single-phase displacements, except that both oil and brine displacements are conducted simultaneously. First, the oil and brine pulse loops are charged with an oil (ethyl butyrate) matched in viscosity and density to the oil used to saturate the core (ethyl benzene) and an NaCl brine (1%) differing in salt concentration from the brine (2%) present in the core. Both oil and brine of the same composition as the saturated core begin to flow through the core at the same fractional flow (but not necessarily the same total flow rate) used to establish the steady-state saturation. Since saturation is a function of fractional flow (if capillary end effects are small), there should be no redistribution of the phases, and the pressure drop across the core should establish itself and stabilize quickly. Once the pressure drop stabilizes, the flow from the pumps can be redirected through the sample loops, creating a pulse or slug displacement of each phase. The two phases can be pulsed simultaneously or separately.

Leaving the core, the fluids enter an on-line, continuous oil-water separator. Fig. 2.23 is a schematic of that device. The two-phase fluid enters the upper portion or chamber of a disk-shaped, horizontal space between two porous membranes which have different wetting behavior. Oil, the less dense phase, rises and contacts the upper, hydrophobic membrane. Water settles and contacts the lower, water-wet membrane. (Membranes used in this study were obtained from Gelman Sciences, Inc., Ann Arbor, MI.)

Because it is hydrophobic, the upper membrane will resist passing water through its pores but will readily admit the non-polar oil. The lower membrane can be wet by either oil or water, but if first wet by water, surface tension effects will prevent oil from entering the pores. Therefore, the first step in operating the separator is to prime it with water to establish a water-wet condition which must be maintained during operation.

Prior to assembly of the separator, the water-wet membrane is saturated using a vacuum to eliminate air from the pore spaces. After assembly, the separator is filled with water to the level of the vent of the siphon-breaker. Without the siphon-breaker, the weight of the water column extending below the separator will tend to pull air into the separator, possibly causing a loss of the water-wet condition. With the siphon-breaker, a few inches of positive water-head can be imposed on the water-wet membrane at all times, thus helping to maintain the water-wet condition.

The oil-water separator passes  $40 \text{ cm}^3/\text{hr}$  of both 2% NaCl brine and ethyl butyrate (combined flow rate of  $80 \text{ cm}^3/\text{hr}$ ) with a pressure differential of less than 69 kPa (10 psi). The volume of the oil-water separator (excluding the siphon-breaker tubing) is about  $0.2 \text{ cm}^3$ .

Because a flowing stream of oil and water can be separated continuously

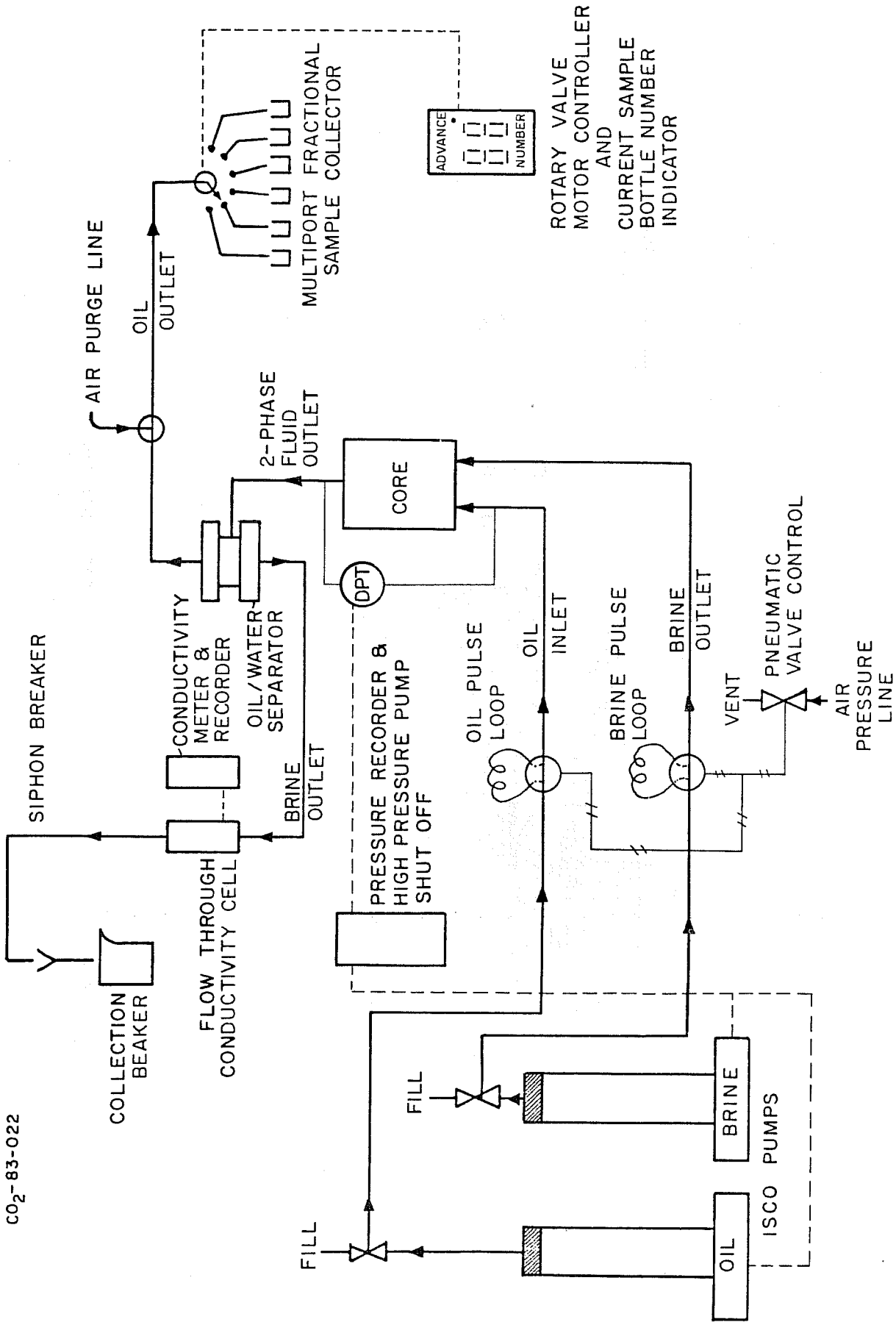


Fig. 2.22 Two-phase displacement apparatus.

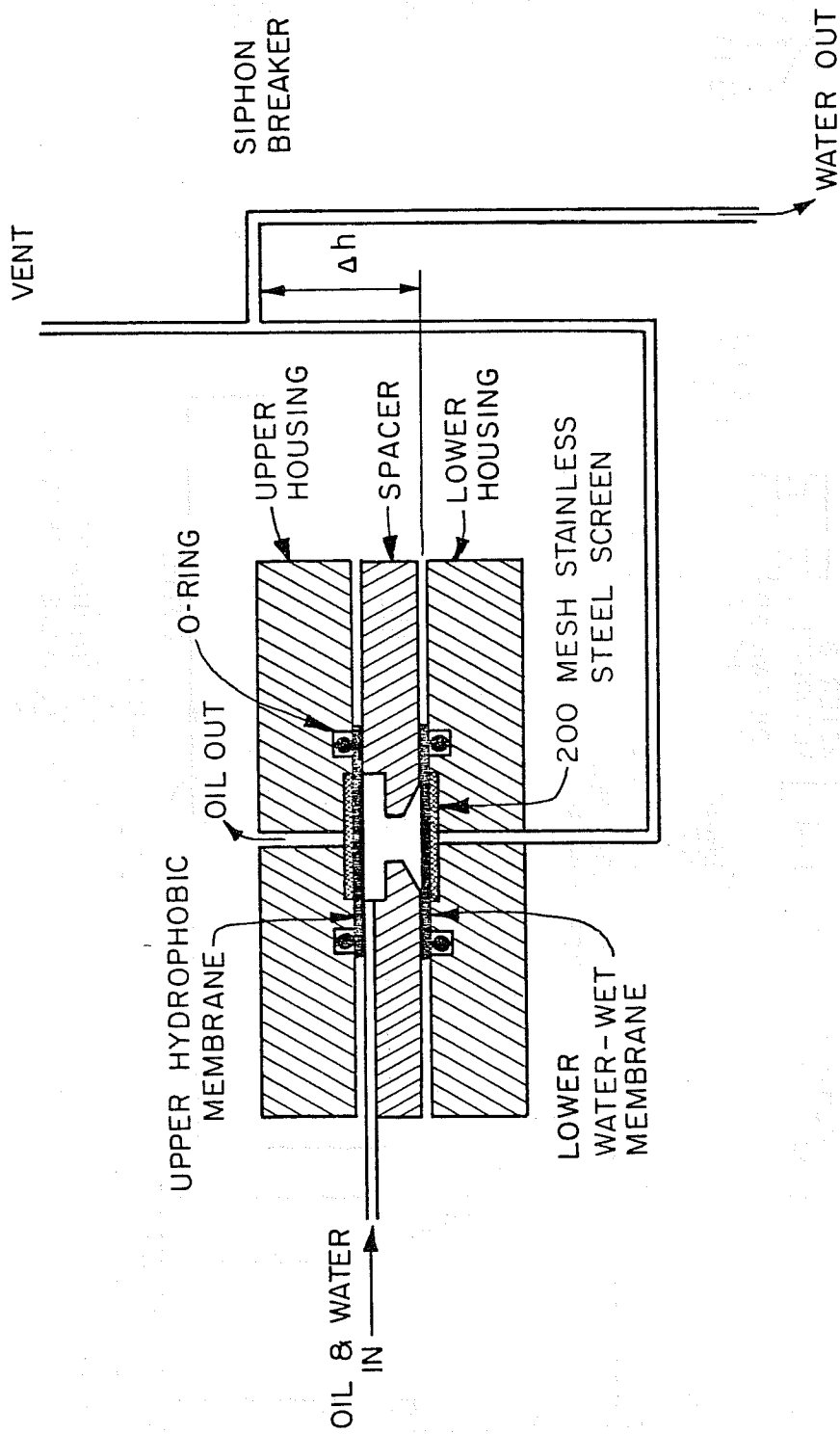


Fig. 2.23 Schematic of the oil-water separator.

without a large volume mixing chamber, it is possible to measure the composition of each phase continuously and on-line. As shown in Fig. 2.22, the brine coming out of the oil-water separator flows to a  $0.3 \text{ cm}^3$  conductivity cell, the output of which is recorded on a strip chart recorder for later digitizing and analysis. In the future, these data will be recorded directly, using an on-line computer and an analog-to-digital converter.

The oil phase flows out of the oil-water separator to a multiport sample collector for later GC analysis. A refractometer which will measure oil composition continuously and on-line will be installed to complete the automation of data collection for this experiment.

### Results and Discussion

Effluent compositions for the oil phase are given in Fig. 2.24 for three two-phase displacements in the Berea core performed at an average interstitial velocity of 12 ft/day. Oil fractional flows were 0.3, 0.5 and 0.75 in the three displacements. In each displacement, an oil pulse of  $5 \text{ cm}^3$  was injected. The oil saturations were .589, .601 and .590, respectively. Fig. 2.25, which compares fractional flows observed here with those calculated from Salter & Mohanty's data for their Berea core, shows that the small changes in saturation with substantial changes in fractional flow were reasonable.

Differences in the performance of the three displacements were also small, since the oil saturations differed only slightly. In all three displacements, injected oil appeared in the effluent at much less than one oil pore volume injected, clear indication that the high water saturation had substantially reduced the fraction of the oil pore space available to the flowing stream. As can be seen from Fig. 2.24, the 50% concentration appeared in all three displacements at approximately 0.3 oil pore volumes injected, in good agreement with the results of Salter & Mohanty (1982), who reported a flowing fraction of 0.3 at an oil saturation of 0.4 in their Berea core. Thus, it appears that the experimental technique in use produces observations consistent with those reported previously.

Fig. 2.26 reports effluent compositions in the brine phase for the displacement at  $f_o = 0.75$  described above. A pulse of  $5 \text{ cm}^3$  of brine was injected. The character of the displacement in the brine phase was quite different from that observed for the oil phase. Breakthrough of injected fluid was much later, at 0.6 brine pore volumes injected. The 50% concentration appeared at 0.72 brine pore volumes injected. Hence, an estimate of the flowing fraction in the brine phase is 0.72 in good agreement with the value of 0.76 reported by Salter & Mohanty. The relatively long concentration tail is consistent with the idea that the brine phase remains connected to the flowing pore volume, but a significant dendritic pore volume exists when water is present (Salter & Mohanty 1982).

The results presented here confirm that the distribution of phases in the pore space can substantially alter mixing between injected and in-place fluid. The remaining challenge is to establish the range of such behavior which may be expected for reservoir cores and to understand how changes in mixing behavior alter the impact of phase behavior on displacement performance.

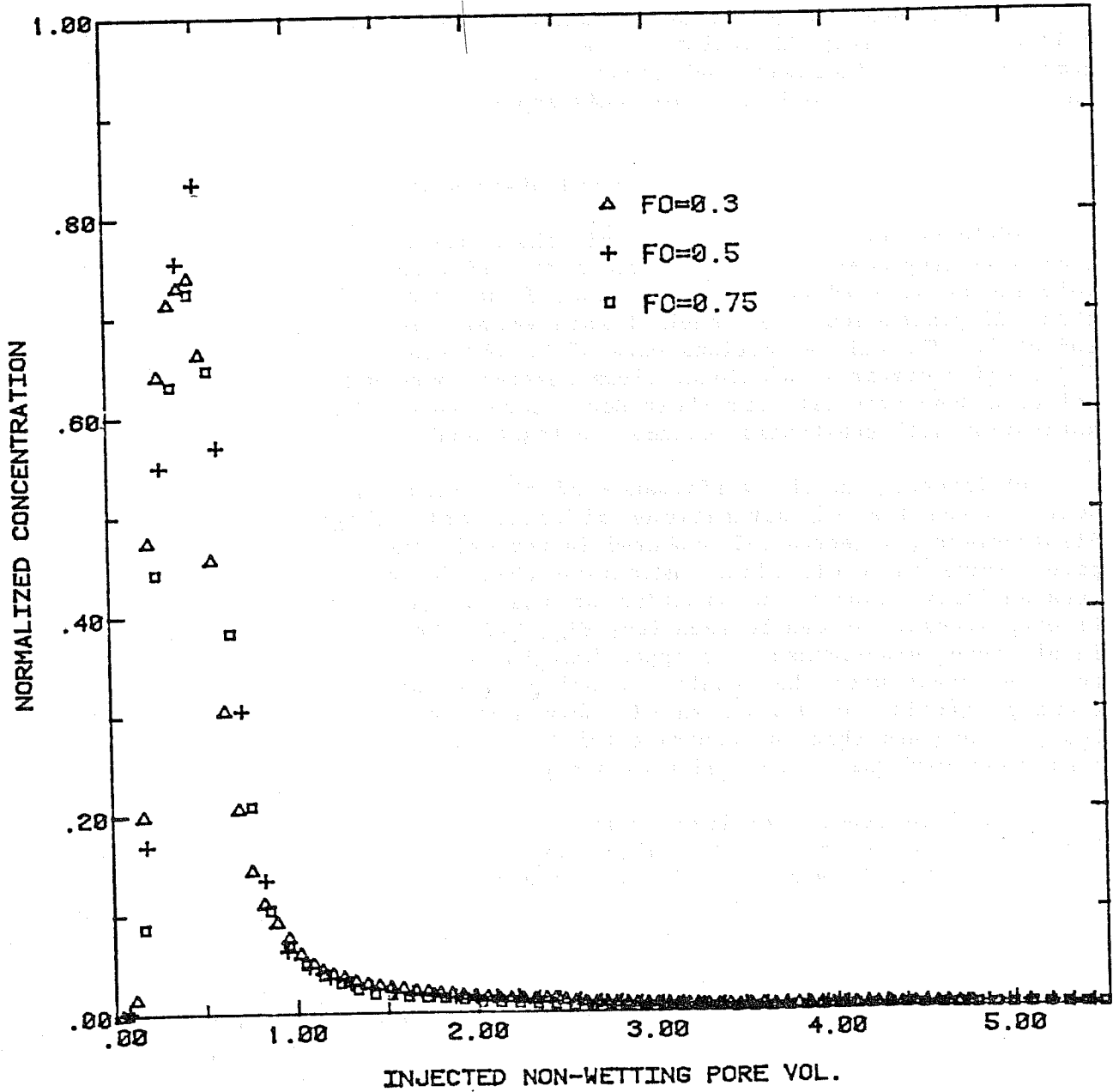


Fig. 2.24 Effluent oil concentration histories at three oil fractional flows in a Berea sandstone core (B-1).

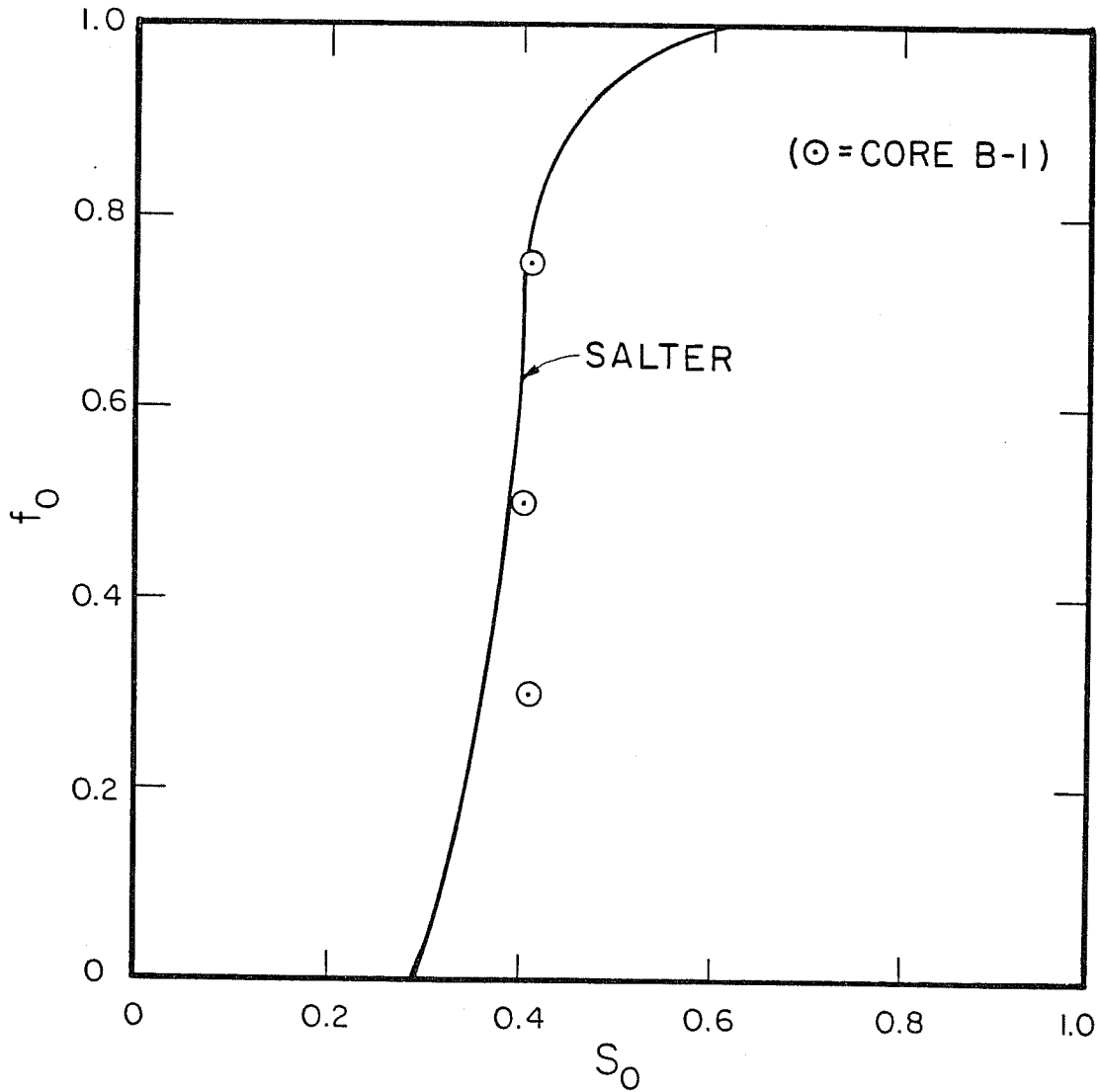


Fig. 2.25 Comparison of a Berea sandstone oil fractional flow curve reported by Salter & Mohanty (1982) with that obtained here for core B-1.

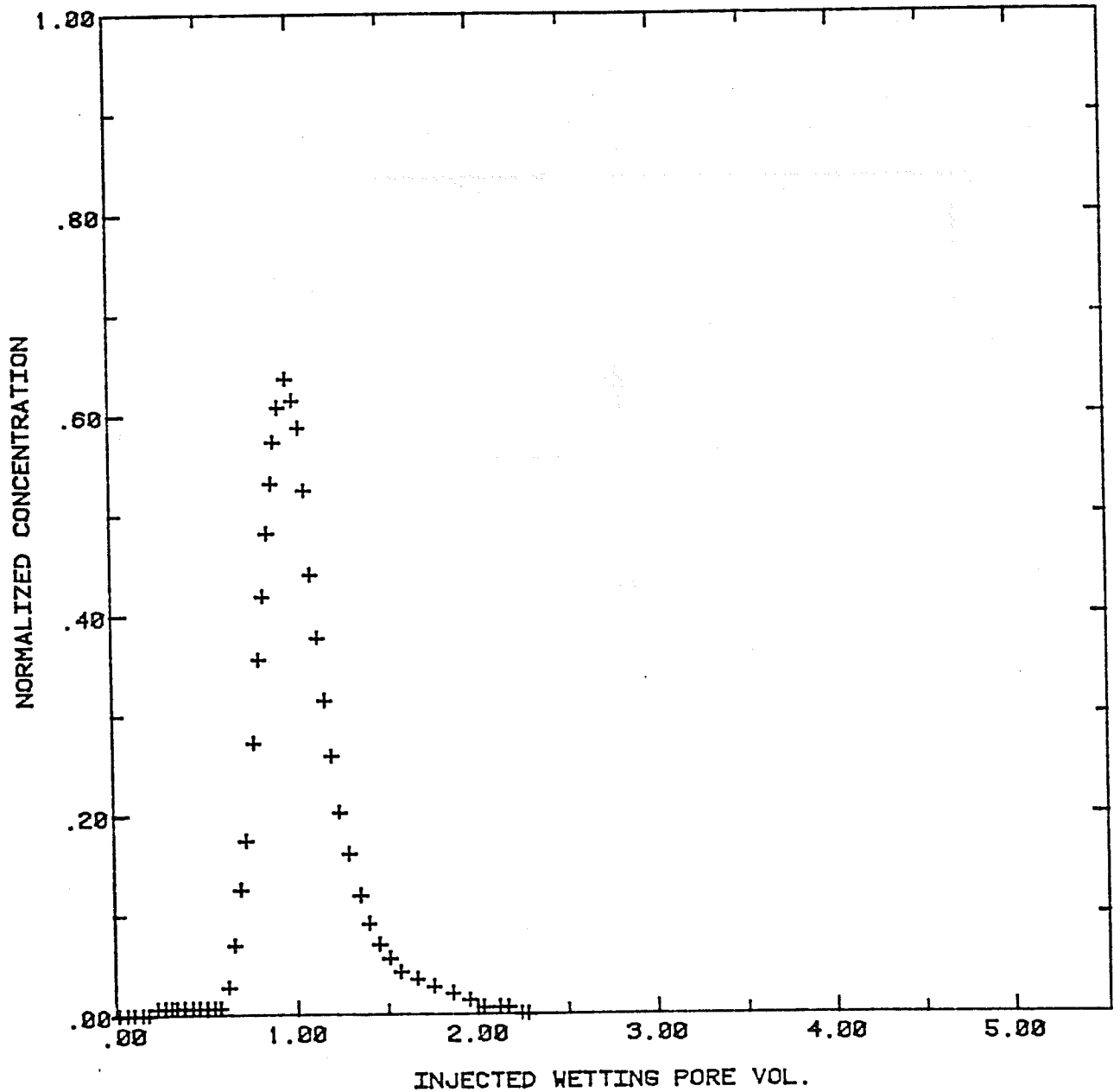


Fig. 2.26 Effluent concentration history for the wetting (brine) phase during a two-phase, steady-state displacement in a Berea sandstone core (B-1).

## 2.5 Conclusions

In §2, the results of parallel experimental investigations of the effects of water saturations on displacement efficiency of both first-contact and multiple-contact miscible displacements are reported. Those investigations yield the following observations and conclusions:

- (1) The design apparatus described for visual observation of CO<sub>2</sub> displacements in glass pore networks is an effective tool for demonstrating flow mechanisms which affect the performance of a CO<sub>2</sub> flood.
- (2) A stable, first-contact miscible displacement of one refined oil by another required 1.15 PV of injection to recover all of the original oil in place from a pore network. Displacement of the same oil by CO<sub>2</sub>, also a first-contact miscible flood, required 1.31 PV to recover all of the oil, because viscous fingering reduced sweep efficiency. In a multicontact miscible displacement of a crude oil by CO<sub>2</sub>, a small residual oil saturation was left behind, and two-phase flow occurred behind the CO<sub>2</sub> front, as predicted by theoretical investigations of the effects of dispersion and viscous fingering (Gardner, Orr & Patel 1981; Gardner & Ypma 1982). Recovery was complete in the crude oil displacement at 1.12 PV injected. Direct observations indicated that the flow length required to develop miscibility was short compared to the length of the model.
- (3) Stable tertiary miscible displacements of one refined oil by another recovered oil much more slowly than secondary displacements with the same fluids, because relatively little of the oil recovered was displaced ahead of the injected fluid. Solvent broke through at the same time oil production started. Most of the oil was recovered by diffusion from ganglia given the shape of dendritic pores by surrounding water. Significant portions of the residual oil present at the start of the tertiary flood remained isolated by water and inaccessible to injected fluid.
- (4) While CO<sub>2</sub> displaced water inefficiently in a tertiary CO<sub>2</sub> flood of a refined oil, it contacted trapped oil by diffusion through the water into the oil. CO<sub>2</sub> displaced crude oil more effectively than it did the refined oil for reasons which are not yet known.
- (5) Improvements to the design of equipment for one- and two-phase displacements in reservoir cores which permit on-line measurements of brine and eventually, oil composition, improve the efficiency of measurements of miscible displacement behavior in reservoir cores. A new device, a continuous oil-water separator of low dead volume was developed to make such measurements possible.

- (6) Single-phase displacements in a Berea sandstone core demonstrated that on-line measurements of brine compositions produce results consistent with those obtained by measurement of oil compositions by chromatography. Those experiments, which yielded dispersion coefficients similar to those reported by other investigators, validated the experimental technique.
- (7) Single-phase displacements in a San Andres dolomite reservoir core clearly demonstrated the effects of pore structure heterogeneity on mixing of injected fluid with that originally in place in the core. Calculations with convection-dispersion and convection-capacitance models suggested that at a minimum, a three parameter model which includes effects of convection, dispersion and capacitance will be required to produce an acceptable match of core flood data.
- (8) Two-phase displacements in a Berea sandstone core showed the impact of a high water saturation on mixing of injected solvent with oil in place. Solvent broke through very early, indicating a low flowing fraction in the oil phase. In the water phase, the flowing fraction was much higher. Good agreement between the experimental observations and those of Salter & Mohanty (1982) suggests that the experimental technique is valid.

### 3. SUPPORTING MEASUREMENTS: PHASE BEHAVIOR AND FLUID PROPERTIES OF CO<sub>2</sub>-CRUDE OIL MIXTURES

Detailed interpretation of flow measurements in which CO<sub>2</sub> displaces crude oil requires independent measurements of the compositions and properties of phases which develop as CO<sub>2</sub> mixes with the oil and water present in the porous medium. For an example of this sort of detailed interpretation for a set of four slim tube displacements, see §4.1. In this section, we report results of single contact PVT experiments for three oils, Wasson stock tank oil, and two recombined oils made with the same dead oil, and 312 and 602 SCF/BBL solution gas. Mixtures of each oil with CO<sub>2</sub> were studied at three temperatures: 90, 105 and 120°F. Those results provide additional confirmation that a CO<sub>2</sub>-rich phase extracts hydrocarbons effectively if the density of CO<sub>2</sub> is high. Furthermore, they suggest a very simple correlation for minimum miscibility pressure in low temperature systems.

Also reported in this section are details of the further development of the continuous multiple contact (CMC) experiment. Minor modifications to the circulation system and major improvements in the control and data acquisition equipment are described. Progress on the development of equipment for measurement of phase viscosities using an oscillating quartz crystal is also reported. Finally, results of CMC measurements to investigate the roles of crude oil composition in determining CO<sub>2</sub>-crude oil phase behavior are given.

#### 3.1 Interpretation of Single Contact PVT Experiments

In a recent paper, Orr and Jensen (1982) reviewed the qualitative behavior of two well-characterized ternary systems, CO<sub>2</sub>-C<sub>1</sub>-C<sub>16</sub> and CO<sub>2</sub>-C<sub>3</sub>-C<sub>16</sub> and concluded that liquid-liquid and liquid-liquid-vapor behavior in CO<sub>2</sub>-crude oil systems is very similar to that of the simpler ternary systems. In this section, we summarize experimental results, also reported in that paper, which show that in low temperature systems, there is some pressure at which the density of the CO<sub>2</sub>-rich phase increases sharply. In addition, we show that the pressure can be estimated easily if the temperature is below about 120°F and that it is a reasonable estimate of the minimum miscibility pressure.

A series of single contact phase behavior experiments was performed with crude oil from the Wasson field (Gaines and Yoakum Counties, Texas). The composition of the oil, determined by gas chromatography (Orr & Taber 1982) is given in Table 3.1, along with the composition of gas added to it. Calculated compositions of two recombined oil mixtures, one containing 312 SCF/BBL and the other 602 SCF/BBL, are also given in Table 3.1. Pressure composition (P-X) phase diagrams were determined for the dead oil and the two recombined oils at three temperatures: 90, 105 and 120°F (32, 41 and 49°C). Results of those experiments are given in Figs. 3.1-3.3.

In Fig. 3.1, the phase behavior of mixtures of CO<sub>2</sub> with the dead oil

Table 3.1 Compositions of Gas, Oil and Recombined Fluids

	<u>Gas</u>	<u>Oil</u>	<u>Oil</u> <u>+ 312 SCF/BBL</u>	<u>Oil</u> <u>+ 602 SCF/BBL</u>
C1	57.36	-	21.33	53.03
C2	19.89	-	7.39	18.39
C3	16.29	-	6.05	15.06
C4	6.46	-	2.41	5.98
C5	-	5.48	3.44	0.41
C6	-	5.37	3.37	0.40
C7	-	7.40	4.65	0.56
C8	-	12.45	7.82	0.94
C9	-	8.71	5.46	0.66
C10	-	6.39	4.02	0.48
C11	-	4.59	2.88	0.34
C12	-	4.63	2.91	0.35
C13	-	3.89	2.44	0.29
C14	-	3.58	2.25	0.27
C15	-	2.84	1.79	0.22
C16	-	2.58	1.62	0.19
C17	-	2.53	1.59	0.19
C18	-	1.79	1.12	0.13
C19	-	2.19	1.37	0.16
C20	-	1.53	0.96	0.11
C21	-	1.43	0.89	0.10
C22	-	1.35	0.85	0.10
C23	-	1.24	0.78	0.10
C24	-	1.14	0.72	0.09
C25	-	1.07	0.67	0.08
C26	-	1.02	0.64	0.07
C27	-	0.66	0.41	0.05
C28	-	0.93	0.59	0.07
C29	-	0.62	0.39	0.04
C30	-	0.60	0.38	0.04
C31	-	0.59	0.37	0.04
C32	-	0.82	0.51	0.06
C33	-	0.45	0.28	0.04
C34	-	0.41	0.26	0.03
C35	-	0.52	0.33	0.04
C36	-	0.29	0.19	0.02
C37+	-	10.92	6.86	0.84
	<u>100.00</u>	<u>100.01</u>	<u>99.99</u>	<u>99.97</u>

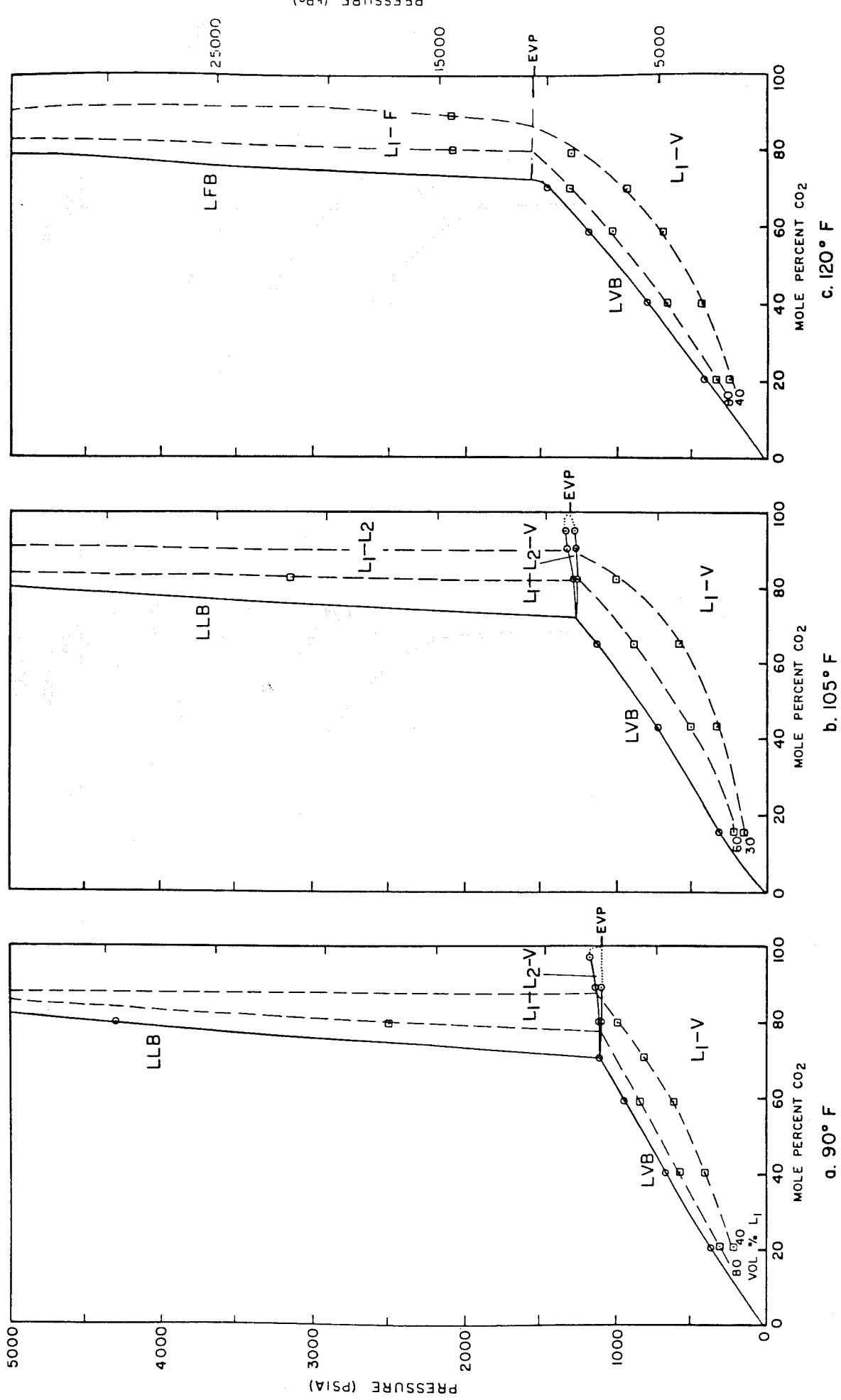


Fig. 3.1 P-X diagrams for mixtures of CO<sub>2</sub> with Wasson oil.

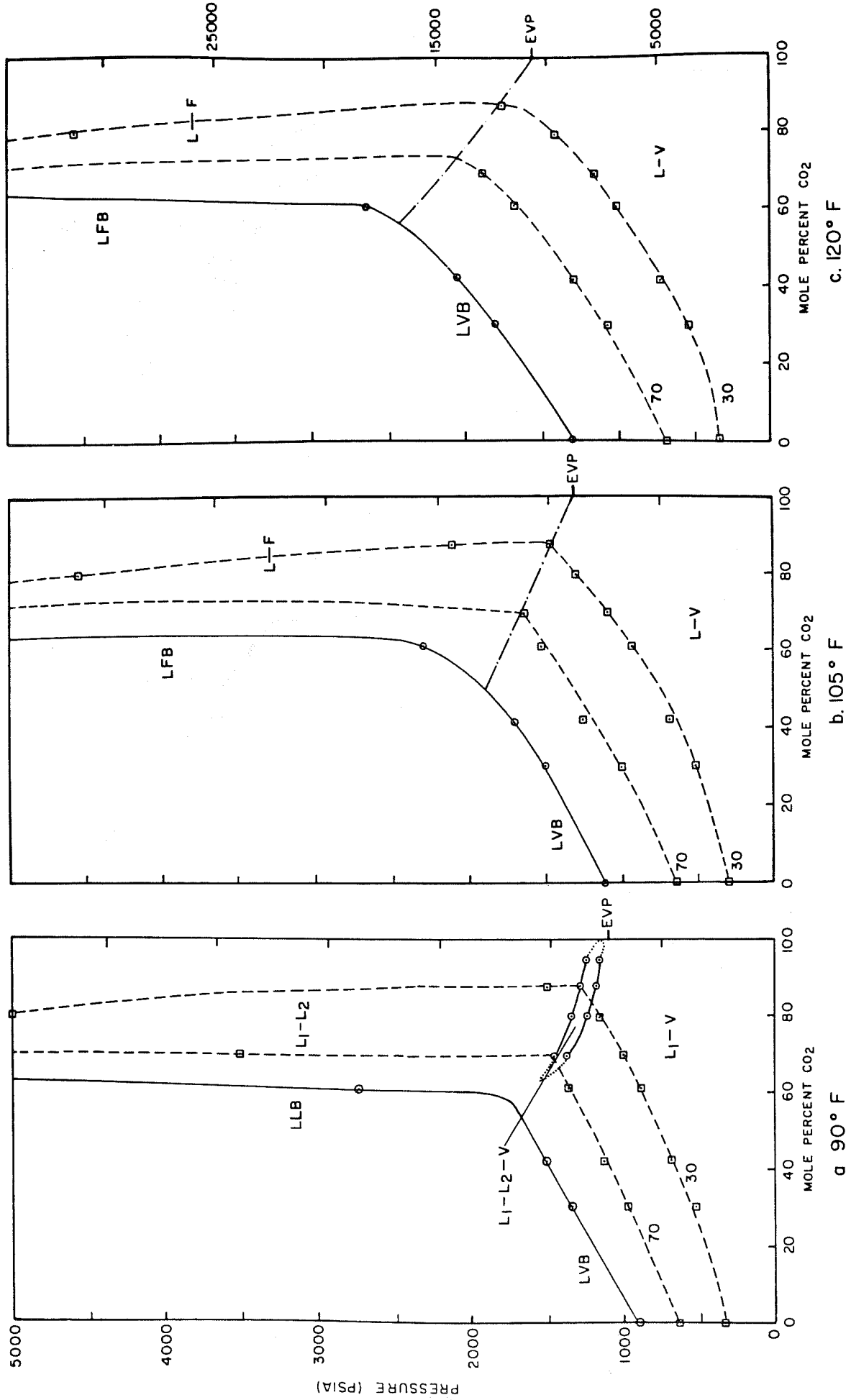


Fig. 3.2 P-X diagrams for mixtures of CO<sub>2</sub> with a recombined Wasson oil containing 312 SCF/BBL.

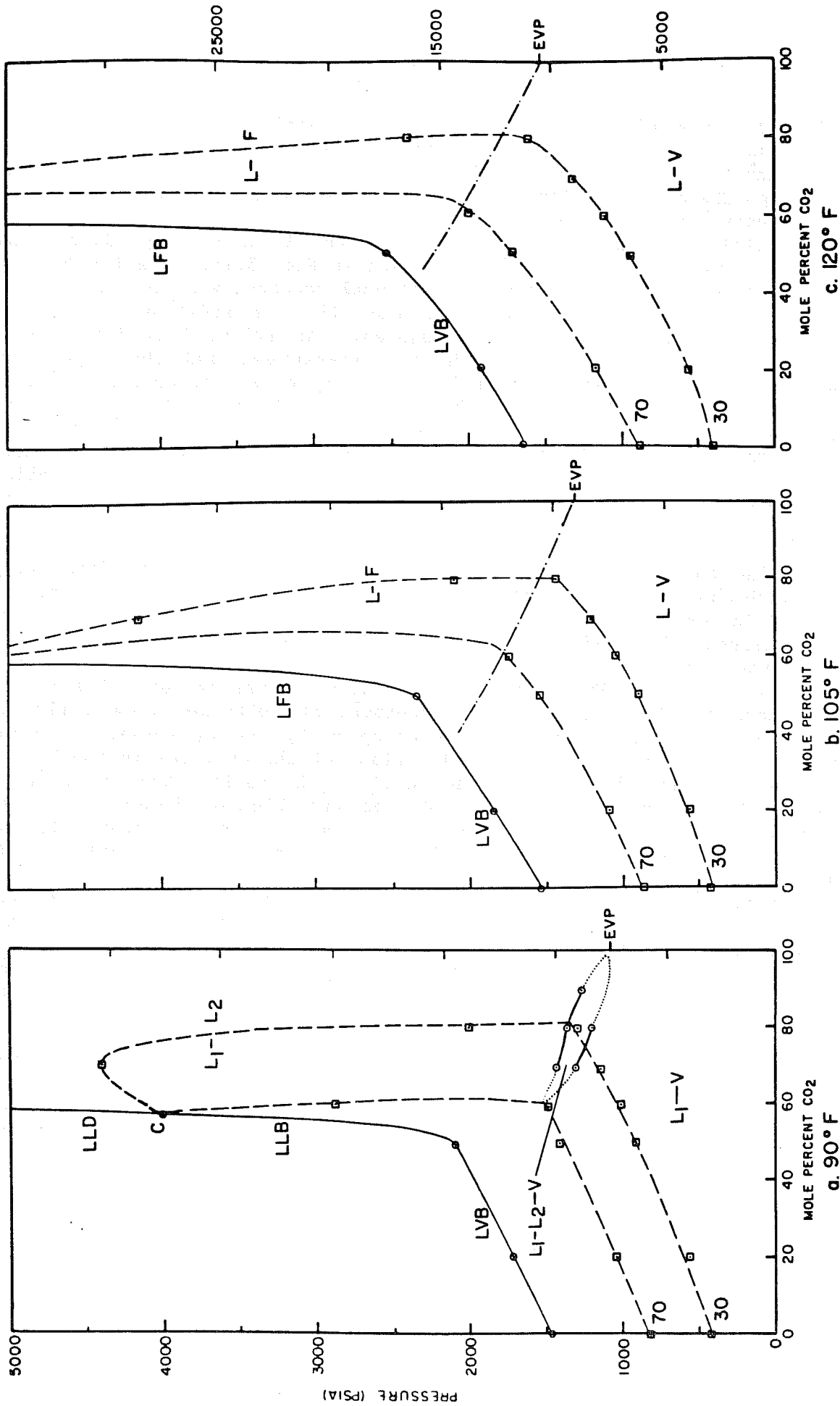


Fig. 3.3 P-X diagrams for mixtures of CO<sub>2</sub> with a recombined Wasson oil containing 602 SCF/BBL.

alone is compared. At 90°F, liquid-vapor bubble points (LVB) were observed for CO<sub>2</sub> concentrations up to about 70 mole percent. At higher CO<sub>2</sub> concentrations, a three-phase (L<sub>1</sub>-L<sub>2</sub>-V) region appeared. At high pressures and high CO<sub>2</sub> concentrations, two liquid phases were present in the cell. The only phase transition observed in the L<sub>1</sub>-L<sub>2</sub> region was a liquid-liquid bubble point (LLB). Hence, no critical point is shown in Fig. 3.1a. Similar behavior was observed at 105°F, as shown in Fig. 3.1b. The L-V bubble point pressure curve shifted upward as additional pressure was required to force the more volatile CO<sub>2</sub> into solution in the oil. In addition, the three-phase region also shifted to higher pressures. At 120°F, Fig. 3.1c, the bubble point curve shifted to still higher pressures, and the L<sub>1</sub>-L<sub>2</sub>-V region disappeared. One mixture, containing 80.1 mole percent CO<sub>2</sub>, was investigated at 115°F (46°C). That mixture did form three phases. Thus, it appears that the maximum temperature for the formation of three phases was between 115 and 120°F for this oil. In Fig. 3.1c, the upper phase at high CO<sub>2</sub> concentrations and high pressures is a dense supercritical phase (F). The L-F bubble point pressures (LFB) increased sharply when the CO<sub>2</sub> concentration reached about 70 mol percent.

Also shown in Fig. 3.1 are contours of constant volume fraction of the oil-rich (L<sub>1</sub>) phase, normally the lowest in the cell. For one mixture containing 89.5 percent CO<sub>2</sub>, however, a phase inversion was observed at 90°F. At pressures above 5800 psia (40,000 kPa), the CO<sub>2</sub>-rich (L<sub>2</sub>) liquid phase, dark orange in color, appeared at the bottom of the cell with the black L<sub>1</sub> phase at the top. Below 5800 psia the L<sub>2</sub> phase was on top. The approximate locations of the volume fraction contours are obtained from a plot of the fraction of the total cell volume occupied by the L<sub>1</sub> phase, an example of which is shown in Fig. 3.4. The locations of the contours in the L<sub>1</sub>-V region are well-defined, but are less so in the L<sub>1</sub>-L<sub>2</sub> region above about 1100 psia (7580 kPa), because the volumes of the two liquid phases are much less sensitive to changes in pressure. Thus, the contours are nearly vertical in the L<sub>1</sub>-L<sub>2</sub> region. Even at 120°F (Fig. 3.1c), the contours climb very steeply at high CO<sub>2</sub> concentrations and high pressures even though the sharp distinction between L<sub>1</sub>-L<sub>2</sub>, L<sub>1</sub>-V separations has disappeared. The pressure at which the volume fraction contours climb steeply (easily identified from plots like Fig. 3.1) indicates the pressure required to force the CO<sub>2</sub>-rich L<sub>2</sub> phase to be a dense, relatively incompressible phase. The locus of pressures at which the L<sub>2</sub> phase became less compressible is shown as an almost horizontal dashed line in Fig. 3.1c.

P-X diagrams for mixtures of CO<sub>2</sub> with a recombined oil containing 312 SFC/BBL are shown in Fig. 3.2. At all three temperatures, the multiphase region was significantly larger than it was for the dead oil. Only at 90°F did an L<sub>1</sub>-L<sub>2</sub>-V region appear. The L<sub>1</sub>-L<sub>2</sub>-V region sloped to lower pressures with increasing CO<sub>2</sub> concentration, and hence, the behavior of this system was similar to that described by Orr & Jensen (1982) for the CO<sub>2</sub>-C<sub>1</sub>-C<sub>16</sub> system. At 90°F, the L<sub>1</sub>-L<sub>2</sub>-V region was clearly separated from the bubble point curve. A mixture containing 61.5 mole percent CO<sub>2</sub> exhibited a liquid-dense phase bubble point at 2750 psia (18960 kPa) but did not form three phases at any lower pressure. Mixtures containing 69.9, 80.0, 87.8 and 95.0 mole percent CO<sub>2</sub>, however, did form three phases.

CO<sub>2</sub>-82-057

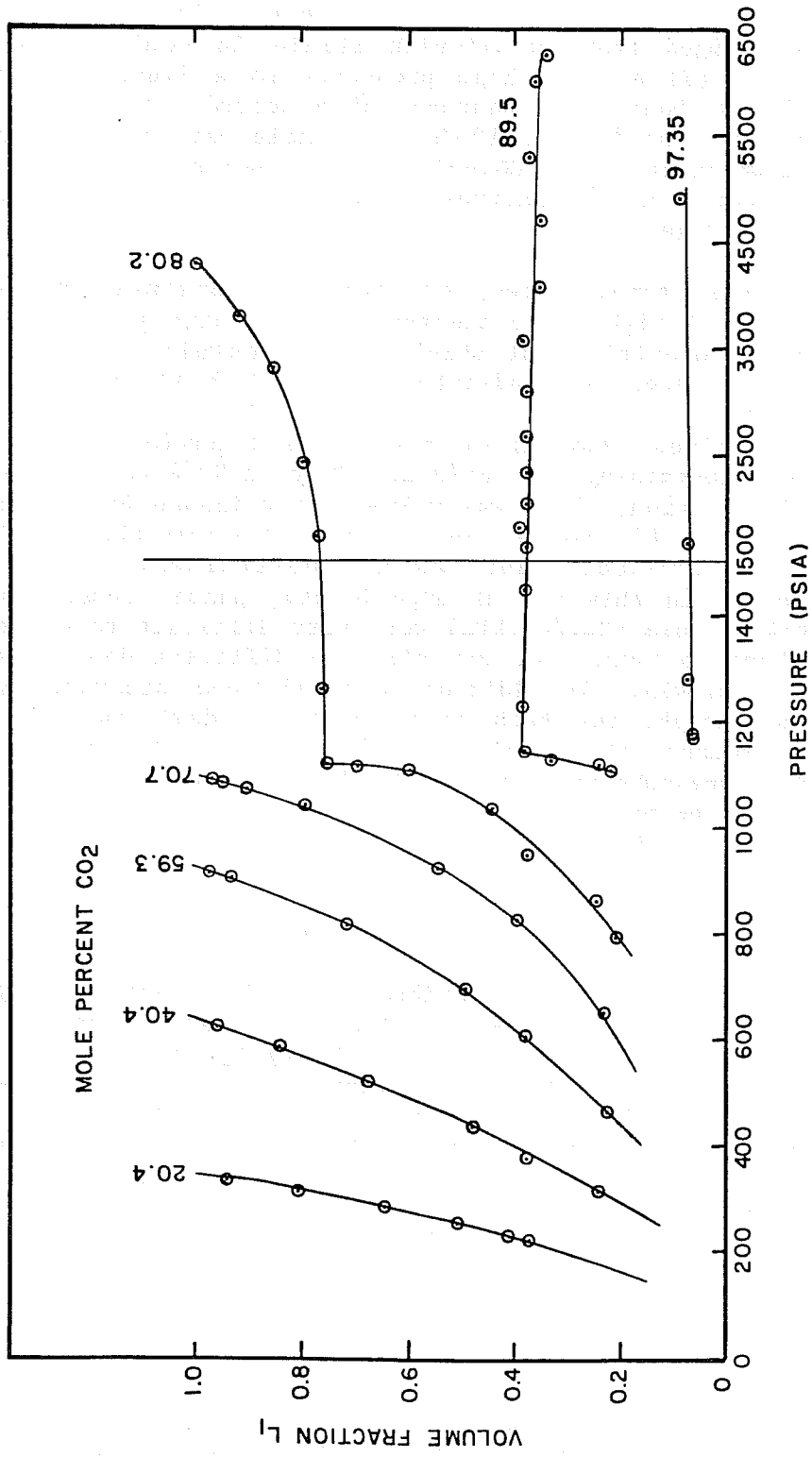


Fig. 3.4 Typical phase volume data for mixtures of CO<sub>2</sub> with Wasson oil at 90°F (32°C).

At 105 and 120°F, no three-phase region was observed. Evidently, the addition of gas to an oil reduces the maximum temperature at which three phases can form. In both cases, mixtures containing more than about 60 mole percent CO<sub>2</sub> changed from an oil-rich liquid in equilibrium with a dense CO<sub>2</sub>-rich liquid (F) at very high pressures to a liquid and a vapor at low pressures, but without the appearance of a second interface. The saturation pressures observed at 105 and 120°F at 60 mole percent CO<sub>2</sub> were bubble point pressures at which the dense CO<sub>2</sub>-rich phase appeared at the top of the cell as the pressure was reduced. Saturation pressures of this type are labeled LFB in Figs. 3.1, 3.2 and 3.3.

At all three temperatures, contours of constant volume fraction L<sub>1</sub> climbed steeply at high CO<sub>2</sub> concentrations and high pressures. The loci of pressures and compositions at which the compressibility of the two-phase mixture dropped sharply are indicated in Fig. 3.2b and c.

Fig. 3.3 gives results of the phase behavior experiments for the recombined oil containing 602 SFC/BBL. Only at 90°F was a three-phase region observed. In addition, there was volumetric evidence for a critical point in the neighborhood of 60 mole percent CO<sub>2</sub> and 4000 psia (27,000 kPa). The exact location of the critical point was not determined. In all the CO<sub>2</sub>-oil mixtures studied in this set of experiments, phase transitions at pressures above about 4000 psia (20,700 kPa) were very difficult to observe because the two dense phases present had only slightly different densities and therefore separated very slowly. In addition, some mixtures separated into two phases if left long enough, but both phases were so dark in color that it was difficult to measure phase volumes. Thus, in all the phase diagrams shown here, the high pressure portions of the diagrams are less precisely known than the portions at low pressures. The locations of the three-phase regions were easily determined, however.

### Discussion

In the ternary systems described by Orr & Jensen (1982), the L<sub>1</sub>-L<sub>2</sub>-V region on the P-X diagram always occurs at pressures near the three-phase pressure for mixtures of CO<sub>2</sub> with the heavy hydrocarbon component. That pressure is, in turn, close to the vapor pressure of CO<sub>2</sub>, extrapolated if necessary for temperatures above that critical to CO<sub>2</sub>. Fig. 3.5 shows how close the three-phase pressure is to the vapor pressure of CO<sub>2</sub> for CO<sub>2</sub>-C<sub>16</sub> mixtures. Thus, the extrapolated vapor pressure of CO<sub>2</sub> is a good estimate of the pressure near which L<sub>1</sub>-L<sub>2</sub>-V behavior will be observed if it occurs (Orr, Lien & Pelletier 1981). A convenient equation for the vapor pressure of CO<sub>2</sub> has been given by Newitt et al (1956)

$$P = 101.3 \exp \left\{ \frac{-2015}{T} + 10.91 \right\} \quad (3.1)$$

where P is the vapor pressure in kPa, and T the temperature in °K.

It is clear from Figs. 3.1-3.3 in which the extrapolated vapor pressure

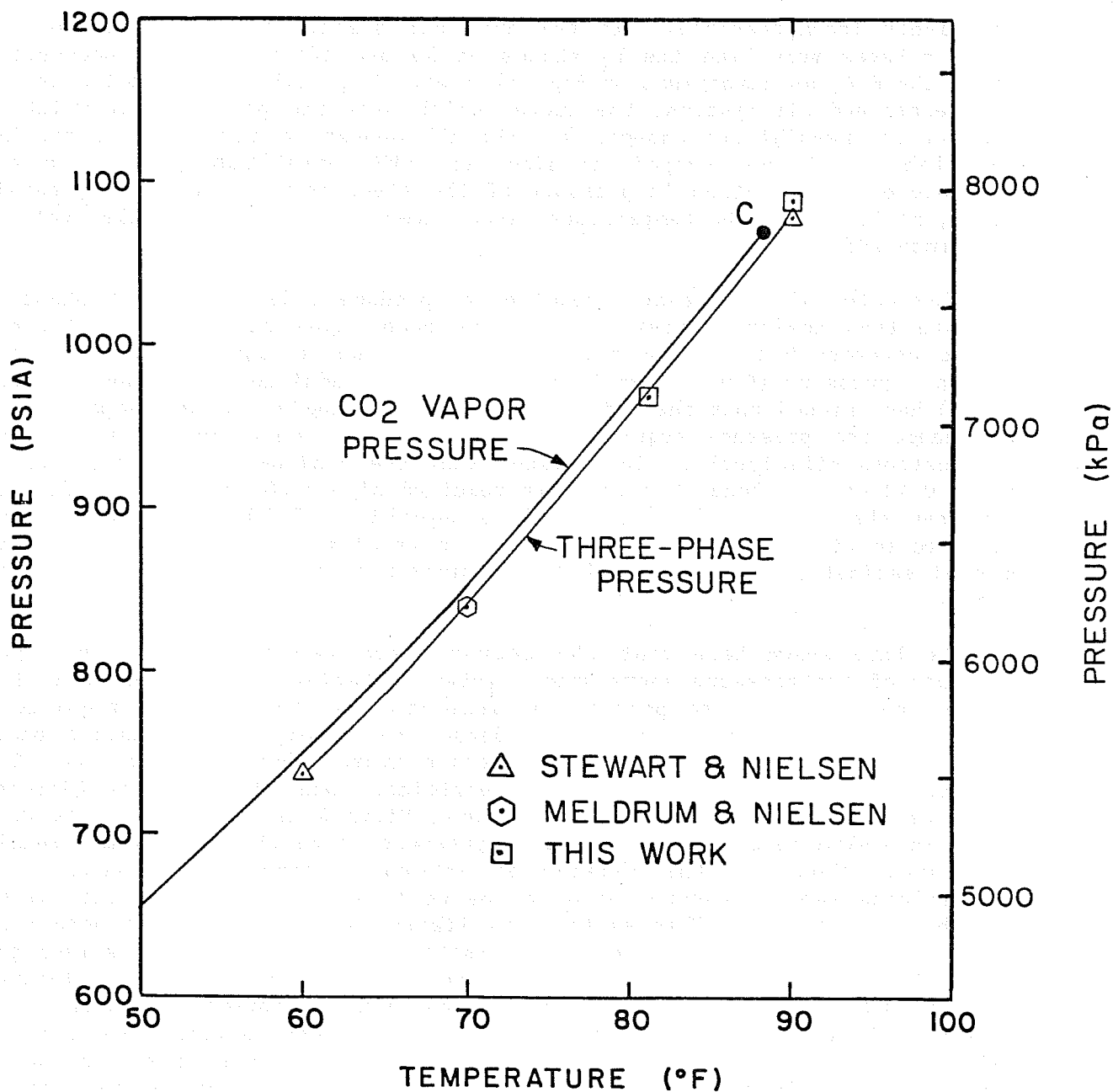


Fig. 3.5 Comparison of three-phase pressures for CO<sub>2</sub>-hexadecane mixtures with the vapor pressure of CO<sub>2</sub>.

is labeled EVP, that the crude oil systems investigated here all show  $L_1$ - $L_2$ -V separations at pressures near the extrapolated vapor pressure, if they show such behavior at all. The extrapolated vapor pressure is also a good estimate of the pressure required to make the  $CO_2$ -rich phase dense enough to be relatively incompressible. In the dead oil system, the  $CO_2$ -rich phase at 120°F behaves much like the  $L_2$  phases at 90 and 105°F when the pressure is above the EVP, as comparison of Fig. 3.1c with Fig. 3.1a and b indicates. In the recombined oil systems, the curves which mark the pressures at which the overall compressibility changes sharply all appear to terminate at the EVP. This behavior is not surprising since the EVP correlation provides a good estimate of the location in pressure of the steep portion of the  $CO_2$  density curve, at least for the temperature range investigated here (Michels, Botzen & Schuurman 1957).

Estimates of the pressure required to produce a dense  $CO_2$ -rich phase are of more than academic interest. It has been shown that a dense  $CO_2$ -rich liquid extracts hydrocarbons more efficiently than a  $CO_2$ -rich vapor phase at the same pressure (Orr, Silva & Lien 1983). In addition, Holm and Josendal (1982) have argued that the principal effect of changing system temperature is to change the pressure required to make the  $CO_2$  dense enough to extract hydrocarbons efficiently. They argued that the minimum density required was about 0.42 g/cm<sup>3</sup>, though heavier oils required higher  $CO_2$  densities. Fig. 3.6 compares the EVP correlation given as equation (3.1) with the pressure required to give a  $CO_2$  density of 0.42. It is clear that the EVP curve gives a good estimate, particularly if the temperature is at a lower end of the range.

We have shown here that the extrapolated vapor pressure is a good estimate of the pressure above which  $L_1$ - $L_2$ -V behavior will be observed if it occurs, and that it also provides an indication of the pressure required to make the  $CO_2$ -rich phase behave as a dense, relatively incompressible phase. It is just such a phase that will extract hydrocarbons efficiently. That extraction will, in turn, lead to an efficient local displacement (Gardner, Orr & Patel 1981; Orr, Yu & Lien 1981; Orr, Silva & Lien 1983) such as would occur in a slim tube displacement at a pressure above the minimum miscibility pressure. Thus, in the absence of other experimental evidence, the extrapolated vapor pressure curve can be used as an estimate of the minimum miscibility pressure. This estimate is likely to be accurate for dead oils, but may be less, if the oil contains substantial quantities of dissolved gas. Figs. 3.1-3.3 clearly show that the pressure required to produce a relatively incompressible  $CO_2$ -rich phase depends on the mixture composition when gas is present, though it is clear that at high  $CO_2$  concentrations, the limiting value of the pressure required is the EVP. It is possible that a  $CO_2$  displacement could still be efficient even if some portion of the process passes through a region where the density of the  $CO_2$ -rich phase is low as long as a dense  $CO_2$ -rich phase is created eventually. This idea has not been tested experimentally, however.

A comparison of the extrapolated vapor pressure estimate of the minimum miscibility pressure (MMP) with measured values reported by a variety of investigators is given in Fig. 3.7. For temperatures below about 140°F, the agreement is excellent, though with a few exceptions. Some of those, however,

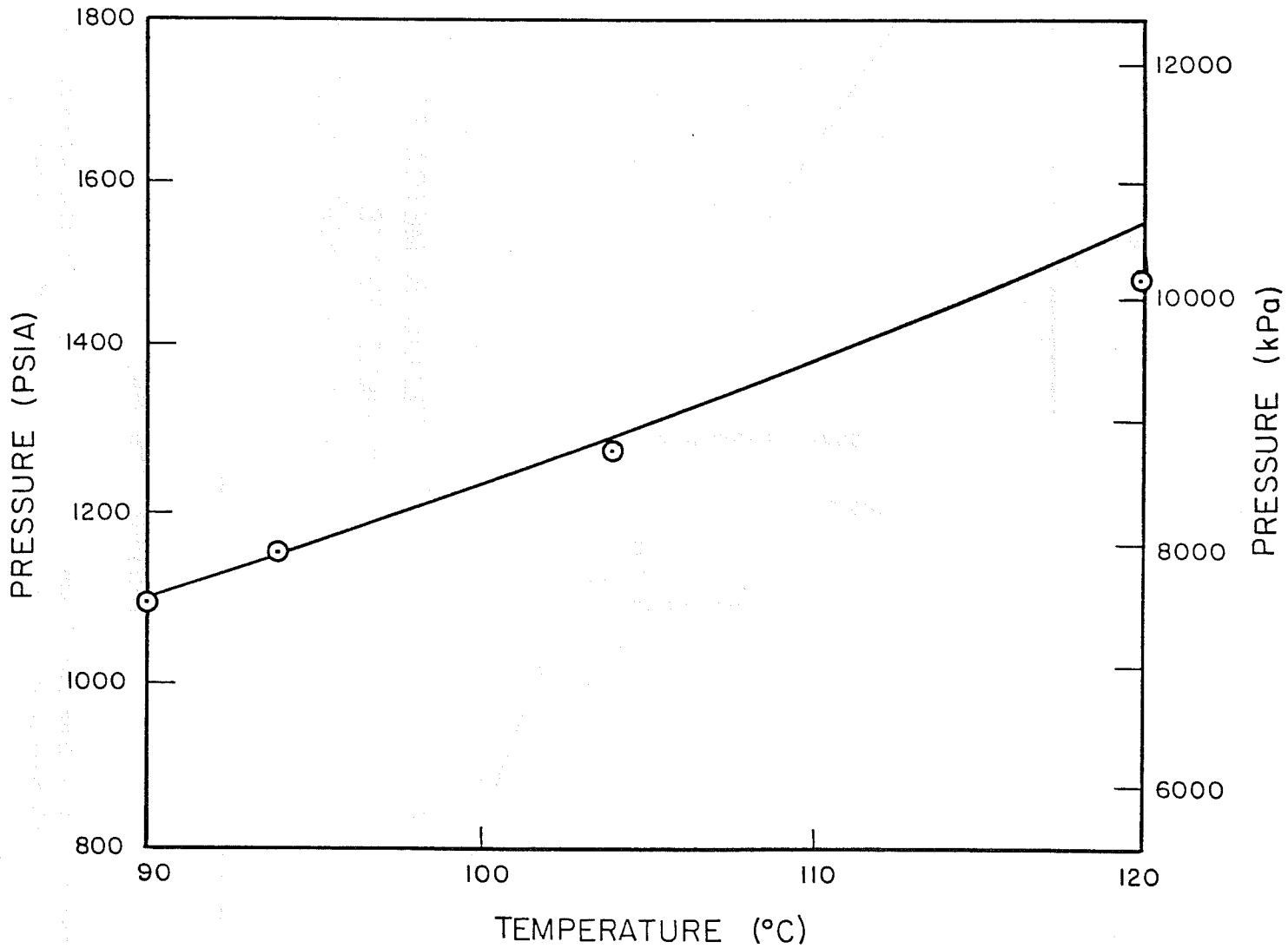


Fig. 3.6 Comparison of the extrapolated vapor pressure (solid line calculated with equation 3.1) of CO<sub>2</sub> with the pressure required to give a CO<sub>2</sub> density of 0.42.

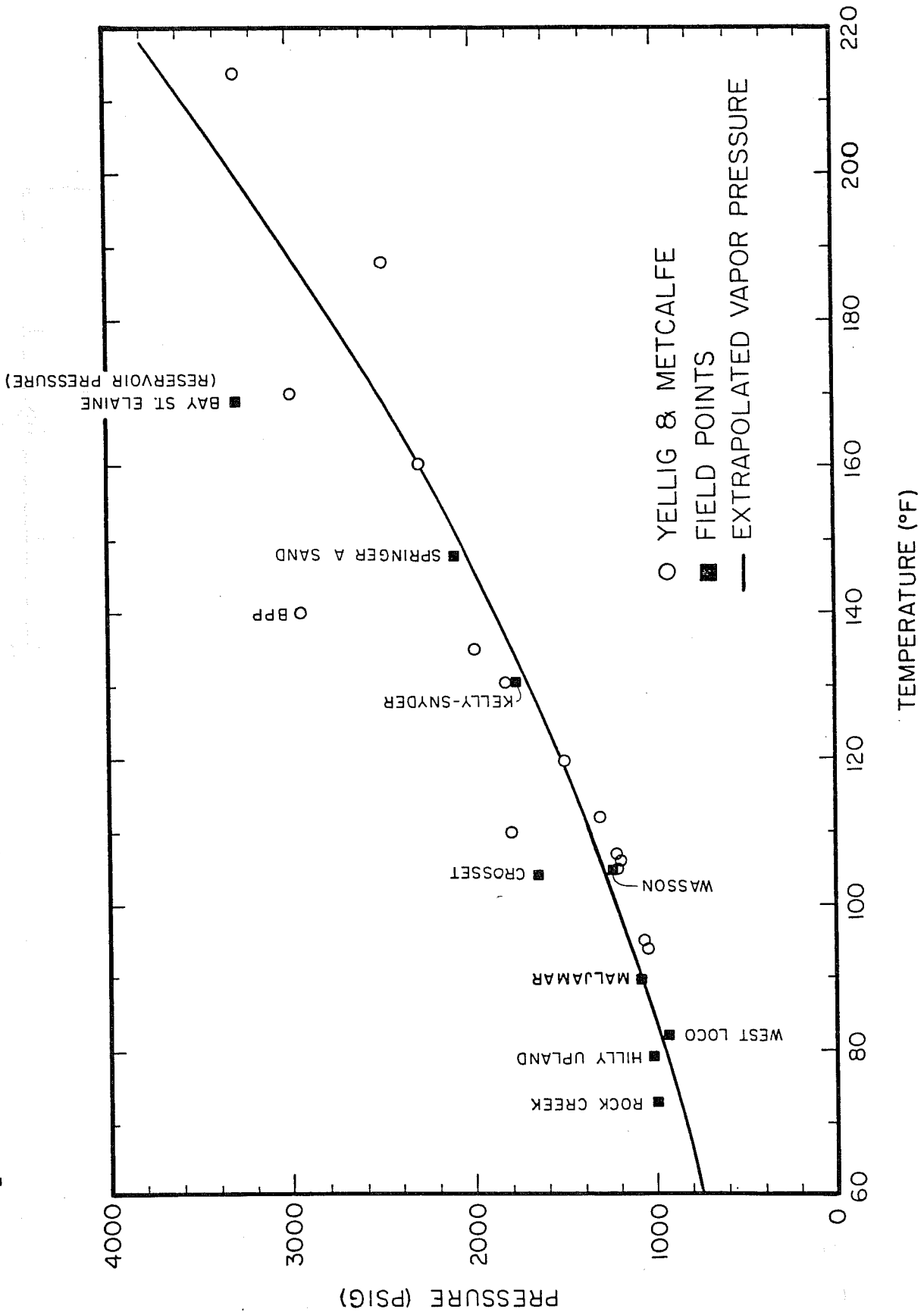


Fig. 3.7 Comparison of extrapolated vapor pressure estimate of the minimum miscibility pressure with measured values reported by other investigators.

were systems in which the investigators did not test pressures below the bubble point. Instead, the bubble point was taken as the MMP, as suggested by Yellig & Metcalfe (1980) and Holm & Josendal (1982). Thus, it is not known whether high recoveries would have resulted at lower pressures. The extrapolated vapor pressure curve is compared with the correlations offered by Yellig & Metcalfe (1980) and Holm & Josendal (1982) in Fig. 3.8. Again, the agreement is good. Thus, the MMP estimate offered here differs little from correlations previously available. It does, however, offer a clear physical explanation for the behavior of such correlations at low temperature. The restriction to low temperatures is, of course, important. At low temperatures, the density of the CO<sub>2</sub>-rich phase climbs so steeply at the extrapolated vapor pressure that effects of oil composition are all but swamped. At higher temperatures where density changes with pressure are more gradual, oil composition would have a larger impact.

### 3.2 Development of the Continuous Multiple Contact Experiment

This section reports results of work on the experimental technique described previously for continuous measurement of phase compositions and fluid properties (Orr, Silva, Lien & Pelletier 1981; Orr & Taber 1982; Orr & Silva 1982; Orr, Silva & Lien 1983).

#### Equipment Modifications

An experimental difficulty was encountered in an attempt to measure phase compositions when the two-phase region was entered through a dew point. In that case, circulation of fluid from the bottom to the top of the cell caused lower phase sample contamination problems, because there was an insufficient volume of lower phase available to satisfy the holdup in the circulation system. To alleviate this problem, additional valves were added to the circulation loop to facilitate reversal of the direction of circulation. The revised system is shown in Fig. 3.9. An additional umbrella was added to the lower sampling port to allow collection of samples from a quiescent zone when the circulation is from top to bottom. The new circulation system allows reversal of flow direction during an experiment. Thus, when a two-phase region has been entered through a bubble point, and progresses to the point where the remaining lower phase volume is too small to permit sampling from the bottom of the cell, the direction of flow can be reversed, and the collection of clean samples through the multiphase region can continue, therefore, a wider range of compositions can be investigated.

While the alterations to the circulation system were minor, much more extensive modifications have been made to the equipment which controls the experiment and records data during the run. The experiment is now controlled by an HP85A microcomputer which:

- Reads densitometer output, calculates and stores upper and

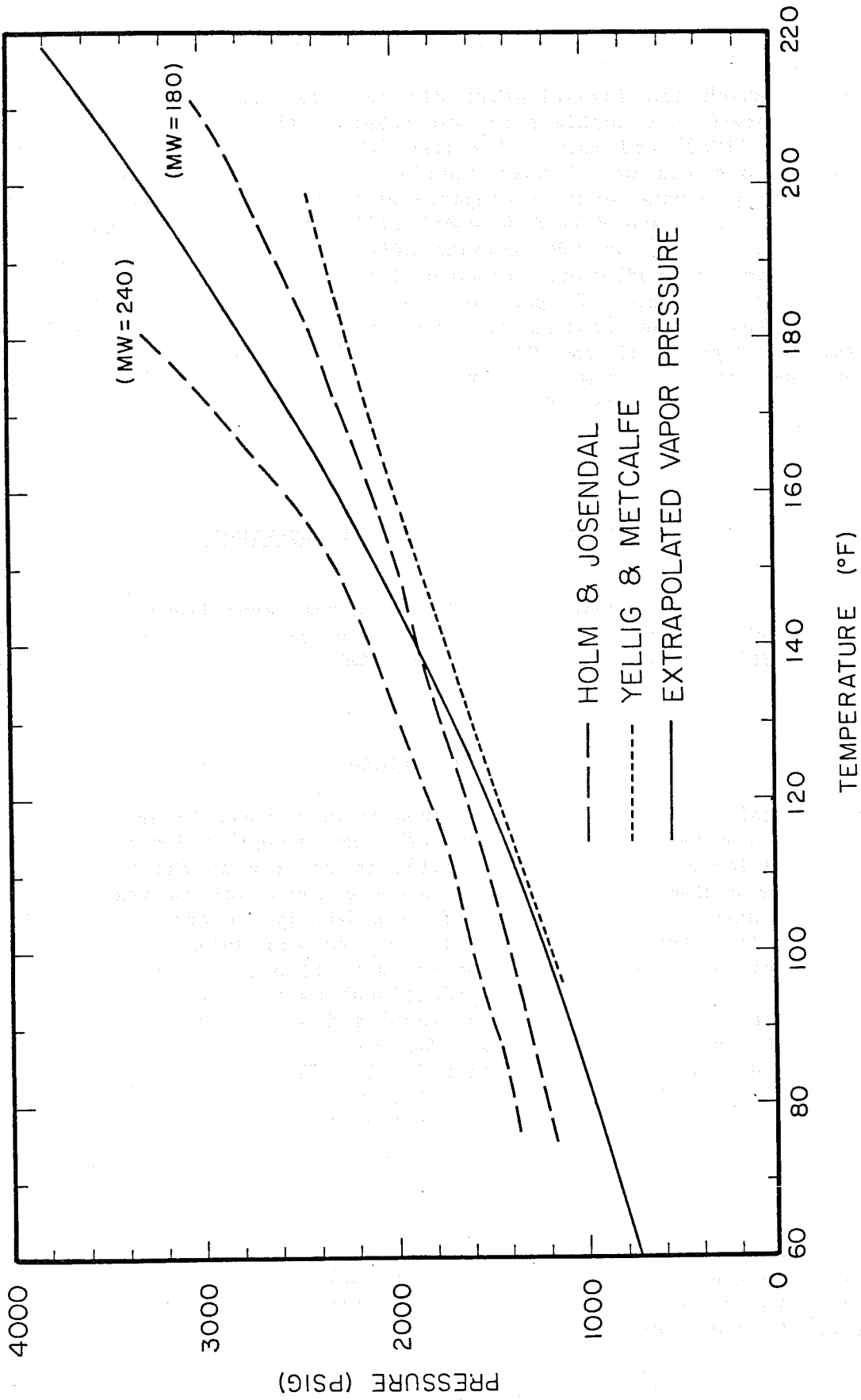


Fig. 3.8 Comparison of extrapolated vapor pressure estimate of minimum miscibility with correlations offered by Yellig & Metcalfe (1980) and Holm & Josendal (1982).

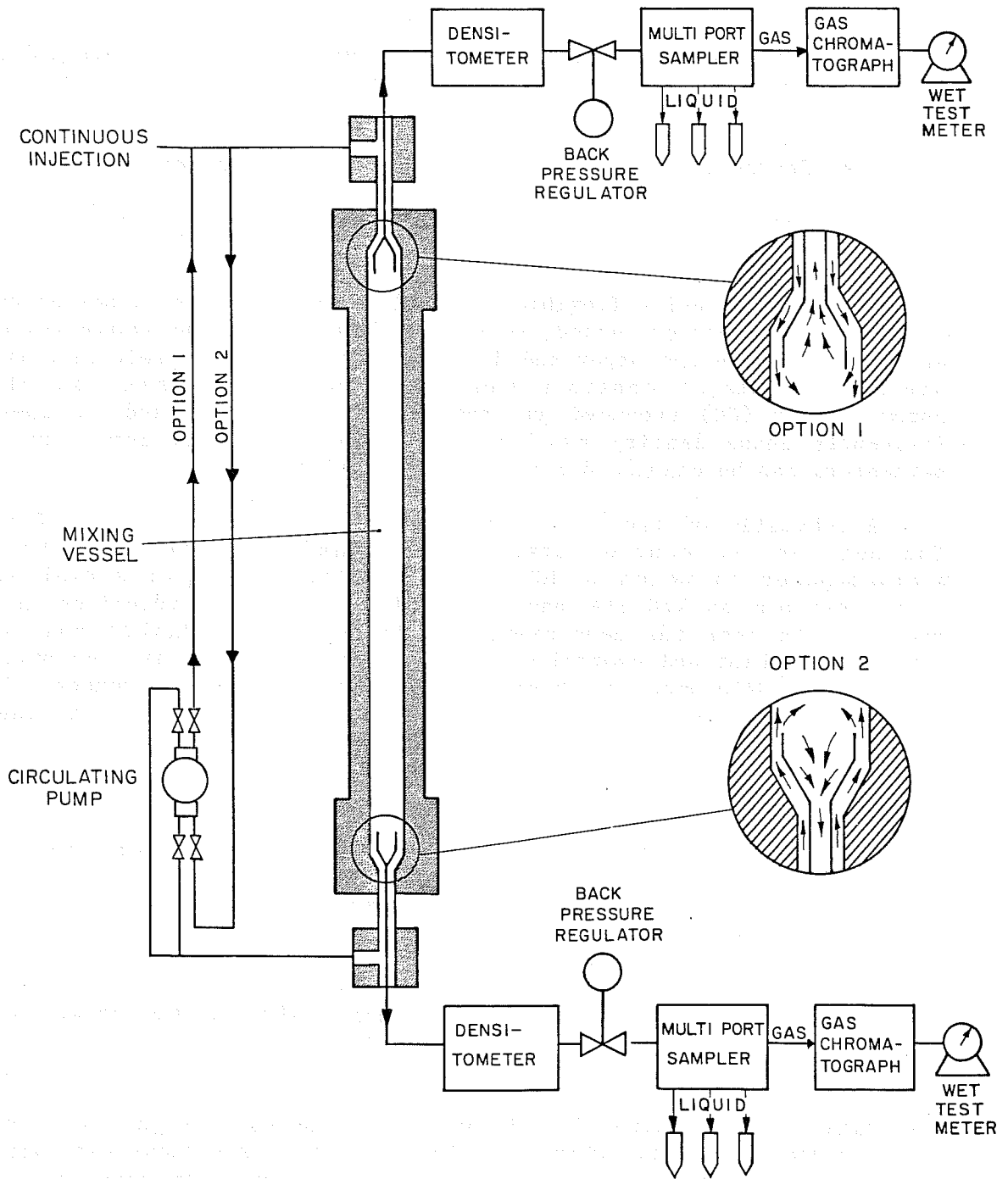


Fig. 3.9 Continuous multiple contact apparatus.

lower phase densities.

- Advances multiport samplers at the end of a sample period; alternates back pressure regulators between the upper and lower phases.
- Selects appropriate (upper or lower) sample streams and sets the position of a sample switching valve in the gas chromatograph.
- Starts gas chromatograph analysis of gas samples.
- Reads and stores results of analysis.

The new system is quite flexible. It allows the operator to select the length of a sample collection period, to specify how rapidly the system switches back and forth between the upper and lower sample streams by selecting which back pressure regulator controls sample production, to set how often gas chromatograph (GC) produced gas samples are analyzed, and to specify how frequently phase density readings are taken. In addition, any of these parameters can be changed during a run if desired.

A schematic of the data communications system is shown in Fig. 3.10. The head of the control system is a standard Hewlett-Packard HP85A microcomputer to which a BCD interface (NP82941A), a serial interface (HP82939A) and an I/O ROM have been added. The BCD interface is used to receive data from the densitometers (Mettler/Paar DMA512) and to handle several switching and control functions. The interface has ten ports. Nine are standard data ports which can receive data from an instrument. The tenth is a special port (port 10) which can be used to transmit data to one or more instruments. The four digits available on the special port are used as follows:

- Digit 1 ( $2^0$ ) - Select upper or lower back pressure regulator.
- Digit 2 ( $2^1$ ) - Advance multiport sampling valves.
- Digit 3 ( $2^2$ ) - Start a GC run.
- Digit 4 ( $2^3$ ) - Switch the GC sample valve to the other sample stream.

When digit 1 is set high (1), the upper back pressure regulator controls the sample production rate. When it is low (0), the lower regulator controls. To advance the multiport sampling valves which are used to separate liquid and vapor downstream of the back pressure regulators, digit 1 is set high for approximately one second and then set low. To start a gas chromatograph run, digit 2 is set high for approximately one second and then set low. The sample valve in the gas chromatograph collects lower phase gas when digit 3 is set

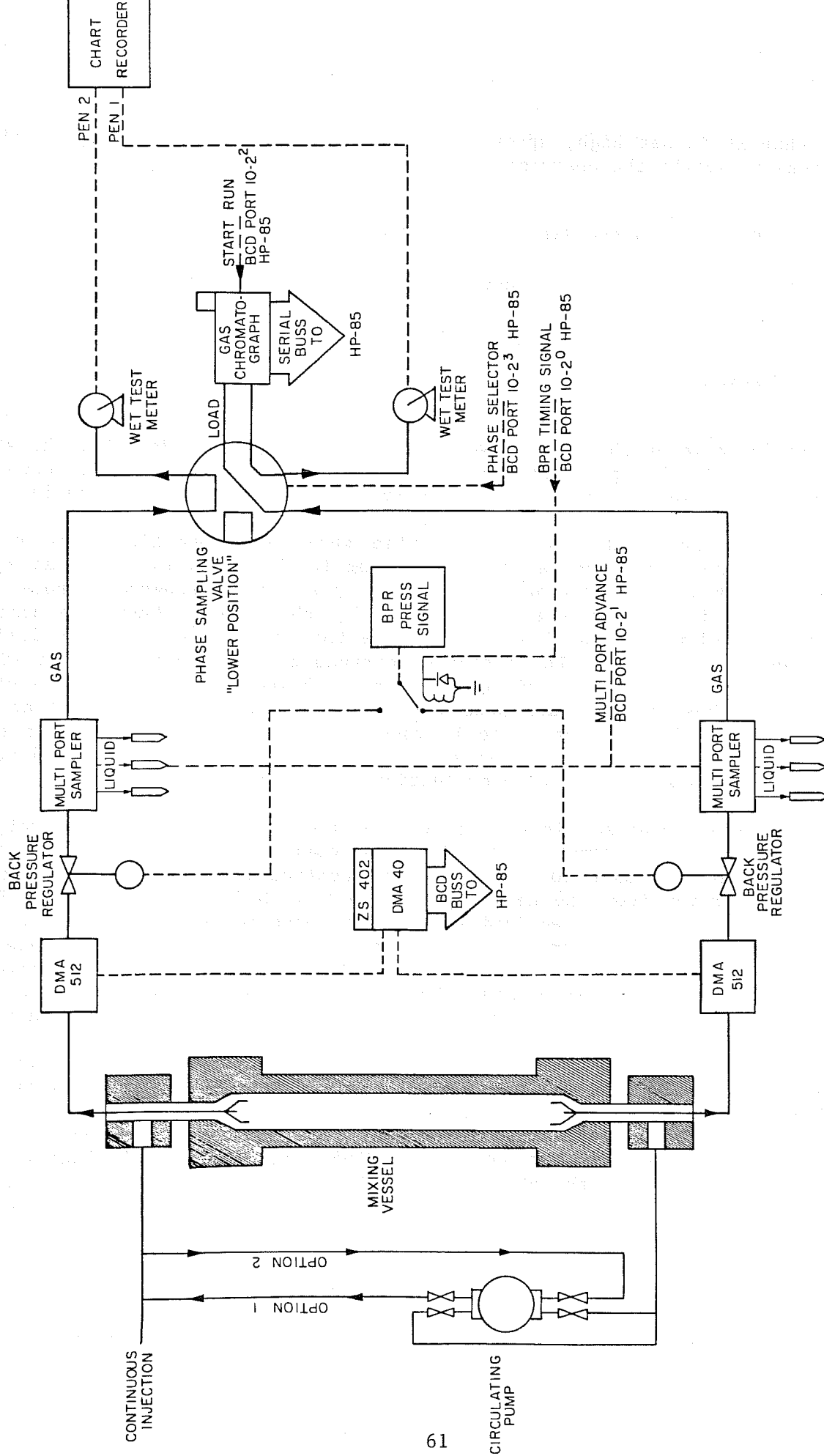


Fig. 3.10 Flowchart of data communications system.

low. When it is set high, upper phase gas is sampled. The timing of these functions is set by the operator. Typical time settings are:

- Collect density data every 4 minutes.
- Alternate the back pressure regulators every 3 minutes.
- Start a GC run every 15 minutes.
- Advance to the next sample every hour.

The sample valve on the GC is always set to switch 6 seconds after the start of a GC run. At that point the sample in the sample loop has been injected on columns and the sample valve is free to begin collecting the next sample.

To avoid conflicts which can arise when two operations are to be performed at the same time, a control program in the HP85A maintains an event queue. Each time an operation is performed, the control program computes the next time for its performance and places it in the queue. Some care must be used in scheduling events, however, because the computer allows only limited simultaneous operations. For instance, changes in the digits on port 10 of the BCD interface cannot be made while data are being read on one of the other BCD ports. Thus, if the back pressure regulators are to be switched at the same time a density reading is to be taken, a conflict can occur. It is a simple matter, however, to requeue any switching events to a time immediately after completion of density data collection and storage.

The serial interface is used solely to receive results of gas analyses from the HP5840 gas chromatograph. When the command is issued to start a GC run (BCD interface, port 10, digit 3), the control program also initiates a transfer operation from the serial interface to a buffer in the HP85. Data from the GC can then be received while other program operations are taking place. When the report from the GC is complete, it transmits an ETX character which signals to the control software that the data from the GC are ready to be processed. The control program then schedules the processing and storage of the GC data for a time when the HP85 is not occupied with other operations.

The new control system eliminates most manual data entry into the computer programs which calculate phase compositions and plot run results, and eliminates the need for operator intervention during a run. The apparatus can now operate unattended. Liquid composition data can be transferred directly from the HP5880 gas chromatograph to the HP85, and reports and plots can be prepared and printed by the HP85. Performing data computations and plotting functions with the HP85 have led to a sharp reduction in costs for central computer time. If desired, however, data can still be transferred to the central computer system for processing a backup data storage.

## Measurement of Viscosities with an Oscillating Quartz Crystal

The continuous multiple contact (CMC) experiment is an efficient technique for measurement of phase compositions and densities. If a measurement of phase viscosities could be added, the experiment would allow simultaneous measurement of fluid properties which would be very useful for estimating the effects of viscous fingering and gravity segregation in a reservoir setting, and for building and testing fluid property correlations. To be suitable for inclusion in the CMC experiment, a viscosity measurement technique should require a small sample volume and should handle conveniently a wide range of viscosities. One technique which appears to meet these requirements uses the damping of the torsional oscillation of a quartz crystal (Mason 1947; Welber 1960; Webeler 1961; De Bock, Grevendonk & Awouters 1967; Collings & McLaughlin 1971; Haynes 1973; Diller 1980; Simon 1982).

A crystal holder similar to that shown in Fig. 3.11 was used to test two mounting schemes. In both, the crystal was capacitively coupled to the driving electric field. Originally, direct plating of platinum electrodes onto the crystal surface was planned, but problems with attaching leads to the crystal led to the arrangement shown in Fig. 3.11. The oscillating electric field is applied to the two pairs of electrodes by an impedance analyzer (Hewlett-Packard HP4192A) which is also used to measure the properties of the crystal. The fluid to be tested resides in the annulus between the electrodes and the crystal. If the crystal is caused to oscillate in a vacuum, it shows a characteristic resonant frequency. In a fluid, the viscous shear at the crystal surface adds damping to the system, which shifts and broadens the resonance peak. The change in the band width of the resonance peak can be used to calculate the product of viscosity and density. It is important, therefore, to minimize the damping of the crystal holder itself. If crystal supports make physical contact only at nodes on the cylinder, the damping induced by the mounting is small. In the fundamental torsional node of oscillation, the cylinder axis is a node, as is the plane which bisects the length of the crystal and is perpendicular to the crystal axis. The two mounting schemes, shown in Fig. 3.12, support the crystal at those two nodes.

The first scheme supports the crystal at the axial node. A toroidal jewel bearing was attached with epoxy to each end of the crystal. Small machined metal points were installed in the end plates of the teflon crystal holder to seat in the toroidal jewels and support the crystal. This method has the advantages of simplicity and mechanical strength, but it proved to have too much damping to allow the crystal to resonate. It also proved difficult to maintain the required orientation of the crystal with respect to the electrodes. Thus, this method appears unlikely to be effective unless a substantial reduction in the damping of the mounting can be achieved.

The second mounting technique is similar to that used by Diller (1980) and Haynes (1973). Two small notches were cut perpendicular to the crystal axis at the crystal midpoint. The crystal was then supported on teflon coated wires seated in the notches and held in place by tension applied to the wires. This mounting scheme is more susceptible to changes in orientation of the crystal in the electric field, but it has much better damping characteristics than the other method. Sharp resonance peaks were obtained in a vacuum and in several fluids.

CO<sub>2</sub>-83-031

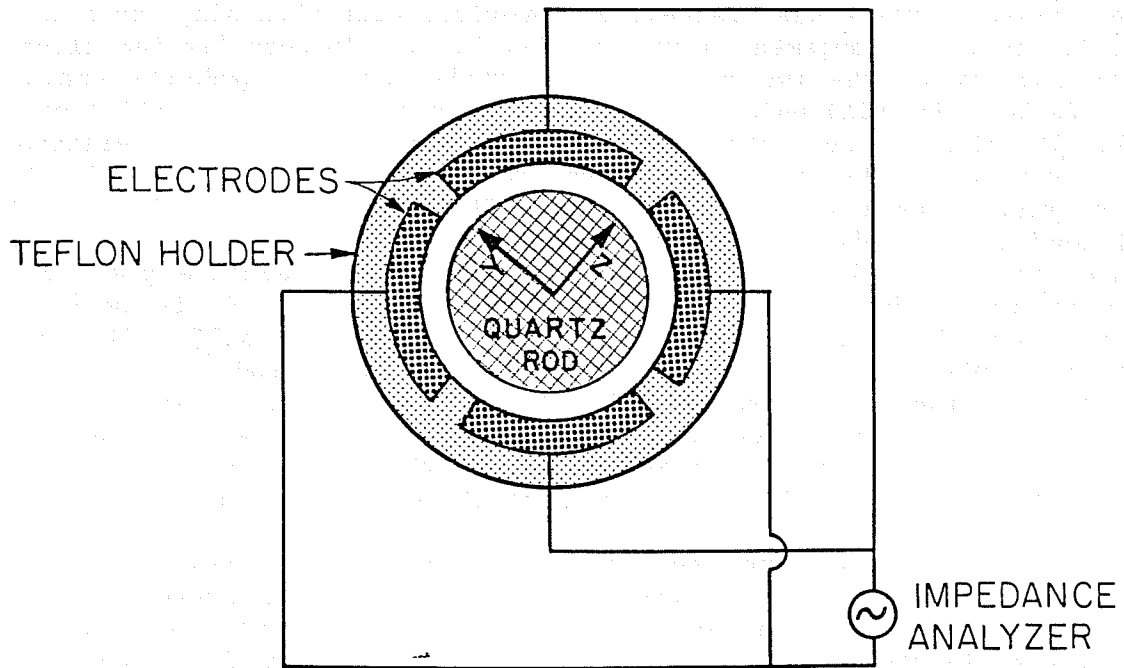


Fig. 3.11 Axial view of a cylindrical crystal holder.

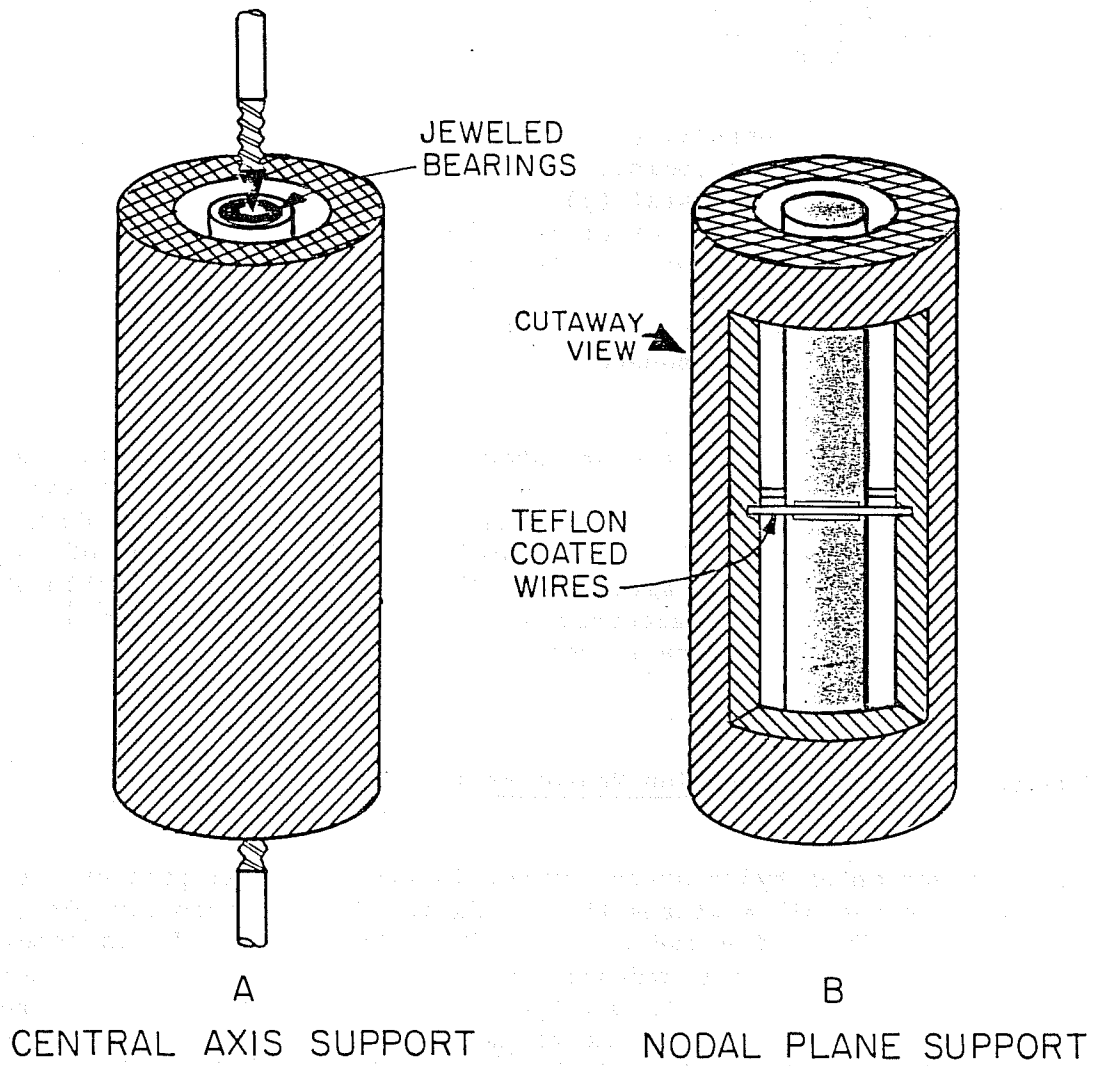


Fig. 3.12 Crystal mounting schemes.

In an actual measurement, the width in frequency of the resonance peak is measured. The viscosity of the fluid can then be calculated as (Webeler 1961, Diller 1980)

$$\eta = \frac{\pi f}{\rho} \left( \frac{M}{S} \right)^2 \left( \frac{\Delta f}{f} - \frac{\Delta f_{\text{vac}}}{f_{\text{vac}}} \right)^2 \quad (3.2)$$

where

- $\rho$  = fluid density (g/cm<sup>3</sup>)
- $\eta$  = viscosity (poise)
- $M$  = mass of crystal (g)
- $S$  = surface area of crystal (cm<sup>2</sup>)
- $f_{\text{vac}}$  = resonant frequency in a vacuum (sec<sup>-1</sup>)
- $\Delta f_{\text{vac}}$  = width of resonance peak in a vacuum (sec<sup>-1</sup>)
- $f$  = resonant frequency in the fluid (sec<sup>-1</sup>)
- $\Delta f$  = width of resonance peak in the fluid (sec<sup>-1</sup>)

Results of typical frequency scans are shown in Figs. 3.13 and 3.14. In those measurements, the crystal was represented as a conductance and a capacitance in parallel. In a partial vacuum, the resonance peak is quite sharp (Fig. 3.13), but in heptane, it is much broader. The viscosity of heptane calculated with equation (3.2) agreed with literature values to within about 6 percent. Work to improve the accuracy of the measurement and develop crystal holders for use at high pressure is underway.

### 3.3 Results of Phase Composition Measurements

The extraction of hydrocarbons by CO<sub>2</sub> is the essential part of the phase behavior of CO<sub>2</sub>-crude oil mixtures that leads to high oil recovery (Orr, Silva & Lien 1983; Orr, Yu & Lien 1981; Holm & Josendal 1982). It is important, therefore, to understand what hydrocarbons are extracted efficiently and how crude oil composition affects the way hydrocarbon components partition between phases. Comparison of measurements of phase compositions of CO<sub>2</sub>-crude oil mixtures with those of CO<sub>2</sub> with well-characterized hydrocarbons indicates that CO<sub>2</sub> extracts greater amounts of hydrocarbons from a crude oil than from a pure oil of similar molecular weight. Fig. 3.15 compares, for instance, tie line slopes for a synthetic oil composed of C<sub>5</sub>, C<sub>10</sub>, C<sub>16</sub> and C<sub>30</sub> paraffins (Orr, Lien & Pelletier 1981) and Maljamar crude oil (Orr & Taber 1982; Orr, Silva & Lien 1983; Silva, Lien, Franklin & Orr 1982a). The tie lines chosen for comparison are the L<sub>1</sub>-L<sub>2</sub> tie lines which bound the L<sub>1</sub>-L<sub>2</sub>-V region. Though the temperatures and pressures were slightly different, it has been shown (Orr, Silva & Lien 1982; Orr & Jensen 1982) that for liquid-liquid systems, the effects of small differences in temperature and pressure are also small. Fig. 3.15 shows clearly that the tie line slope for the crude oil system is significantly more favorable. Thus, differences in oil compositions can affect component partitioning in a way which affects the pressure required to produce tie line slopes that generate high recovery in a slim tube displacement.

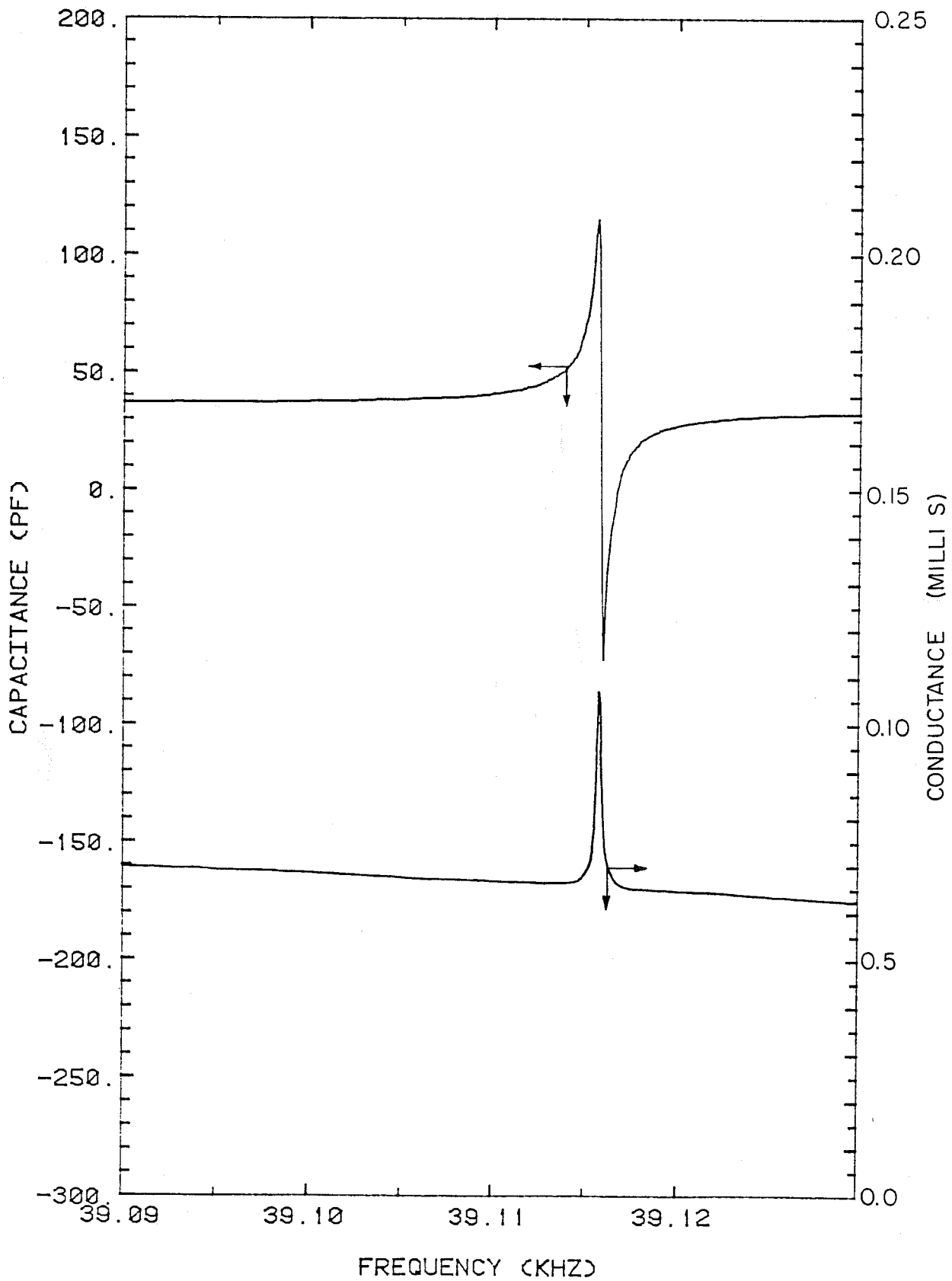


Fig. 3.13 Quartz crystal resonance in air at 26 mm Hg.

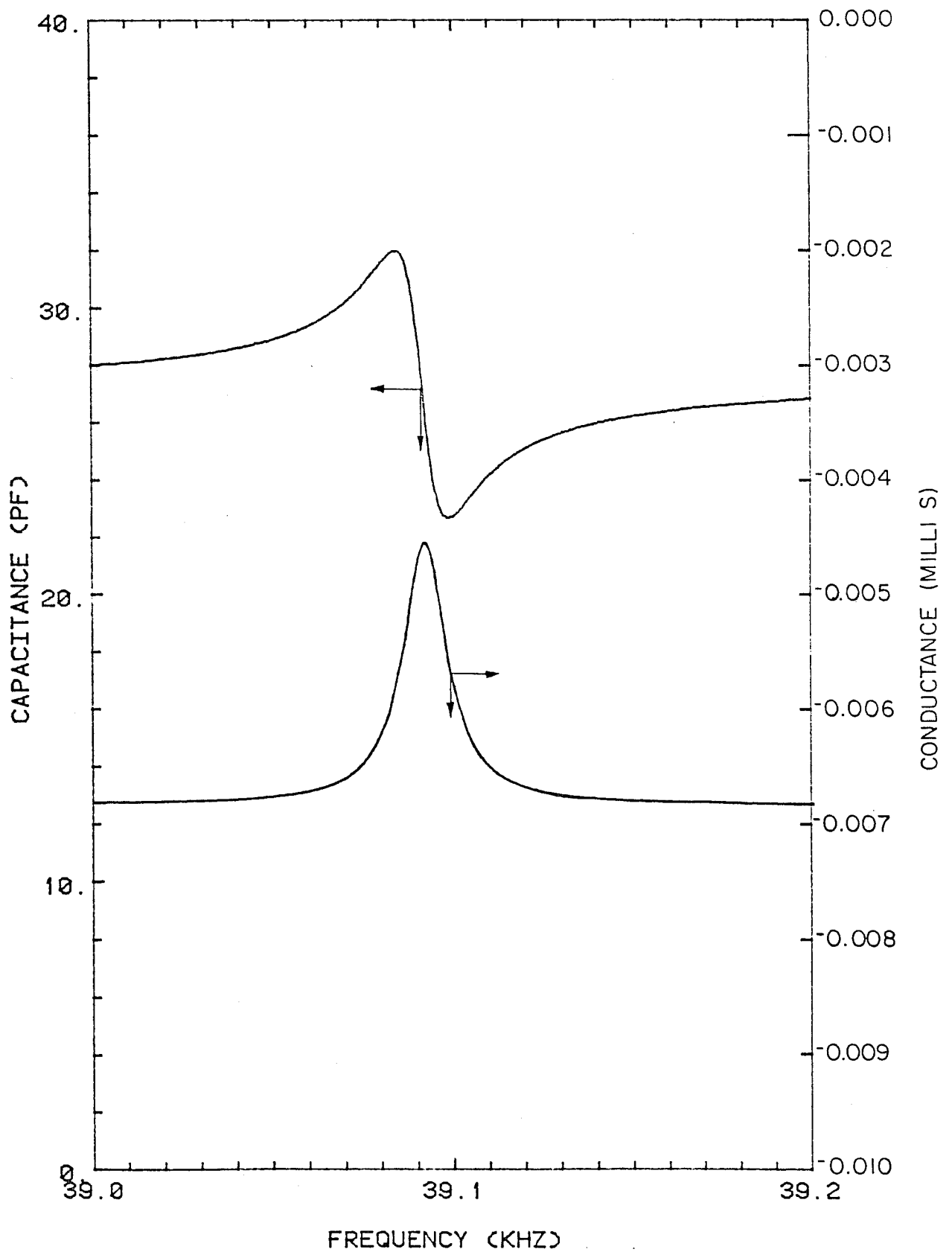
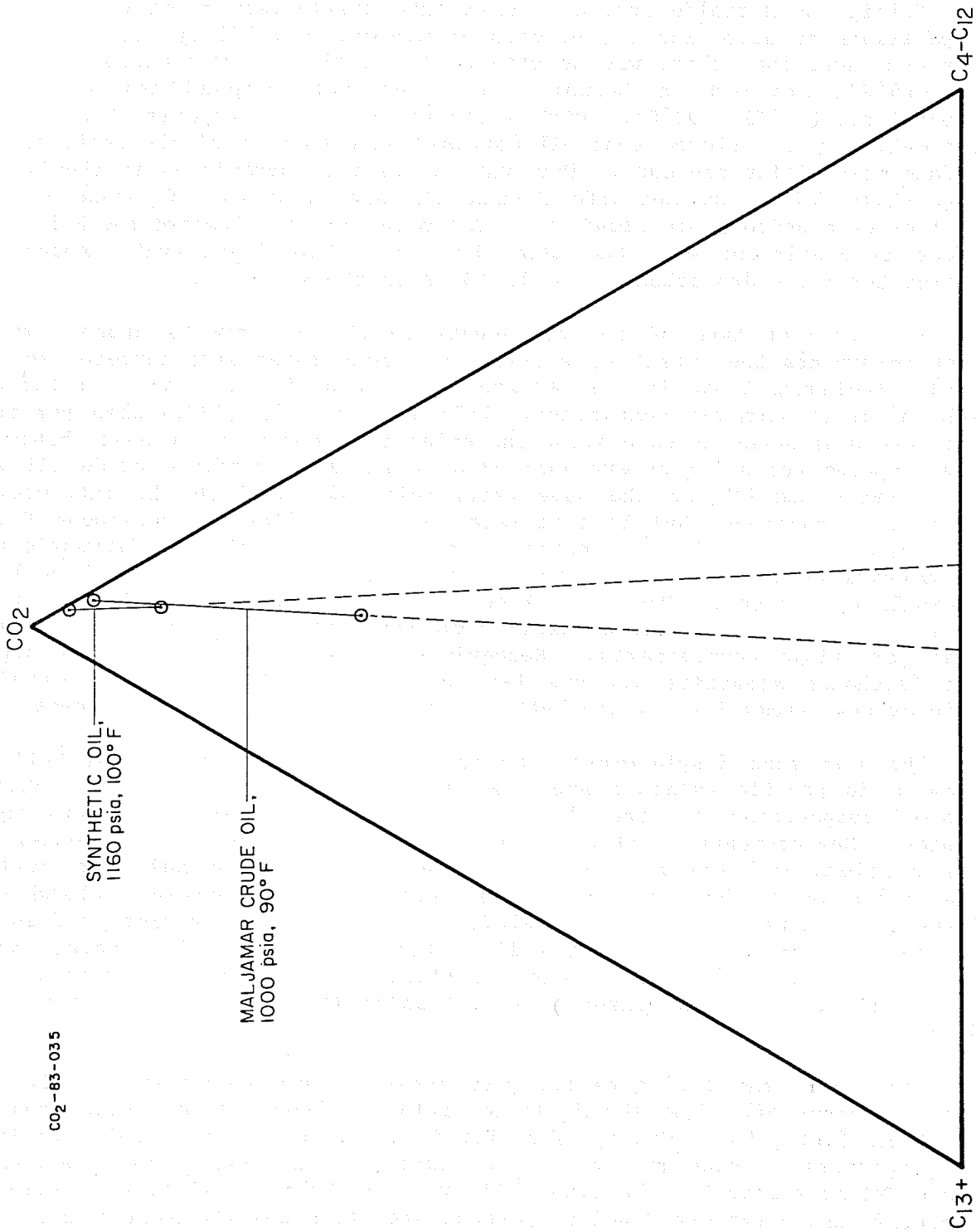


Fig. 3.14 Quartz crystal resonance in heptane.



CO<sub>2</sub>-83-035

SYNTHETIC OIL,  
1160 psia, 100°F

MALJAMAR CRUDE OIL,  
1000 psia, 90°F

Fig. 3.15 Comparison of tie line slopes for a synthetic oil composed of C<sub>5</sub>, C<sub>10</sub>, C<sub>16</sub>, and C<sub>30</sub> paraffins and Maljamar crude oil.

Yellig and Metcalfe conducted slim tube displacements for different oil compositions to determine the effects on minimum miscibility pressure (MMP). They concluded that there was no effect at relatively low temperatures (95°F and 118°F), and only a "minor effect" of oil composition at higher temperatures (150°F, 192°F). With a similar series of experiments, Holm and Josendal, however, showed that oil composition does appreciably influence the minimum miscibility pressure. They varied the oil composition in the C<sub>5</sub> - C<sub>9</sub> range while Yellig and Metcalfe changed the amount of C<sub>2</sub> - C<sub>6</sub> present. The addition of a hydrocarbon blend (C<sub>5</sub> - C<sub>9</sub>) significantly lowered the MMP. That effect is consistent with the idea that the intermediate hydrocarbons help extract heavier hydrocarbons into the CO<sub>2</sub>-rich phase.

The chemical type of the components in the oil may be another factor which determines the extent of extraction. Some reservoirs targeted for CO<sub>2</sub> floods, including those in the Permian Basin, contain oils with a relatively high amount of aromatic components. Holm and Josendal (1982) also performed slim tube displacements to examine the effects of aromatics on phase behavior. They compared the oil recovery and MMP of a highly paraffinic crude oil with the recovery and MMP of the same paraffinic oil in which the intermediate range of hydrocarbons had been replaced by intermediate hydrocarbons from a more aromatic crude oil. Oil recovery was greater for the more aromatic oil. The authors concluded that increasing aromaticity correlated with a lower miscibility pressure. However, those results seem inconsistent with the observation that individual aromatic components are less soluble in CO<sub>2</sub> than their paraffinic counterparts. Recognizing this, Holm and Josendal argued that "although aromatics ... are less compatible with CO<sub>2</sub> than paraffin hydrocarbons, aromatics ... are better solvents for petroleum heavy ends."

The slim tube displacements performed by Holm & Josendal and Yellig & Metcalfe do provide evidence about how minimum miscibility pressure changes with oil composition, but they do not provide any direct evidence as to why it changes. Measurements of phase compositions can provide that evidence. In this section, we compare results of these continuous multiple contact experiments which shed some additional light on the reasons behind such changes. Results of continuous multiple contact phase behavior studies for CO<sub>2</sub>-separator crude oil systems (Silva, Lien, Franklin & Orr 1981a, 1981b) were compared with results of one additional experiment to determine the effects of aromatics on component partitioning (Silva, Lien, Franklin & Orr 1982b).

Figs. 3.16 and 3.17 give the pseudo-ternary representation of CO<sub>2</sub> with separator crude oils from the Maljamar field, Lea County, New Mexico and the Rock Creek field, Roane County, West Virginia, respectively. Table 3.2 lists the properties of each system and the experimental conditions. Based on proton NMR measurements, the crude oil from the Maljamar field was estimated to contain approximately 8 weight percent aromatics and the highly paraffinic Rock Creek oil, less than 2 weight percent aromatics. The slopes of the tie lines and geometry of the two-phase envelopes of the two systems are similar, as shown in Figs. 3.16 and 3.17. Thus, the presence of the aromatics in the Maljamar crude oil had no obvious effect on component partitioning. A more detailed comparison of partitioning in the two systems is shown in Fig. 3.18, which reports equilibrium ratios for individual carbon number cuts. In each

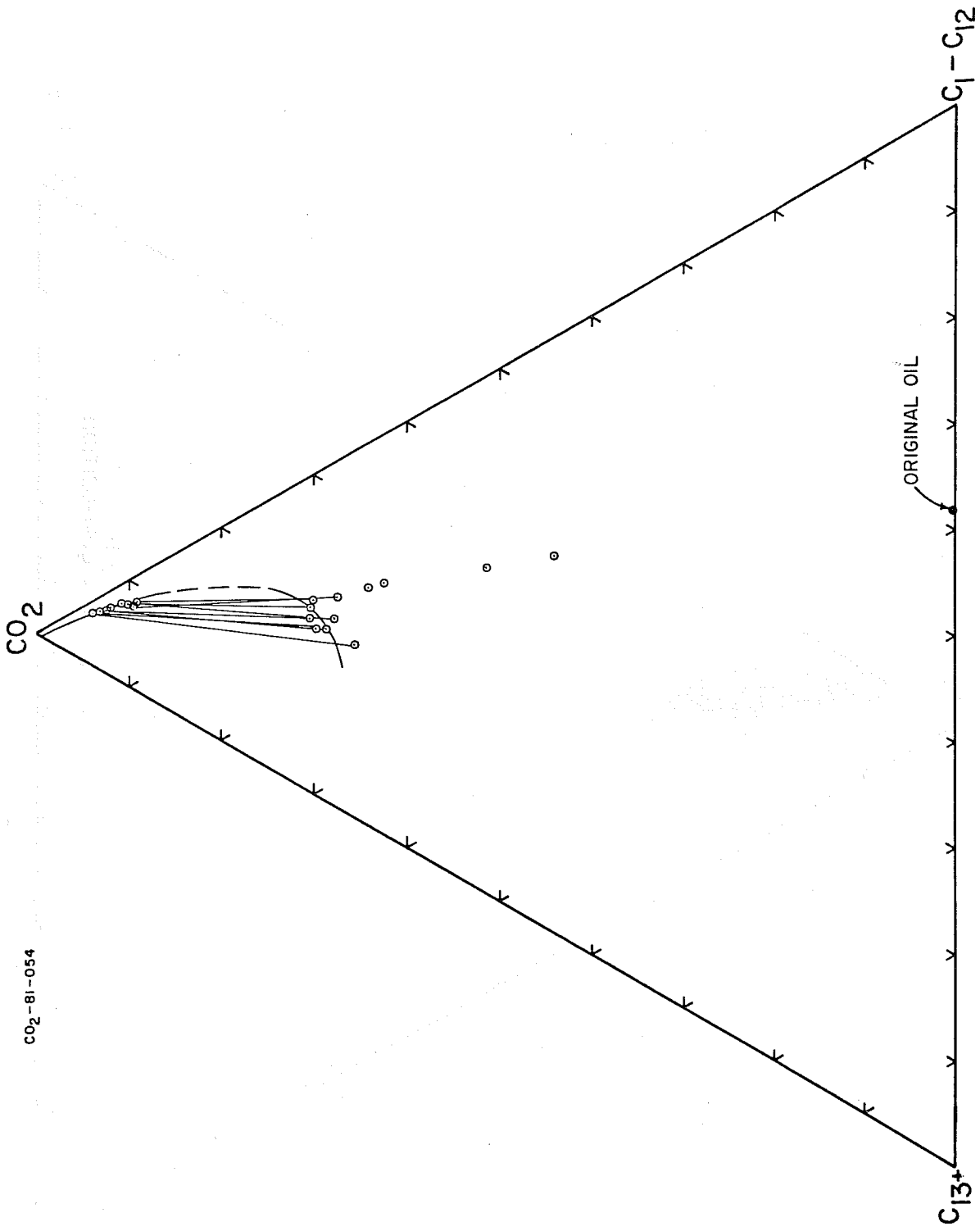


Fig. 3.16 Pseudo-ternary representation of phase compositions of mixtures of CO<sub>2</sub> with Maljamar separator oil at 1200 psia and 90°F.

CO<sub>2</sub>-81-055b

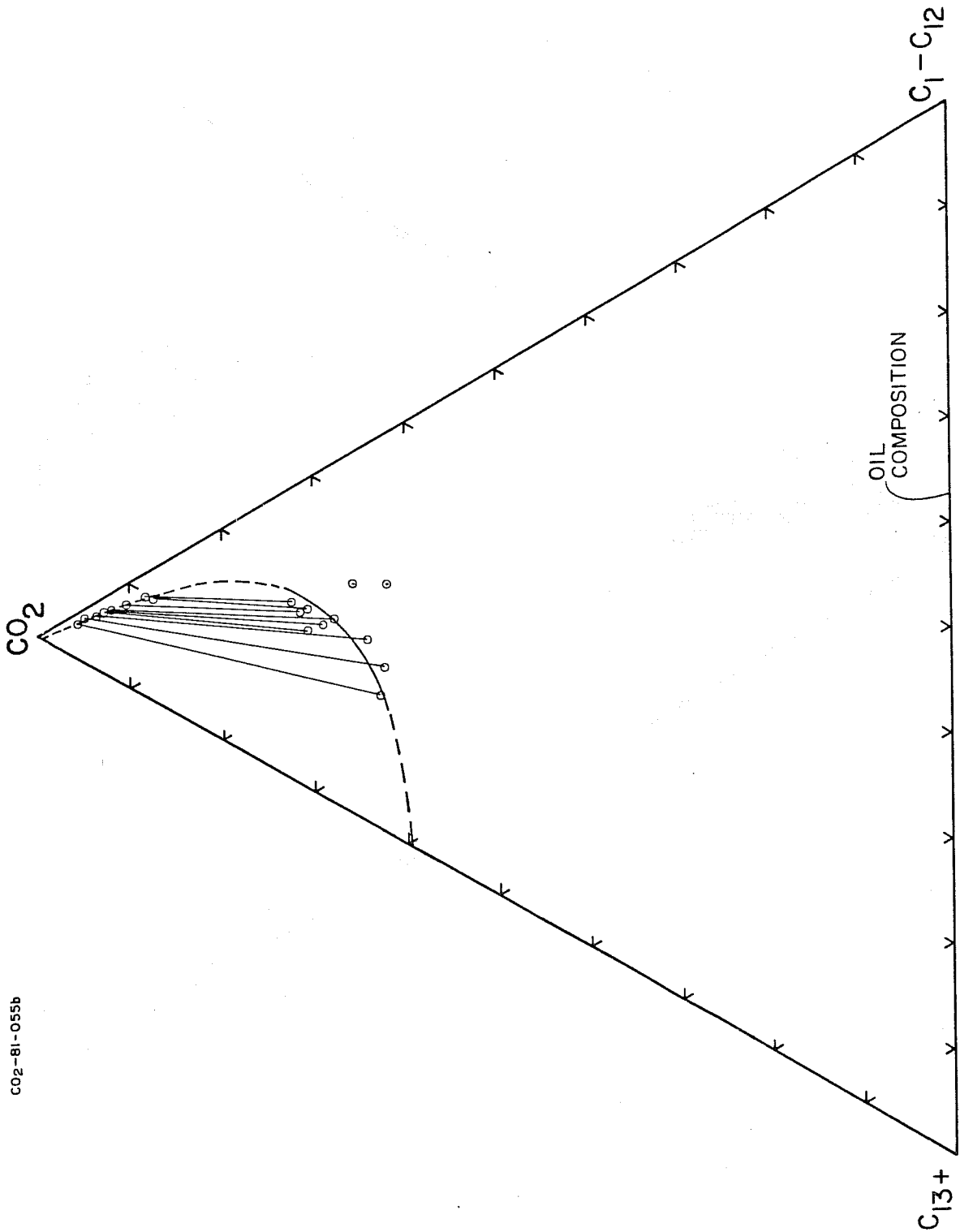


Fig. 3.17 Pseudo-ternary representation of phase compositions of mixtures of  $CO_2$  with Rock Creek separator oil at 1300 psia and 75°F.

Table 3.2

Comparison of Oil Properties and Run Conditions for Continuous Multiple Contact Experiments for Maljamar and Rock Creek Crude Oils

	<u>Maljamar Separator Oil</u>	<u>Rock Creek Separator Oil</u>	<u>Rock Creek Separator Oil with selected aromatics</u>
Aromatic Content (wt. %)	8	<2	14.8
Molecular Weight	200	190	174
Density (gm/cm <sup>3</sup> )	0.832	0.797	0.813
Temperature (°F)	90	75	75
Pressure (psia)	1200	1300	1300

Table 3.3

Composition of Mixture of Aromatic Hydrocarbons Added to Rock Creek Crude Oil

<u>Component</u>	<u>Wt. %</u>	<u>Mole %</u>
Toluene	30.98	40.24
1,2,4-Trimethylbenzene (TMB)	27.13	27.24
2-Methylnaphthalene (2MN)	23.85	19.51
Phenanthrene	18.03	13.01

Calculated Molecular Weight = 119.02

Table 3.4

Composition of Rock Creek Crude Oil Mixed with Selected Aromatic Hydrocarbons

<u>Component</u>	<u>Wt. %</u>	<u>Mole %</u>
Rock Creek	85.21	78.30
Aromatics	14.79	21.70

Calculated Molecular Weight = 174.6

Measured Molecular Weight = 173.5

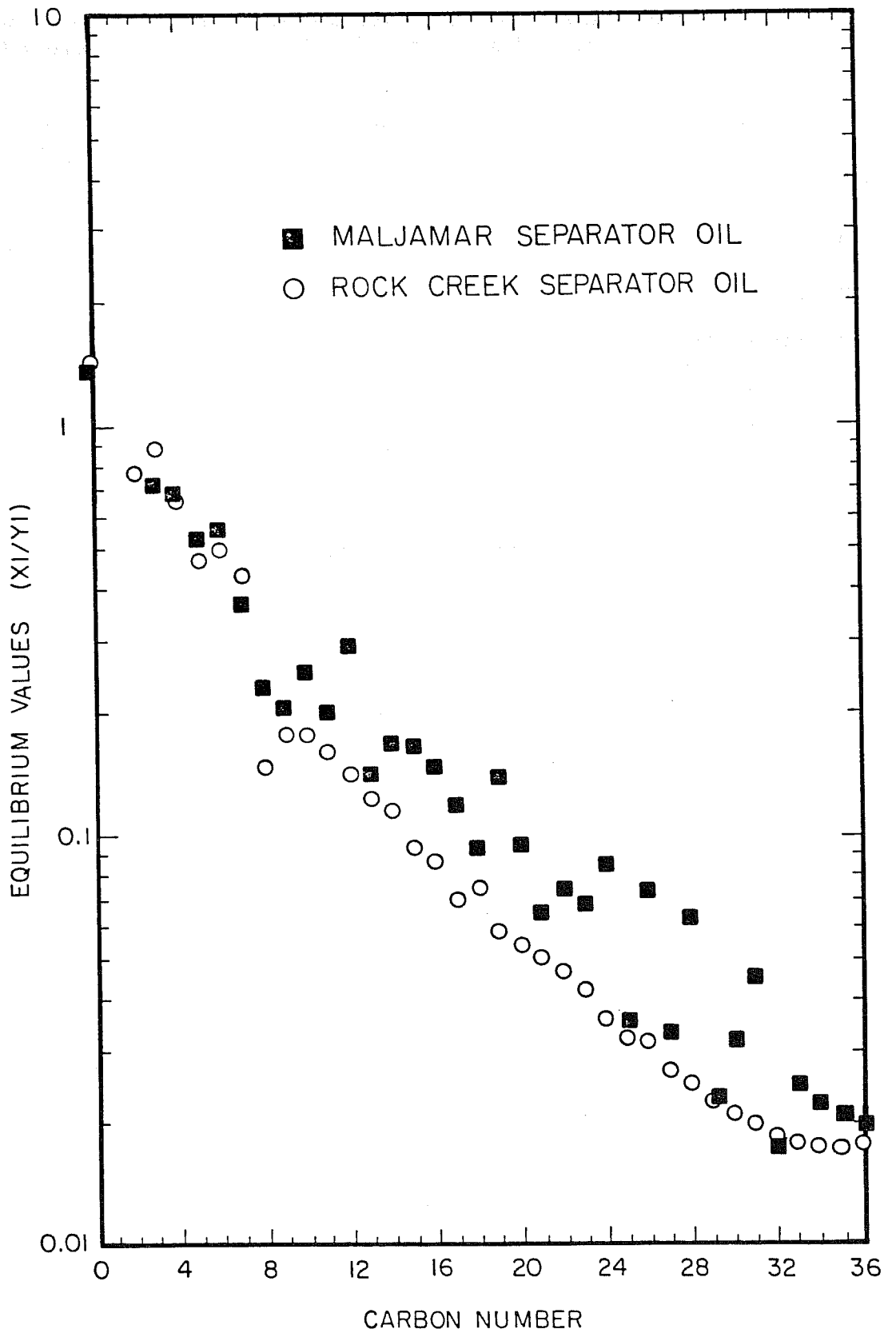


Fig. 3.18 Comparison of component partitioning for Rock Creek separator oil and Maljamar separator oil.

case, the K-values reported are for samples in the two-phase region that have an equal mole fraction of carbon dioxide in the upper phase. Again, there is little evidence of a substantial effect of the aromatics present in the Maljamar oil on component partitioning.

To examine further the role of aromatics in component partitioning, a continuous multiple contact experiment was performed for the Rock Creek oil to which a mixture of aromatics had been added. Table 3.3 gives the composition of the aromatic mixture added to the crude oil, and Table 3.4 reports the composition of the mixture. A more detailed discussion of sample preparation is given by Silva et al (1982b).

The phase behavior of the Rock Creek separator oil plus aromatics, presented in Fig. 3.19, shows a change in the shape of the phase envelope and the tie line slopes, though the magnitude of the change is not large. The two-phase region extended further toward the light hydrocarbon apex when aromatics were added. The change in the slopes of the tie lines is favorable, but it is at least partly compensated by the enlargement of the two-phase region, which displaces the critical tie line to higher concentrations of light hydrocarbons ( $C_1$ - $C_{12}$ ), an unfavorable change in the phase diagram (Orr, Jensen & Silva 1981).

Fig. 3.20 compares equilibrium ratios of individual components for samples in the two-phase region for Rock Creek separator oil and Rock Creek separator oil with aromatic spikes. The addition of selected aromatics to the paraffinic oil results in a redistribution of the hydrocarbons in the two phases which is consistent with the observed change in tie line slopes seen in Fig. 3.19. Hydrocarbons lighter than  $C_8$  partitioned more strongly into the upper phase when the aromatics were present, while those heavier than  $C_8$  showed about the same equilibrium ratios.

Fig. 3.21 gives the weight fraction liquid collected in the separator vials downstream of the back pressure regulators for the Rock Creek separator oil and Rock Creek separator oil with aromatics plotted against a dimensionless time scale (Orr & Silva 1982). As the experiment proceeded and  $CO_2$  was added to the system, the weight fraction liquid declined until the overall composition reached the two-phase region. The weight fraction liquid for both systems was identical in the two-phase region indicating that the addition of aromatics to a paraffinic oil did not change the total amount of hydrocarbons extracted into the upper phase by carbon dioxide, though the distribution of hydrocarbons extracted did change.

The experimental results presented here do not give a definitive answer concerning the effect of aromatics on  $CO_2$ -crude oil displacement behavior. It is not clear, for instance, whether the differences observed in the phase diagrams shown in Figs. 3.17 and 3.19 are the result of the addition of aromatics or the result of adding hydrocarbons of low molecular weight. An additional experiment, in which a paraffin mixture, with a molecular weight distribution similar to that of the aromatic mixture, is added to the crude oil combined with one-dimensional simulations (see §4), will be needed to assess the effect of molecular type in these multicomponent systems.

CO<sub>2</sub>-81-037

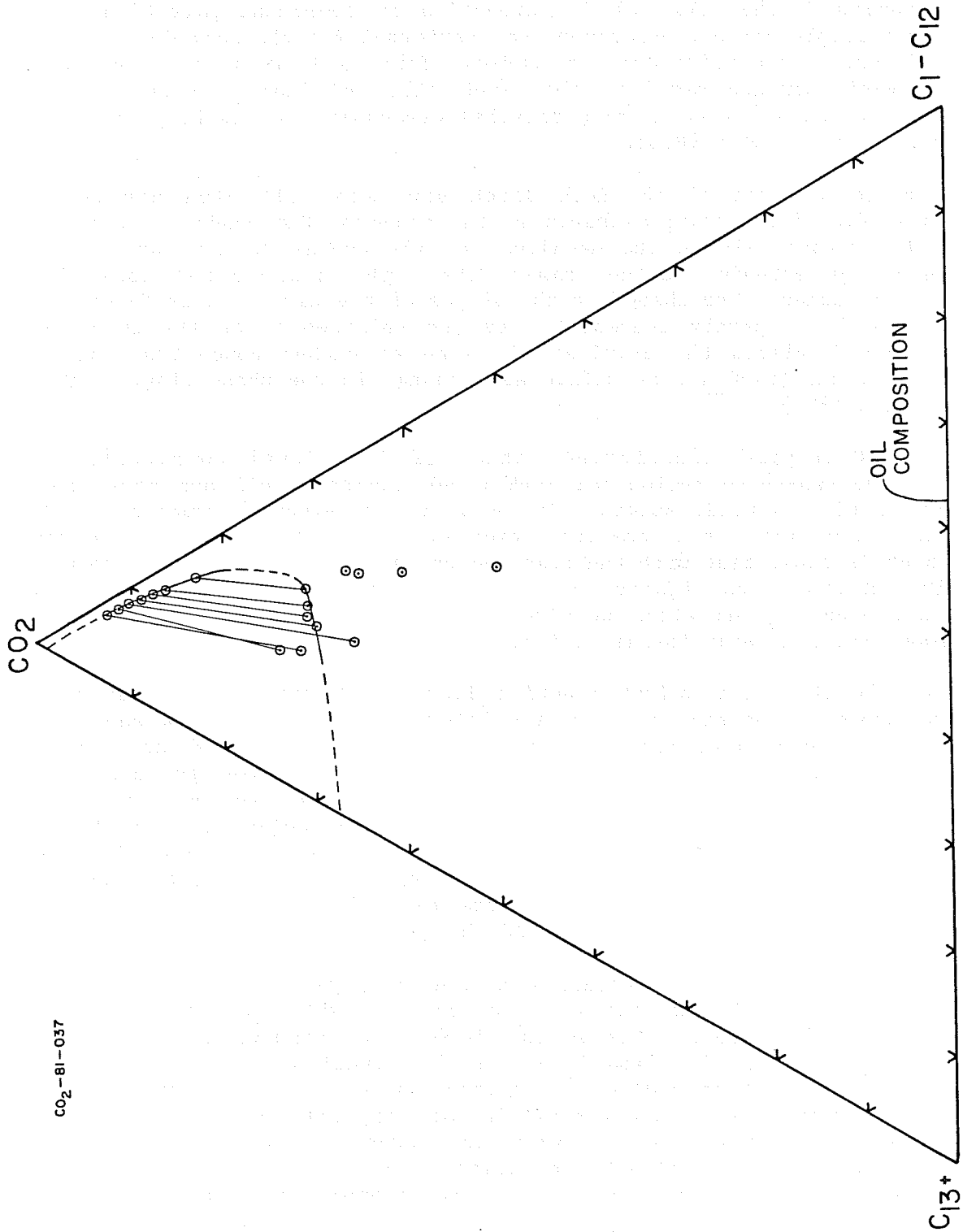


Fig. 3.19 Pseudo-ternary representation of phase compositions of mixtures of CO<sub>2</sub> with Rock Creek separator oil with aromatic spikes at 1300 psia and 75°F.

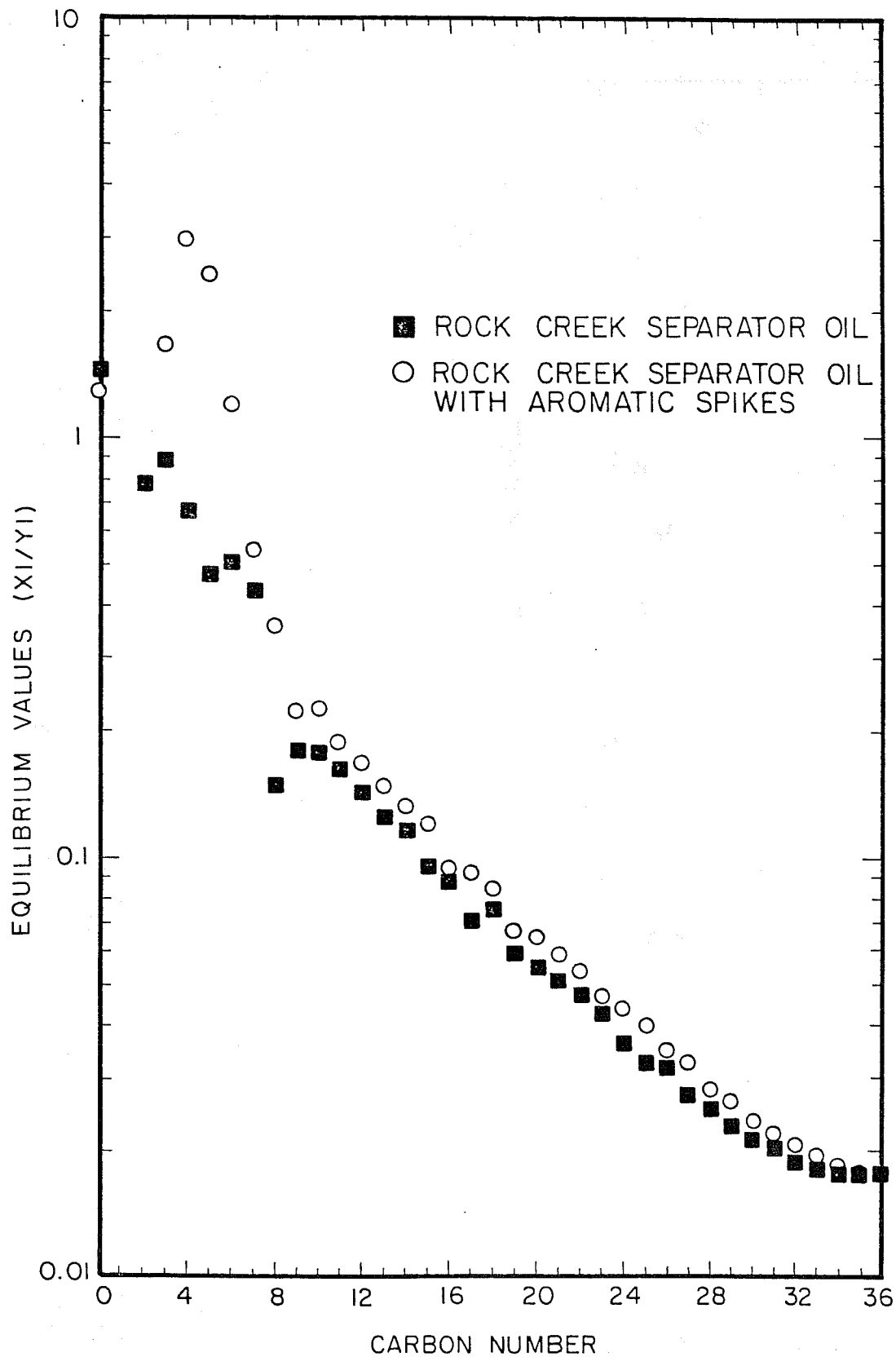


Fig. 3.20 Comparison of component partitioning for Rock Creek separator oil and Rock Creek separator oil with aromatic spikes.

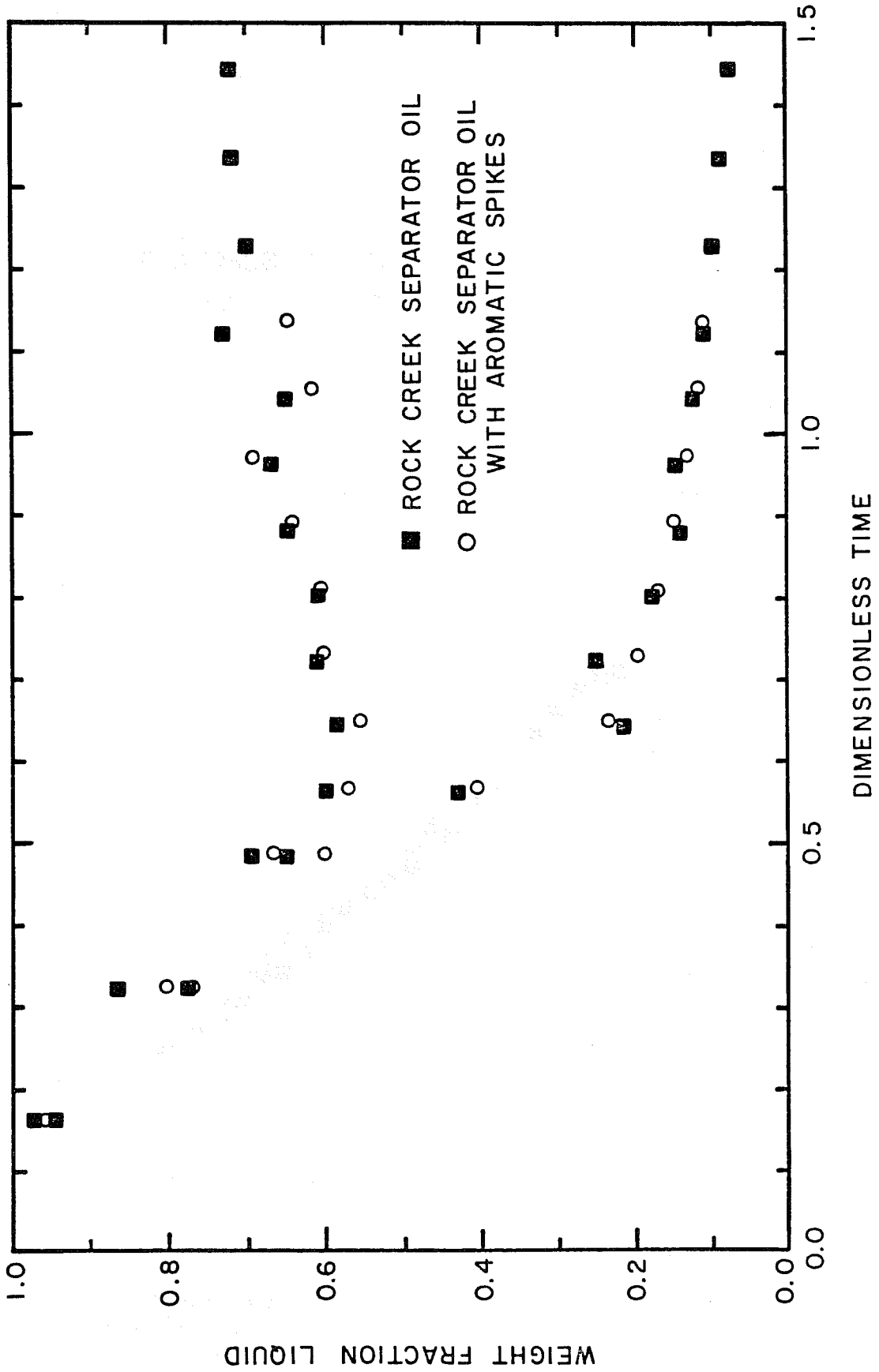


Fig. 3.21 Comparison of weight fraction liquid for Rock Creek separator oil and Rock Creek separator oil with aromatic spikes.

### 3.4 Conclusions

Results of measurements of the volumetric, compositional and fluid property behavior of CO<sub>2</sub>-crude oil mixtures lead to the following observations and conclusions:

- (1) The maximum temperature at which L<sub>1</sub>-L<sub>2</sub>-V phase separation occurs depends on the composition of the oil. Addition of solution gas to a dead oil reduces the maximum temperature for L<sub>1</sub>-L<sub>2</sub>-V formation.
- (2) For both dead and live oils, the L<sub>1</sub>-L<sub>2</sub>-V region occurs, if it occurs at all, at pressures close to the vapor pressure of CO<sub>2</sub>, extrapolated if the temperature is greater than the critical temperature of CO<sub>2</sub>. For temperatures below about 140°F, even if an L<sub>1</sub>-L<sub>2</sub>-V region does not occur, because the system temperature exceeds the maximum for such separations, the density of the CO<sub>2</sub>-rich phase increases sharply at the extrapolated vapor pressure.
- (3) The extrapolated vapor pressure is a reasonable estimate of the pressure required to make a CO<sub>2</sub>-rich phase dense and relatively incompressible. Such a phase should extract hydrocarbons efficiently. Thus, the extrapolated vapor pressure, plus a suitable safety margin, can be used as an estimate of the minimum miscibility pressure, as long as the temperature is below about 140°F.
- (4) Modifications to the circulation system of the continuous multiple contact apparatus allow larger portions of a phase diagram to be investigated. Control of the experiment and control of data acquisition by microcomputer improve its efficiency and reliability.
- (5) Preliminary testing of the use of an oscillating quartz crystal to measure viscosities of high pressure CO<sub>2</sub>-crude oil mixtures suggests that the measurement is feasible.
- (6) Addition of an aromatic mixture to a paraffinic crude oil changed the distribution of hydrocarbons extracted by a CO<sub>2</sub>-rich phase, but did not alter the total weight of hydrocarbons extracted.
- (7) Additional experiments are needed to delineate the effects of crude oil composition on CO<sub>2</sub>-crude oil phase behavior.

#### 4. ONE-DIMENSIONAL SIMULATION OF CO<sub>2</sub> DISPLACEMENTS

The complexity and variety of the physical effects which combine to determine the performance of a field scale CO<sub>2</sub> flood makes detailed simulation of a field displacement process a formidable task. No simulator currently available models all of the factors known to influence CO<sub>2</sub> flood performance (Orr, Silva, Lien & Pelletier 1981; Orr & Taber 1982). Nevertheless, simulation of even a limited collection of the process mechanisms is an important part of building understanding of the interactions of mechanisms inherent in the complex flows which develop during a CO<sub>2</sub> flood. Sensitivity of process performance to variations in phase behavior, fluid properties and other process variables can be investigated far more rapidly by simulation than by experiments. Such studies are convincing, however, only if the simulator can be shown to be quantitatively reasonable for the flows it attempts to model. In this section we report results of a test of the accuracy of the one-dimensional simulator by predicting the performance of slim tube displacements. While those displacements are substantially simpler than the flows which occur in reservoir rocks, they are a useful test of the predictive power of the simulator because the flow is very nearly one-dimensional and is strongly influenced by phase behavior. Clearly, it is important to establish whether the simulator is accurate for simple flows before more complex tests are attempted.

In addition, modifications to the one-dimensional simulator to include a model of the effects of an oil saturation which is inaccessible to injected fluid when the water saturation is high are described, and sample computational results are presented. Those calculations are part of a study aimed at improving understanding of interactions of changes in mixing of oil and CO<sub>2</sub>, caused by the presence of water, with the phase behavior of CO<sub>2</sub>-crude oil mixtures, which produces high oil recovery in stable secondary displacements.

##### 4.1 Quantitative Prediction of Slim Tube Displacement Performance

Simulations of slim tube displacements of Maljamar crude oil by CO<sub>2</sub> at four pressures were performed using a simple one-dimensional simulator similar to those described by Pope & Nelson (1978), Gardner, Orr & Patel (1981) and Orr (1980) but with one important difference. It models the effects of volume change on mixing by allowing each component to have a different density in each phase. In it, the oil is represented as two components, with CO<sub>2</sub> as the third component. Material balance equations for the three components are solved by an explicit finite difference method which allows the use of numerical dispersion to model qualitatively the effects of physical dispersion.

The calculations performed in the simulator are based on the following assumptions:

- (1) Darcy's law describes the flow of each of up to three phases.
- (2) The flow system has uniform cross section and properties, and fluids are uniform and well mixed in the direction transverse to flow.
- (3) Capillary pressure effects are negligible.
- (4) Local chemical equilibrium exists between phases.
- (5) The density of a phase can be calculated as a volume weighted average of constant apparent densities of each component in that phase.
- (6) Changes in pressure over the length of the displacement have negligible effect on the compositions and densities of the CO<sub>2</sub>-hydrocarbon mixtures.
- (7) CO<sub>2</sub>-crude oil phase behavior can be represented in terms of three components: CO<sub>2</sub>, light hydrocarbons, and heavy hydrocarbons.

Material balance equations for each component in the system have the form

$$\frac{\partial}{\partial \tau} \sum_j \rho_j x_{ij} S_j + \frac{1}{q_i} \frac{\partial}{\partial \xi} \sum_j \rho_j x_{ij} f_j q = 0 \quad i = 1, n_c \quad (4.1)$$

where  $\tau = (q_i t)/(\phi A L)$  is the dimensionless time scale based on the volumetric injection rate  $q_i$ ,  $t$  the time,  $\phi$ ,  $A$  and  $L$  the porosity, cross-sectional area and length of the slim tube,  $\rho_j$ ,  $S_j$  and  $f_j$  the molar density, fractional flow and saturation of phase  $j$ ,  $x_{ij}$  the mole fraction of component  $i$  in phase  $j$ ,  $\xi = x/L$  the dimensionless length, and  $q$  the local volumetric flow rate. The molar density of phase  $j$  is defined as

$$\rho_j = \left[ \sum_i (x_{ij}/\rho_{ij}) \right]^{-1} \quad (4.2)$$

where  $\rho_{ij}$  is the apparent molar density of component  $i$  in phase  $j$ . The fractional flow of phase  $j$  is defined as

$$f_j = \frac{k_{rj}/\mu_j}{\sum_i k_{ri}/\mu_j} \left\{ 1 - \frac{A k g \sin \alpha}{q} \left[ \sum_i \frac{k_{ri}}{\mu_i} (M_i \rho_i - M_j \rho_j) \right] \right\} \quad (4.3)$$

where  $\alpha$  is the dip angle,  $g$  gravity, and  $M_i$  and  $M_j$  are average molecular weights of phases  $i$  and  $j$ .

In finite difference form, equation (4.1) is

$$\left( \sum_j \rho_j x_{ij} S_j \right)_m^{n+1} = \left( \sum_j \rho_j x_{ij} S_j \right)_m^n - \frac{\Delta \tau}{q_i \Delta \xi} \left\{ \left( \rho_j x_{ij} f_{j,q} \right)_m^n - \left( \rho_j x_{ij} f_{j,q} \right)_{m-1}^n \right\} \quad (4.4)$$

where  $m$  is the grid block and  $n$  the time step. Equation (4.4) is used to calculate new overall compositions in each grid block. Phase behavior and fluid property routines then calculate new phase compositions, densities, and viscosities. Finally, fractional flows and local flow rates are calculated and the process repeated. The finite difference form applied here allows the use of time truncation error to cancel a portion of the spatial truncation error which provides some control of the level of numerical dispersion (Lantz 1971). Numerical dispersion can be used to model physical dispersion quantitatively as long as only one phase is flowing. When two phases are flowing, however, less control is possible because the nonlinearity of the fractional flow functions alters the level of numerical dispersion in such a way that it is no longer constant throughout the grid (Lantz 1971; Orr 1980). For instance, the composition and saturation profiles in Fig. 4.6 show evidence of more numerical dispersion in the single phase regions than in the two-phase portions of the flow. The simulations reported here were all performed with 100 grid blocks and a time step size of 0.00125, which represents a compromise between numerical dispersion, stability and computation cost. It should be noted that the dispersion, numerical or physical, does alter computed composition paths and hence oil recovery (Gardner, Orr & Patel 1981).

Simple polynomial representations of ternary diagrams are used to enter the phase behavior data into the simulator. Phase behavior of mixtures of CO<sub>2</sub> with Maljamar crude oil was measured using the continuous multiple contact experiment (see Orr, Silva & Lien 1983 for details of the experiments). Pseudo-ternary phase diagrams obtained in those experiments, all of which were performed at 32°C (90°F), are shown in Figs. 4.1 - 4.4 for four pressures, 5520, 6890, 8270 and 9650 kPa (800, 1000, 1200 and 1400 psia).

Detailed gas, liquid, and phase composition data are available separately (Silva et al 1981d; Silva et al 1982a; Silva et al 1981a; Silva et al 1981c). In the displacement at 5520 kPa, only a small portion of the phase diagram was scanned because very small amounts of hydrocarbons were extracted into the upper (vapor) phase (Fig. 4.1). The vapor phase was nearly pure CO<sub>2</sub> and hence, the composition of the oil in the cell changed little during the displacement. A CO<sub>2</sub> flood of Maljamar separator oil at 5520 kPa would be immiscible.

At 6890 kPa (Fig. 4.2), the phase diagram is much more complex. The displacement entered the liquid-liquid (L<sub>1</sub>-L<sub>2</sub>) region first and then with continued CO<sub>2</sub> injection reached the liquid-liquid-vapor (L<sub>1</sub>-L<sub>2</sub>-V) region. The tie lines shown in the L<sub>1</sub>-L<sub>2</sub> region confirm that more efficient extraction of C<sub>1</sub>-C<sub>12</sub> hydrocarbons takes place in the L<sub>1</sub>-L<sub>2</sub> region than in the L<sub>1</sub>-V region. At 8270 kPa (Fig. 4.3), the displacement passed only through the liquid-liquid region in which extraction of hydrocarbons was much more efficient. Similar

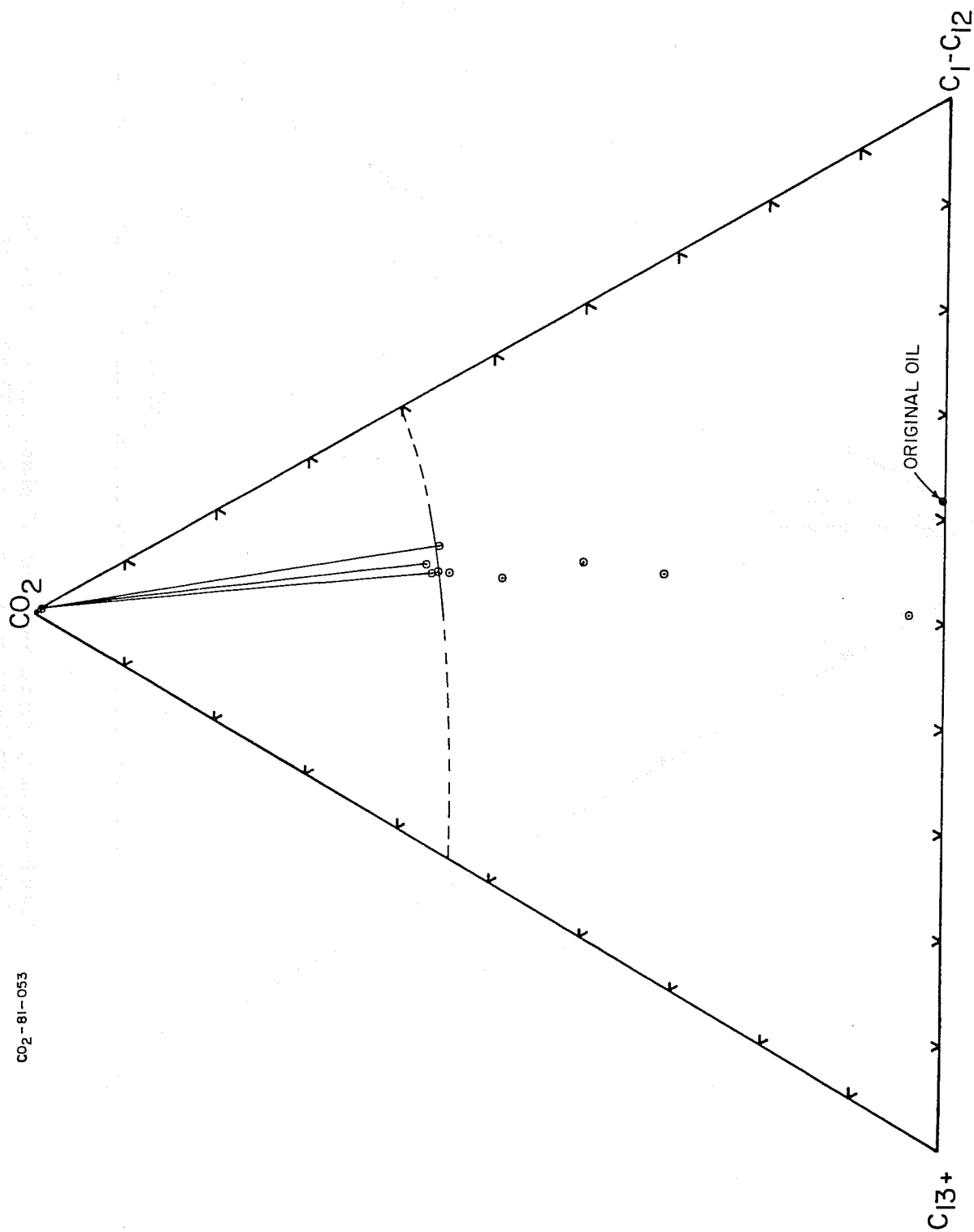


Fig. 4.1 Pseudo-ternary representation of phase compositions for mixtures of CO<sub>2</sub> with Maljamar separator oil at 5520 kPa and 32°C.

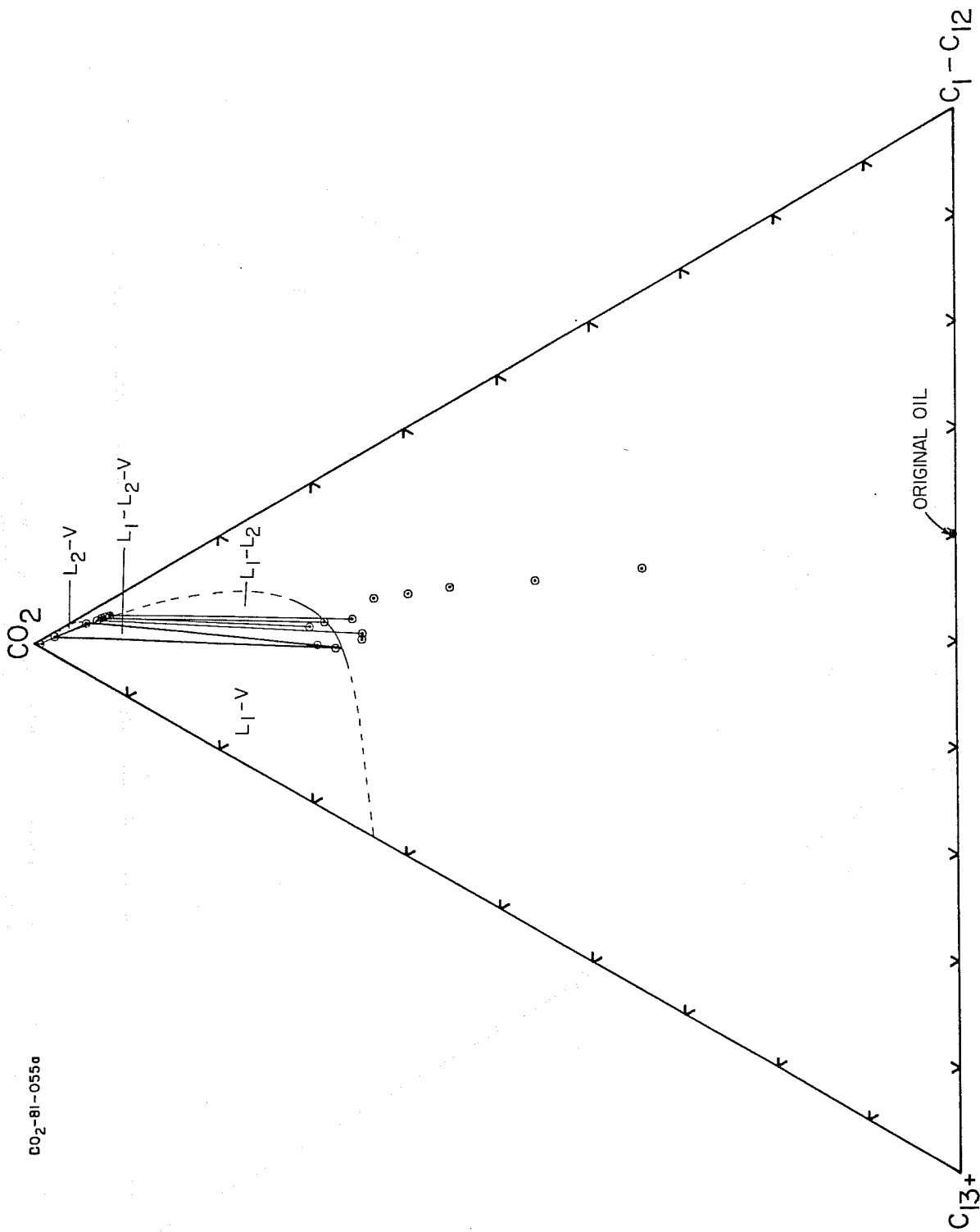


Fig. 4.2 Pseudo-ternary representation of phase compositions for mixtures of CO<sub>2</sub> with Maljamar separator oil at 6890 kPa and 32°C.

CO<sub>2</sub>-81-054

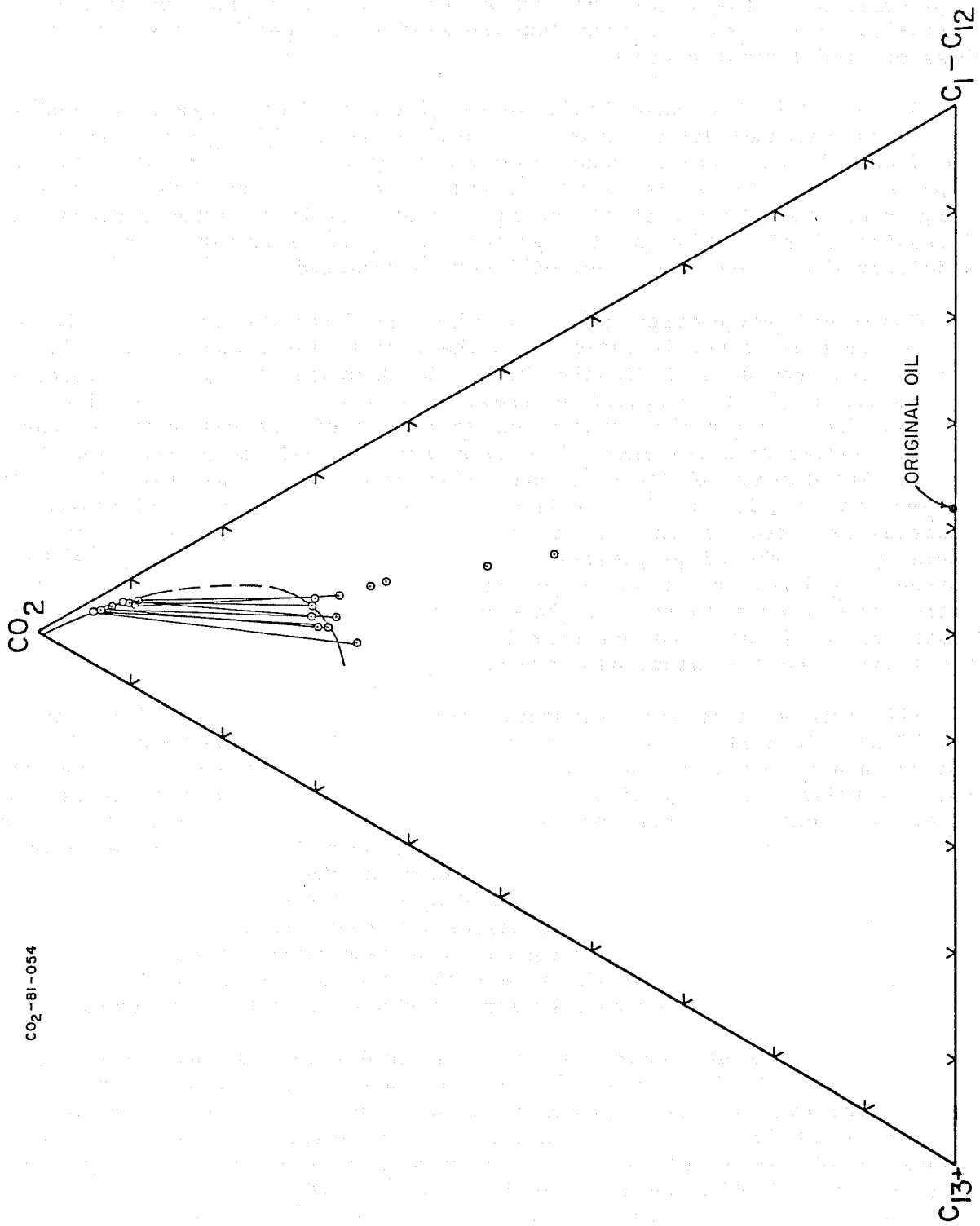


Fig. 4.3 Pseudo-ternary representation of phase compositions for mixtures of CO<sub>2</sub> with Maljamar separator oil at 8270 kPa and 32°C.

behavior was observed at 9650 kPa (Fig. 4.4). The differences between the two displacements at the higher pressures were smaller because compositions of liquid-liquid systems are much less sensitive to pressure changes than are those of liquid-vapor systems.

Gas-oil relative permeability data given by Naar, Wygal & Henderson (1962) for unconsolidated sands were used without adjustment. Because the experimentally determined phase diagrams reported here match closely those proposed by Orr, Yu & Lien (1981) based on single contact PVT data and an analysis of the behavior of binary and ternary CO<sub>2</sub>-hydrocarbon systems, their discussion of simulation of the effects of phase behavior on displacement efficiency also applies here and will not be repeated.

Component properties used in the simulations of the slim tube displacements are given in Table 4.1. The viscosities shown in Table 4.1 were interpolated from data of Michels, Botzen & Schuurman (1957). The viscosities and densities of the hydrocarbon pseudo-components were estimated (McCain 1973) so that the overall density and viscosity of the oil matched measured values. Hydrocarbon component densities were assumed to be the same in all phases. The density of CO<sub>2</sub> in a vapor phase was taken to be that of pure CO<sub>2</sub>. The apparent density of CO<sub>2</sub> in liquid phases, however, was calculated from densities measured in the continuous multiple contact experiment. For simulations of the displacements at 8270 and 9650 kPa, slightly different apparent CO<sub>2</sub> densities in the CO<sub>2</sub>-rich liquid were used in different regions of the phase diagram to reflect the experimental observation that the apparent density of CO<sub>2</sub> is not constant over large ranges in composition (Orr, Silva & Lien 1983). The two values used are also given in Table 4.1.

Slim tube studies were performed using a 12.2 m (40 ft.), 0.635 cm (1/4 in.) ID stainless steel tube packed with 170-200 mesh glass beads. The slim tube had a pore volume of 147.3 cm<sup>3</sup> and a permeability of 5800 md. The packed tube was rolled into a 25.4 cm (10 in.) diameter coil, and installed in a temperature controlled water bath. In all slim tube displacements, the bead pack was first completely saturated with oil, then CO<sub>2</sub> was injected into the top, and fluids were produced from the bottom of the coiled tube. Just prior to the start of CO<sub>2</sub> injection, oil was displaced through the pack at the run displacement rate to establish a pressure gradient, with the pressure at the outlet controlled to the test pressure by a back pressure regulator. Then, CO<sub>2</sub> injection was started at the same rate. The amount of oil recovered was determined by weight rather than by less accurate volumetric measurements.

Results of displacements at the same conditions as those used in the continuous multiple contact experiments are given in Fig. 4.5. The scales used to plot Fig. 4.5 deserve some comment. The time scale is presented as pore volumes of CO<sub>2</sub> injected. Because the run temperature was very near the critical temperature of CO<sub>2</sub>, its density was sensitive to the change in pressure gradient which occurred as low viscosity CO<sub>2</sub> replaced high viscosity oil. The volume of CO<sub>2</sub> injected at a point during the run was calculated as the volume of mercury injected into the thermostatted CO<sub>2</sub> supply vessel plus the expansion of the total volume of CO<sub>2</sub>.

It is clear from Fig. 4.5 that the volume of CO<sub>2</sub> calculated as described

CO<sub>2</sub>-81-055

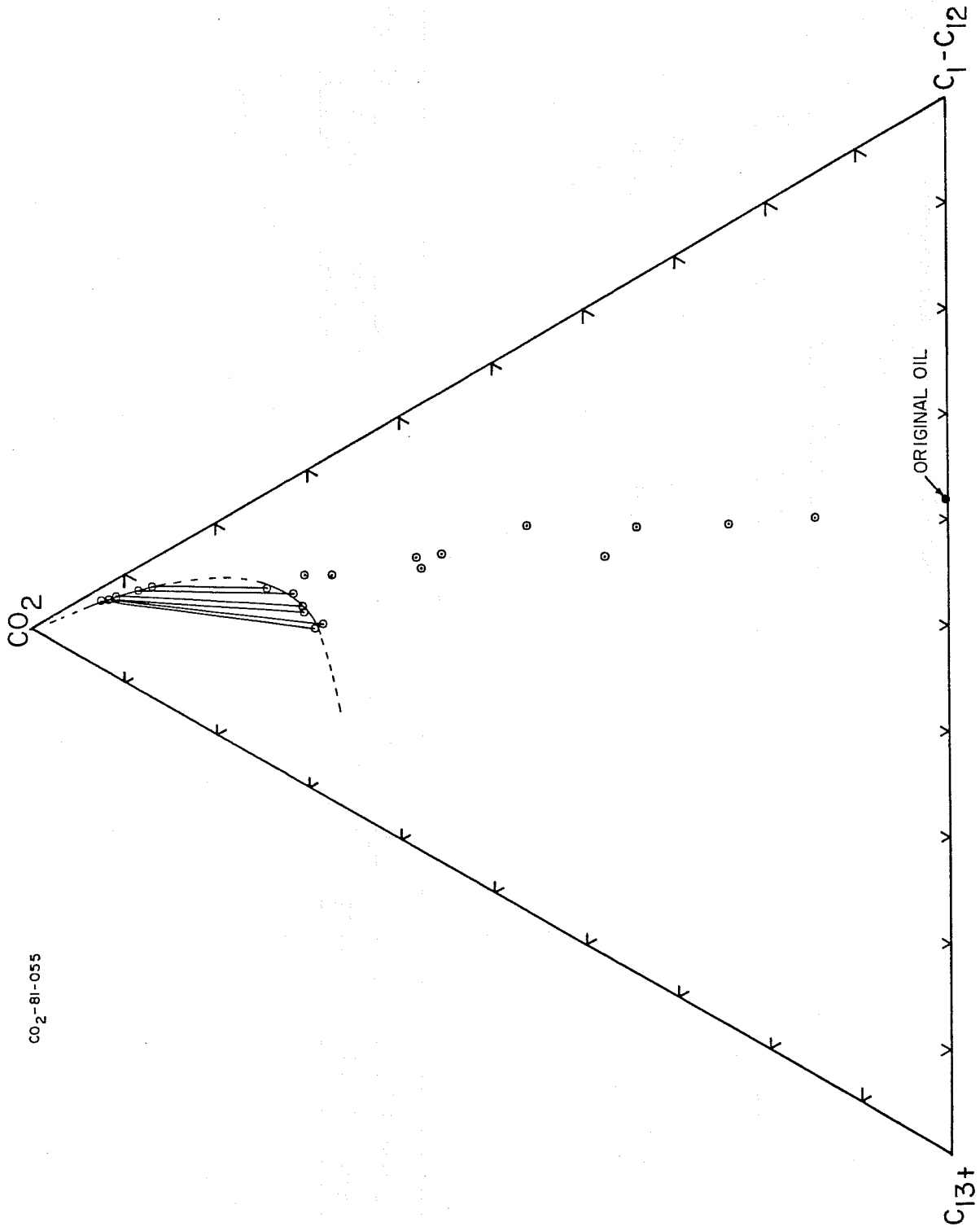


Fig. 4.4 Pseudo-ternary representation of phase compositions for mixtures of CO<sub>2</sub> with Maljamar separator oil at 9650 kPa and 32°C.

Table 4.1 Component Properties for Simulations of Slim Tube Displacements

Component	Molecular Weight	Viscosity (mPa·s)			
		5520 kPa	6890 kPa	8270 kPa	9650 kPa
CO <sub>2</sub>	44	0.0176	0.021	0.052	
C <sub>5</sub> -C <sub>12</sub>	119	0.89	0.89	0.89	0.89
C <sub>13+</sub>	323	18.96	18.96	18.96	18.96

Component	Density (g/cm <sup>3</sup> )											
	5520 kPa		6890 kPa		8270 kPa		9650 kPa		CO <sub>2</sub> -rich		Oil-rich	
	Vapor	Liquid	Vapor	Liquid	Vapor	Liquid	Vapor	Liquid	Liquid	Liquid	Liquid	Liquid
CO <sub>2</sub>	0.143	0.918	0.2313	0.780	0.898	0.898	0.74, 0.82	0.895	0.79, 0.83	0.893	0.893	0.893
C <sub>5</sub> -C <sub>12</sub>	0.689	0.689	0.696	0.696	0.696	0.696	0.702	0.702	0.708	0.708	0.708	0.708
C <sub>13+</sub>	0.978	0.978	0.978	0.978	0.978	0.978	0.978	0.978	0.978	0.978	0.978	0.978

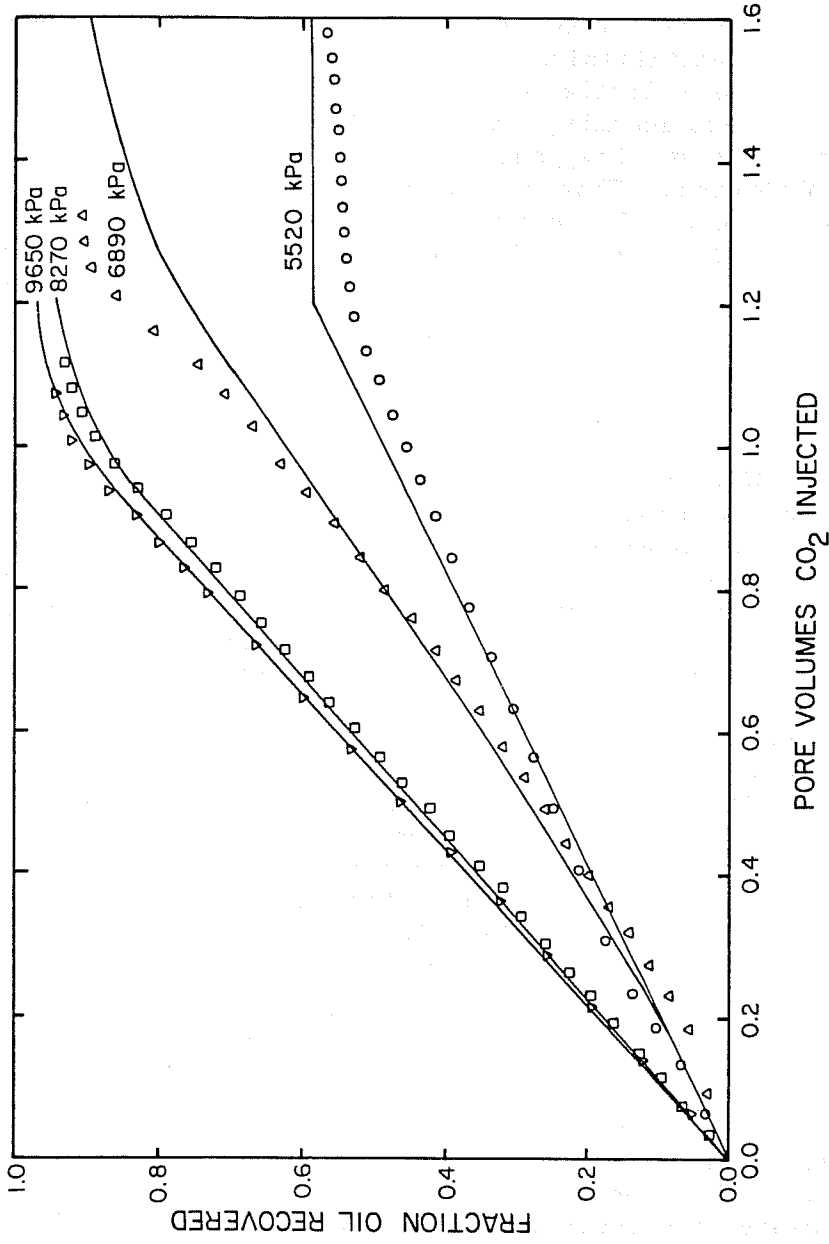


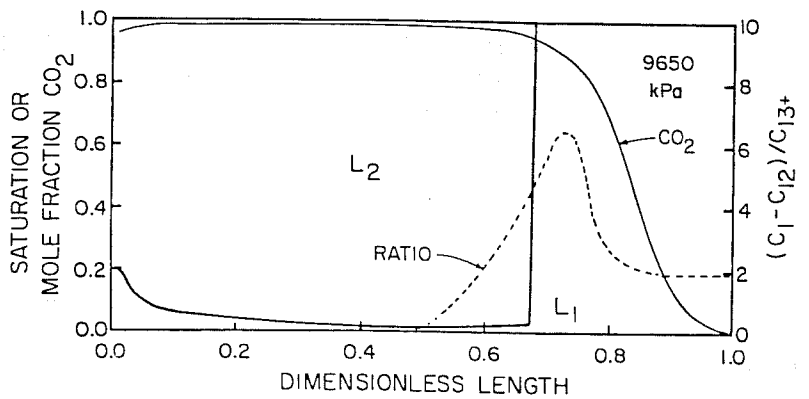
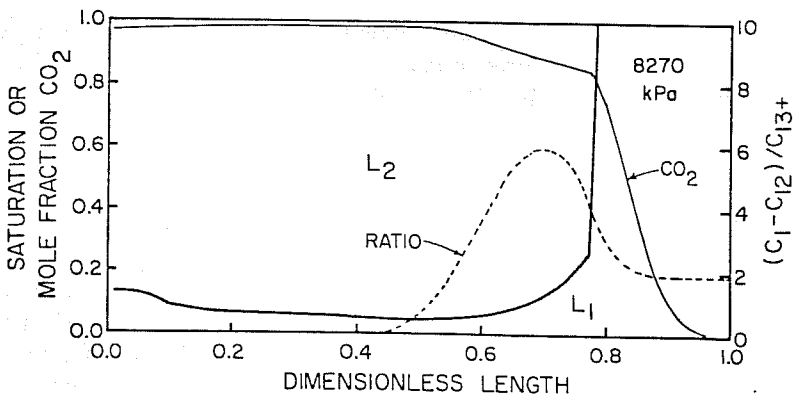
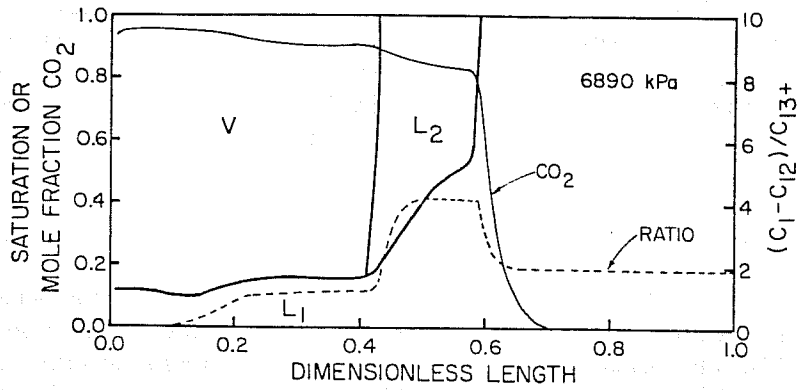
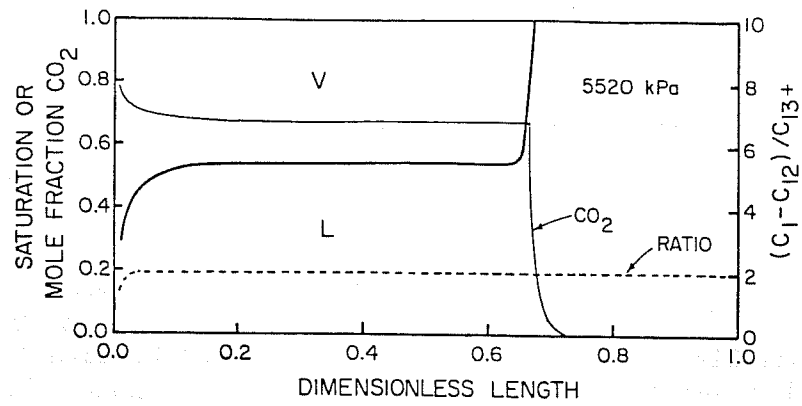
Fig. 4.5 Comparison of calculated (line) and experimental (symbols) oil recovery in slim tube displacements of Maljamar separator oil by CO<sub>2</sub> at 32°C.

above is not an accurate measure of the actual volume of oil displaced at 5520 and 6890 kPa (800 and 1000 psia). In those displacements, the amount of oil recovered early in the runs was significantly less than the apparent volume injected, and in both runs CO<sub>2</sub> breakthrough occurred at an apparent injection of more than one pore volume. The explanation for the observed behavior lies in the interplay of the solubility of CO<sub>2</sub> in the oil, volume change on mixing, and the effect of component partitioning on displacement efficiency. In the displacement at 5520 kPa, very little extraction of hydrocarbons by CO<sub>2</sub> occurred (see Fig. 4.1). Consequently, the displacement was immiscible, the local displacement efficiency was low, and almost 50 percent of the oil was left behind at CO<sub>2</sub> breakthrough. That oil was saturated with CO<sub>2</sub>, however, and since the quantity of oil left behind was large, the amount of CO<sub>2</sub> required to saturate it was also large. The apparent density of CO<sub>2</sub> dissolved in the oil (defined as the mass of CO<sub>2</sub> dissolved divided by the volume increase of the swollen oil over original oil) is, however, much greater than the density of pure CO<sub>2</sub> at the same pressure. Thus, the effect of the volume change of CO<sub>2</sub> upon dissolution in the oil is to reduce the effective volume of CO<sub>2</sub> injected.

The displacements at 8270 and 9650 kPa (1200 and 1400 psia) were affected much less by volume change on mixing for two reasons. First, the density of pure CO<sub>2</sub> was much nearer the apparent density of CO<sub>2</sub> in solution, so that there was much less volume change. Second, the local displacement efficiency was much higher, and hence there was much less oil remaining to be saturated with CO<sub>2</sub>. Thus, the corrections for volume change were much smaller at the higher pressures. Simulation results reported below confirm this explanation.

It is evident from the results shown in Fig. 4.5 that the displacement of oil by vapor phase CO<sub>2</sub> at 5520 kPa was much less efficient than the displacements in which a CO<sub>2</sub>-rich liquid phase was present. The phase compositions presented above clearly indicate that extraction of hydrocarbons by a CO<sub>2</sub>-rich liquid is more efficient than that of a vapor, but that fact alone does not prove that more efficient extraction is responsible for the dramatic improvement in oil recovery at 6890 kPa over that obtained at 5520 kPa. The solubility of CO<sub>2</sub> in the oil changes with pressure as does its viscosity and density. Assessment of the relative importance of variations of extraction, solubility and fluid properties is a task for simulation.

Fig. 4.5 also compares calculated oil recoveries with the experimental results. With the exception of the run at 6890 kPa, the agreement is good. Calculated oil recoveries increase with increasing pressure, and the rates of recovery in the simulated displacements match well with the experimental rates. Fig. 4.6 shows computed saturation distributions for each displacement at 0.8 PV injected (based on the density of pure CO<sub>2</sub> at the displacement pressure). At 5520 kPa, the liquid phase occupies more than 50% of the volume of the swept zone though part of that volume is dissolved CO<sub>2</sub>. Also plotted in Fig. 4.6 is the ratio of the mole fraction of the light hydrocarbon pseudo-component (C<sub>5</sub>-C<sub>12</sub>) to that of the heavy hydrocarbon pseudo-component (C<sub>13+</sub>). Because the vapor phase at 5520 kPa extracts only small quantities of hydrocarbons, the ratio hardly changes. The only compositional effect in that displacement comes from the solubility of the CO<sub>2</sub> in the oil. Because the displacement is relatively inefficient and the solubility and apparent density



CO<sub>2</sub>-82-014

Fig. 4.6 Calculated saturation and composition profiles at 0.8 pore volumes CO<sub>2</sub> injected.

of CO<sub>2</sub> are both high, much of the injected CO<sub>2</sub> simply dissolves in the oil rather than displacing it. Thus, the displacement proceeds slowly as shown in Fig. 4.5.

At 6890 kPa, a CO<sub>2</sub>-rich liquid (L<sub>2</sub>) displaces oil and is in turn displaced by CO<sub>2</sub>-rich vapor. The residual liquid phase is much smaller, and the ratio of light to heavy hydrocarbons indicates a zone in which the L<sub>2</sub> phase has preferentially extracted light hydrocarbons. Because the residual oil phase is smaller and because the injected CO<sub>2</sub> is denser, there is less volume change and the displacement proceeds more rapidly on a time scale based on the volume of pure CO<sub>2</sub> injected. At 8270 kPa, the displacement is still more efficient. The saturation of the residual L<sub>1</sub> phase is smaller and the ratio of light to heavy hydrocarbons indicates more efficient extraction. At 9650 kPa, the transition zone enriched in light hydrocarbons is sharper and the residual saturation is slightly smaller than at 8270 kPa. Both displacements recover well over 90% of the oil in place (see Fig. 4.5).

The difference between the computed and observed recovery at 6890 kPa deserves comment. The total amount of oil recovered in the simulation is nearly the same as that observed, but the time scale in the simulation is obviously not correct late in the run. This occurs because the representation of phase densities in the simulator is too simple. Measurements at 6890 kPa (Orr, Silva & Jensen 1982) suggest that the density of the CO<sub>2</sub>-rich liquid declines rapidly as the overall composition approaches the liquid-liquid-vapor region. That fact is not modeled in the simulator, which treats the density of CO<sub>2</sub> in the CO<sub>2</sub>-rich liquid as constant. Therefore, late in the calculated displacement, the CO<sub>2</sub> present in the CO<sub>2</sub>-rich liquid occupies less volume than in the experiment, and hence the calculated rate of fluid production is too low.

As Fig. 4.5 indicates, recovery of oil in slim tube displacements increases with increasing pressure, as has long been known. Even in a very simple porous medium, however, displacement of oil by CO<sub>2</sub> is the result of a complex interplay of phase behavior, fluid properties and multiphase flow. Sensitivity studies with the simulator used here, as well as with the version which does not allow volume change on mixing, lead to the following observations:

- (1) The viscosity of CO<sub>2</sub>, or of a CO<sub>2</sub>-rich phase, is sufficiently low that the increase in that viscosity with pressure produces a negligible increase in oil recovery if all other factors are held constant. The efficiency of such adverse mobility displacements remains low. Thus, changes in the viscosity of CO<sub>2</sub> do not account for improved recovery with increasing pressure.
- (2) An increase in the density of dissolved CO<sub>2</sub>, with other factors constant, reduces oil recovery because the volume occupied by CO<sub>2</sub> in the oil phase is lower.
- (3) An increase in the solubility of CO<sub>2</sub> in oil increases recovery because the fraction of the remaining oil phase which is

actually oil is reduced. However, the solubility of CO<sub>2</sub> in crude oil usually does not exceed 60-80 mol % at reasonable pressures and typical CO<sub>2</sub> volume fraction at such pressures would be less than 0.50. Thus, solubility increases alone do not explain recoveries of 95%.

- (4) Improvement in the efficiency with which CO<sub>2</sub> extracts light and intermediate hydrocarbons from the oil, with all other factors constant, does produce an increase in recovery. Simulations presented here and by Gardner, Orr & Patel (1981) and Orr, Yu & Lien (1981) clearly establish that improved extraction can account for improved recovery with increasing pressure in CO<sub>2</sub>-crude oil systems in which the temperature is low enough that liquid-liquid phase behavior occurs.
- (5) Total recovery is determined by phase behavior, but the rate of recovery is determined by volume change on mixing.

The combination of simulations and experiments presented offers some guidance on the selection of pressure levels for field projects. Because extraction by a dense CO<sub>2</sub>-rich liquid phase is so much more efficient than that of a low density vapor phase, and because extraction (or vaporization in systems too high in temperature to show liquid-liquid behavior) accounts for the high local displacement efficiency which is a fundamental part of any successful CO<sub>2</sub> flood, it seems reasonable to select an operating pressure which avoids the presence of a phase of high mobility and low extractive power. The simple correlation discussed in §3 can be used to estimate that pressure. It has been suggested, however, that it might be beneficial to operate a CO<sub>2</sub> flood in the liquid-liquid-vapor region to take advantage of the mobility control which might result from the interference to flow of multiple phases (Henry and Metcalfe 1980; Yellig 1981). In any case, the pressure ranges over which three phases coexist are fairly small, so that controlling field pressure to stay within that range in a significant fraction of a reservoir might be difficult. We believe that it would be preferable to err on the high-pressure side of the liquid-liquid-vapor region where extraction is known to be more efficient.

The simulator used here is, by design, simple in its mathematical approach and in the representation of the complex phase behavior of CO<sub>2</sub>-crude oil systems. Nevertheless, it produces results which agree well with experimental displacements. Given the simplicity of the representations used for the phase behavior and density effects, the agreement obtained is remarkable. We emphasize that no attempt was made to adjust the phase behavior, fluid properties, or relative permeabilities used in the simulations. The calculated oil recoveries are, therefore, predictions based solely on independent measurements of phase compositions and densities for the CO<sub>2</sub>-crude oil system used. The fact that good quantitative agreement was obtained between prediction and experiment offers encouragement that representations of CO<sub>2</sub>-crude oil phase behavior in terms of a small number of pseudo-components may be feasible. Such representations are essential if field scale simulations which account for phase behavior are to be successful.

#### 4.2 Effect of a Trapped Oil Saturation on One-Dimensional Displacement Performance

To assess the potential impact of the existence of some fraction of the oil saturation which is isolated by water and hence inaccessible to injected fluid, the one-dimensional simulator described in §4.1 was modified to include a very simple model of trapping. This preliminary model is based on the following assumptions:

- (1) Only nonwetting phase(s) may be trapped.
- (2) The fraction of the total nonwetting saturation which is trapped is a function of the water saturation only.
- (3) If more than one nonwetting phase is present, a fraction of each is trapped. The total trapped saturation is distributed between phases in proportion to their saturations.
- (4) A trapped phase does not mix with flowing fluid or other trapped phases.
- (5) A trapped phase has a uniform composition.

The algorithm used in the calculations is:

- (1) From the overall composition in the flowing phase, calculate compositions and saturations.
- (2) Calculate phase properties, relative permeabilities and fractional flows.
- (3) From the water saturation, calculate the total trapped saturation.
  - If the total trapped saturation has increased from the previous time step, calculate the amount of each component to be added to the number of moles of that component already trapped in each phase.
  - If the total trapped saturation has decreased from the previous time step, calculate the amount of each component to be released from each phase to the flowing stream.
- (4) Use material balance equations to calculate new overall compositions:

$$\left\{ \begin{array}{l} \text{Moles of} \\ \text{component } i \\ \text{present in} \\ \text{flowing stream in} \\ \text{grid block} \\ \text{at } t + \Delta t \end{array} \right\} = \left\{ \begin{array}{l} \text{Moles of} \\ \text{ } i \text{ present in} \\ \text{flowing stream} \\ \text{at } t \end{array} \right\} + \left\{ \begin{array}{l} \text{Net} \\ \text{Inflow} \\ \text{of } i \end{array} \right\} - \left\{ \begin{array}{l} \text{Moles of} \\ \text{ } i \text{ trapped} \\ \text{during} \\ \text{time step} \end{array} \right\}$$

$$\left\{ \begin{array}{l} \text{Moles of} \\ \text{component } i \\ \text{trapped in} \\ \text{grid block at} \\ \text{ } t + \Delta t \end{array} \right\} = \left\{ \begin{array}{l} \text{Moles of } i \\ \text{trapped at} \\ \text{ } t \end{array} \right\} + \left\{ \begin{array}{l} \text{Moles of} \\ \text{ } i \text{ trapped} \\ \text{during} \\ \text{time step} \end{array} \right\}$$

Return to step (1).

This algorithm treats the trapped phases as if they are individually mixed, even though fluids trapped at different times have different compositions. Physically, this is not strictly correct. Fluids which become isolated at different times are probably physically segregated. Unfortunately, a calculation which rigorously accounted for the compositions of fluids trapped at different times and, for instance, released first that fluid which was trapped last, would require a set of compositions to be stored for each time step. The computer memory required would be unacceptable even for a one-dimensional calculation. In the calculations reported here, therefore, the simulator maintained only a total of the number of moles of a component trapped in any of the up to three nonwetting phases. It should be noted that it has not been established that nonwetting phases trap in proportion to their saturations. That question has not been investigated. We make the assumption only because some recipe for trapping nonwetting phase must be specified in the simulator. In the absence of experimental evidence or theory to the contrary, the assumption appears to be as reasonable as others we considered.

#### Sample Calculations

To test the operation of the simulator and to obtain a preliminary indication of the potential impact of an interaction of phase behavior and trapping, a series of one-dimensional simulations were performed using the phase behavior for CO<sub>2</sub>-Maljamar oil mixtures at 90°F and 1000 psia, shown in Fig. 4.2. Gas-oil and water-oil relative permeability data reported by Corey (1956) for a sandstone and measurements of trapped oil saturations reported by Salter & Mohanty (1982) for a Berea core were used in the simulations. The following calculations were each performed with and without the model of trapping for two sets of initial saturations, oil plus connate water

(secondary displacements), and residual oil plus water (tertiary displacements):

- (1) Continuous CO<sub>2</sub> injection
- (2) Simultaneous injection of CO<sub>2</sub> and water
  - 70% CO<sub>2</sub> - 30% water by volume
  - 50% CO<sub>2</sub> - 50% water
  - 30% CO<sub>2</sub> - 70% water
- (3) Alternate injection of CO<sub>2</sub> and water slugs (each 0.2 PV of injection was divided as follows)
  - 70% CO<sub>2</sub> - 30% water by volume
  - 50% CO<sub>2</sub> - 50% water
  - 30% CO<sub>2</sub> - 70% water.

Results of the thirteen simulations are summarized in Figs. 4.7-4.10. Reported are the fractions of light and heavy components recovered after one pore volume of total fluid injection (based on the density of pure CO<sub>2</sub>). Results of the secondary displacements are compared in Figs. 4.7 and 4.8. About 86% of the oil in place was recovered at one pore volume injected by continuous CO<sub>2</sub> injection (Fig. 4.7). In that case, trapping had no effect because there was no mobile water present. Simultaneous injection of CO<sub>2</sub> and water led to slightly lower recovery when the volume fraction of water in the injected fluid was 30% and 50%. The calculated recovery for the trapped oil version was only slightly lower than that of the original simulator because the water saturation was low enough that only a small portion of the oil was isolated from mixing with the CO<sub>2</sub>. At 70% water in the injected fluid, both models predicted higher recoveries than that for continuous CO<sub>2</sub> injection, though the recovery with trapping was lower. The recovery with and without trapping was higher because the high water saturation (82%) reduced the relative permeability of CO<sub>2</sub> enough that CO<sub>2</sub> breakthrough was delayed and hence the recovery of oil was greater at one pore volume injected. That effect is, of course, the rationale behind the injection of water simultaneously or alternately with CO<sub>2</sub>. The water is intended to reduce the mobility of CO<sub>2</sub>, hence reducing the tendency for viscous fingering. It is clear from Fig. 4.7 that effects of trapping offset some of the benefits of that mobility reduction. In all the cases investigated, however, injection of CO<sub>2</sub> with water recovered more oil than did water alone.

The oil recoveries shown in Fig. 4.7 are not, however, an accurate representation of the benefits of water injection in multidimensional flows. There can be no viscous instability in one-dimensional displacements, so the recoveries calculated for continuous CO<sub>2</sub> injection in one dimension are higher

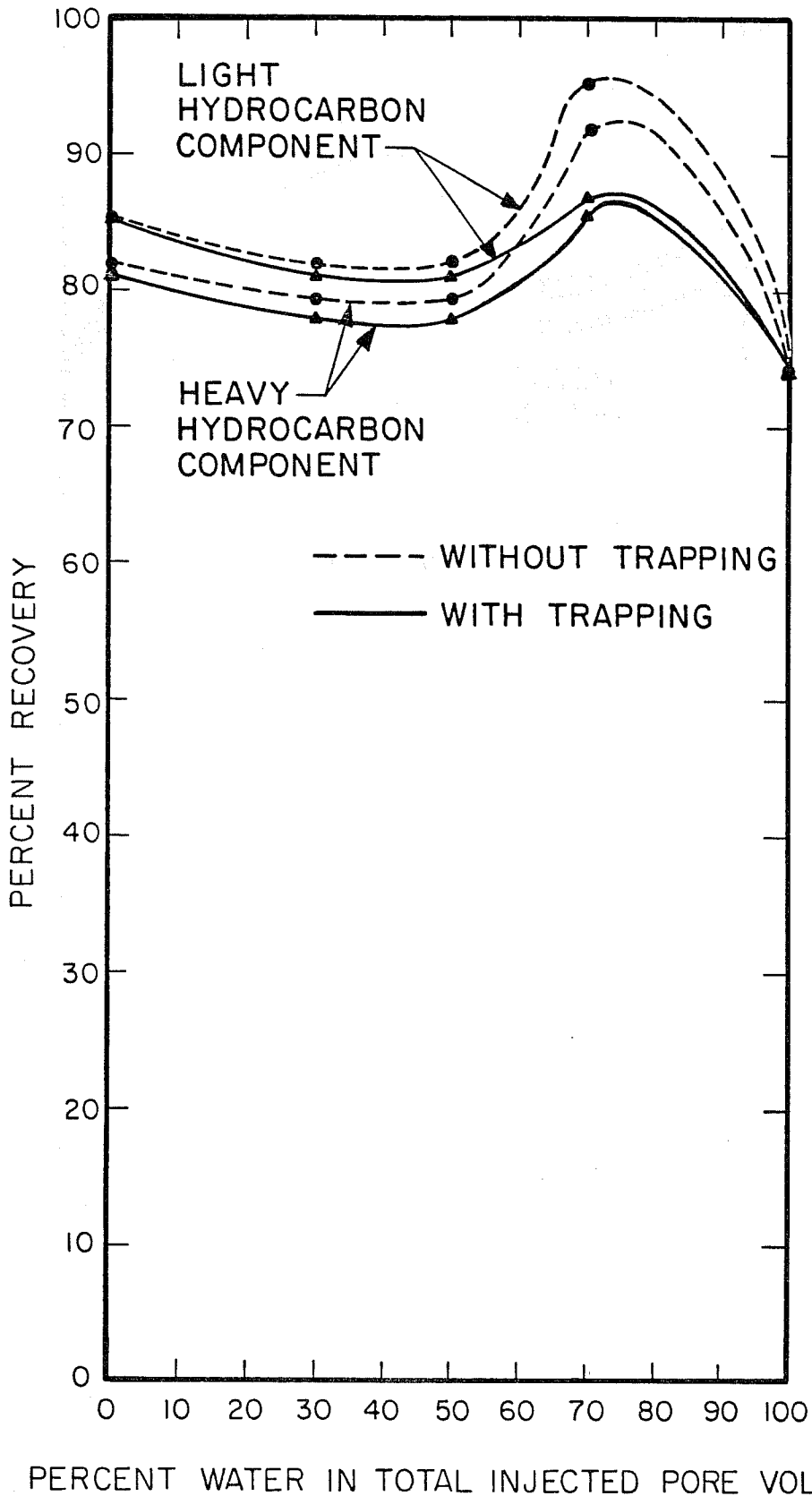


Fig. 4.7 Secondary oil ( $S_{wi} = 0.312$ ) recovered by simultaneous injection of CO<sub>2</sub> and water.

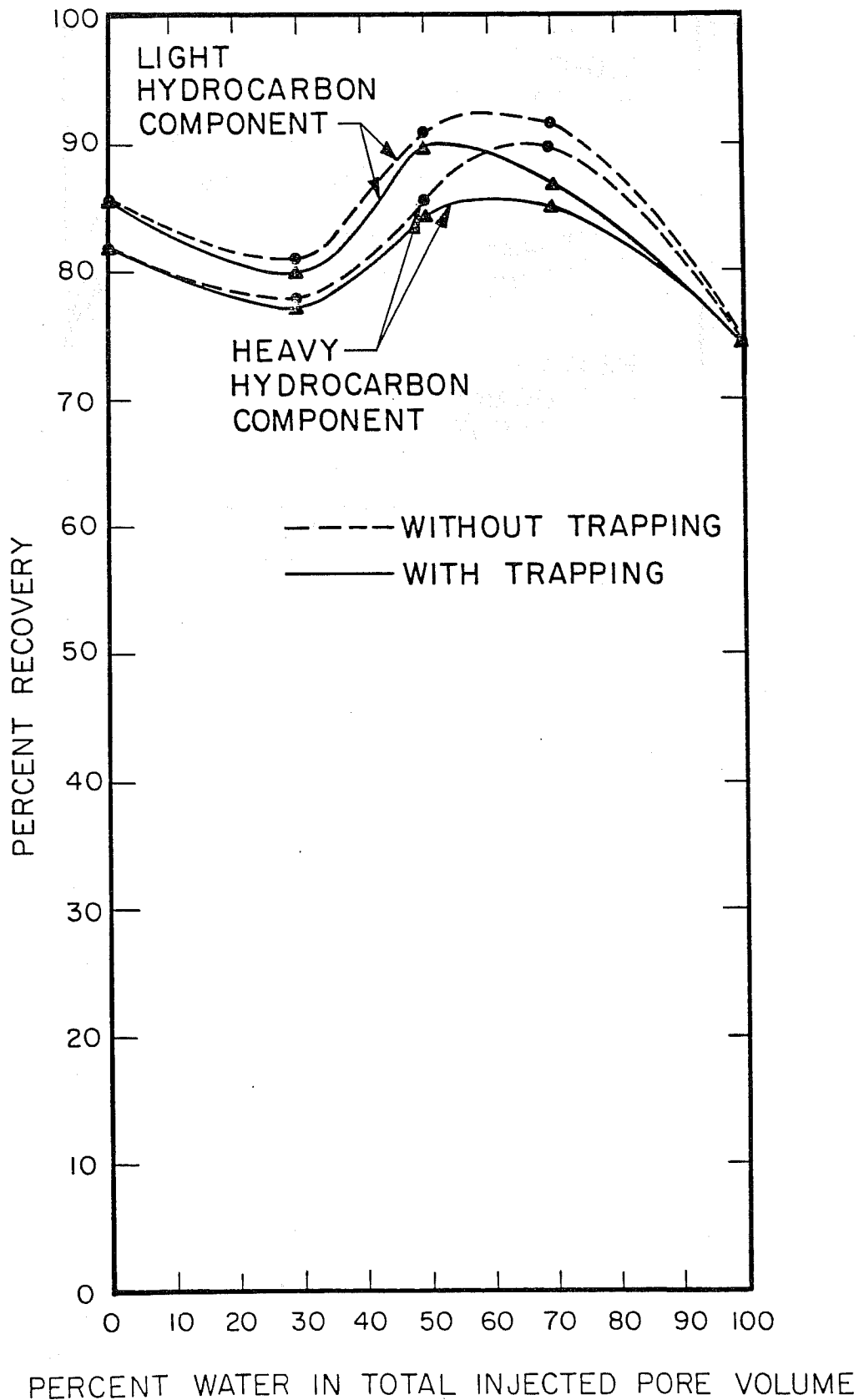
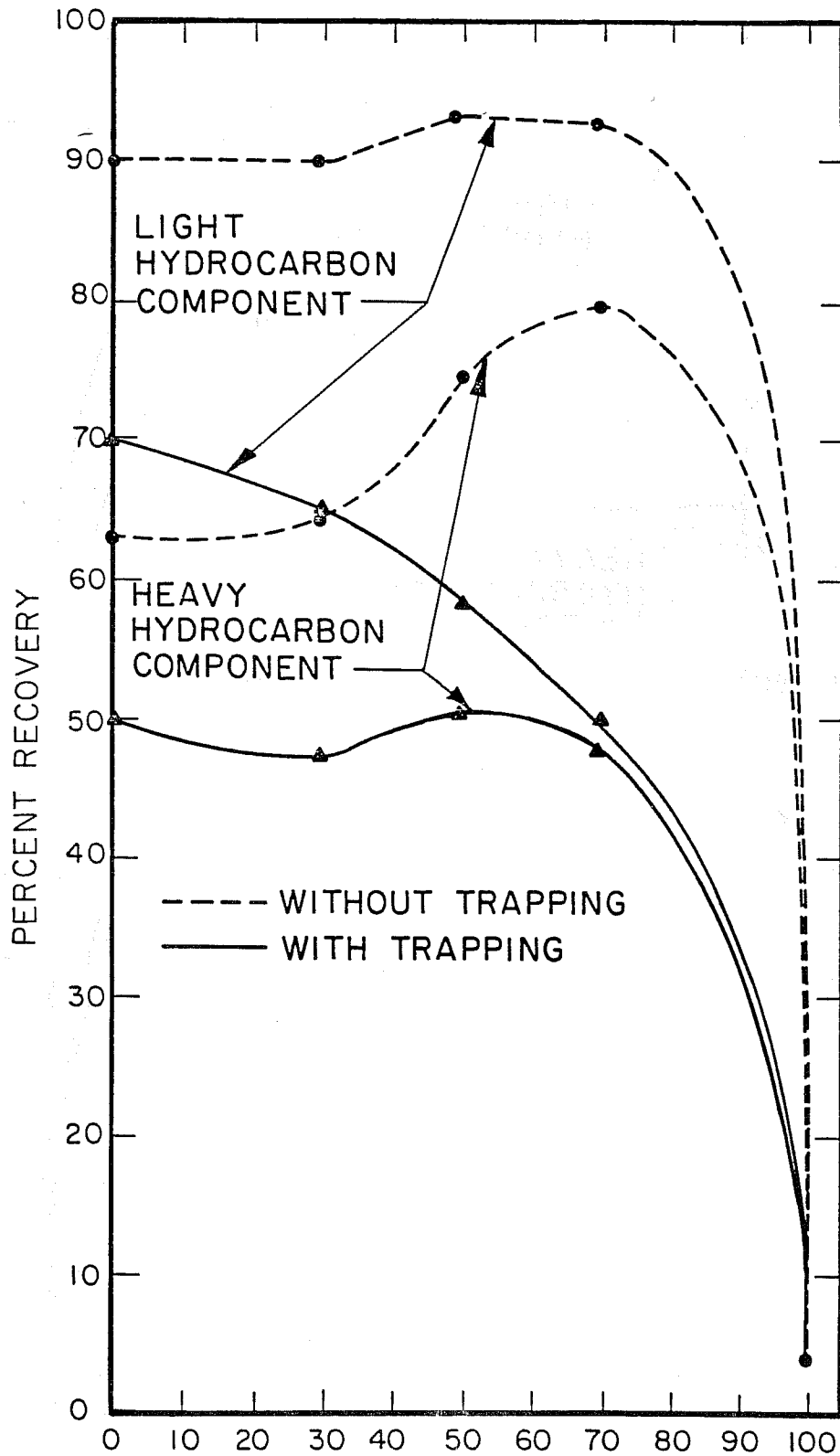
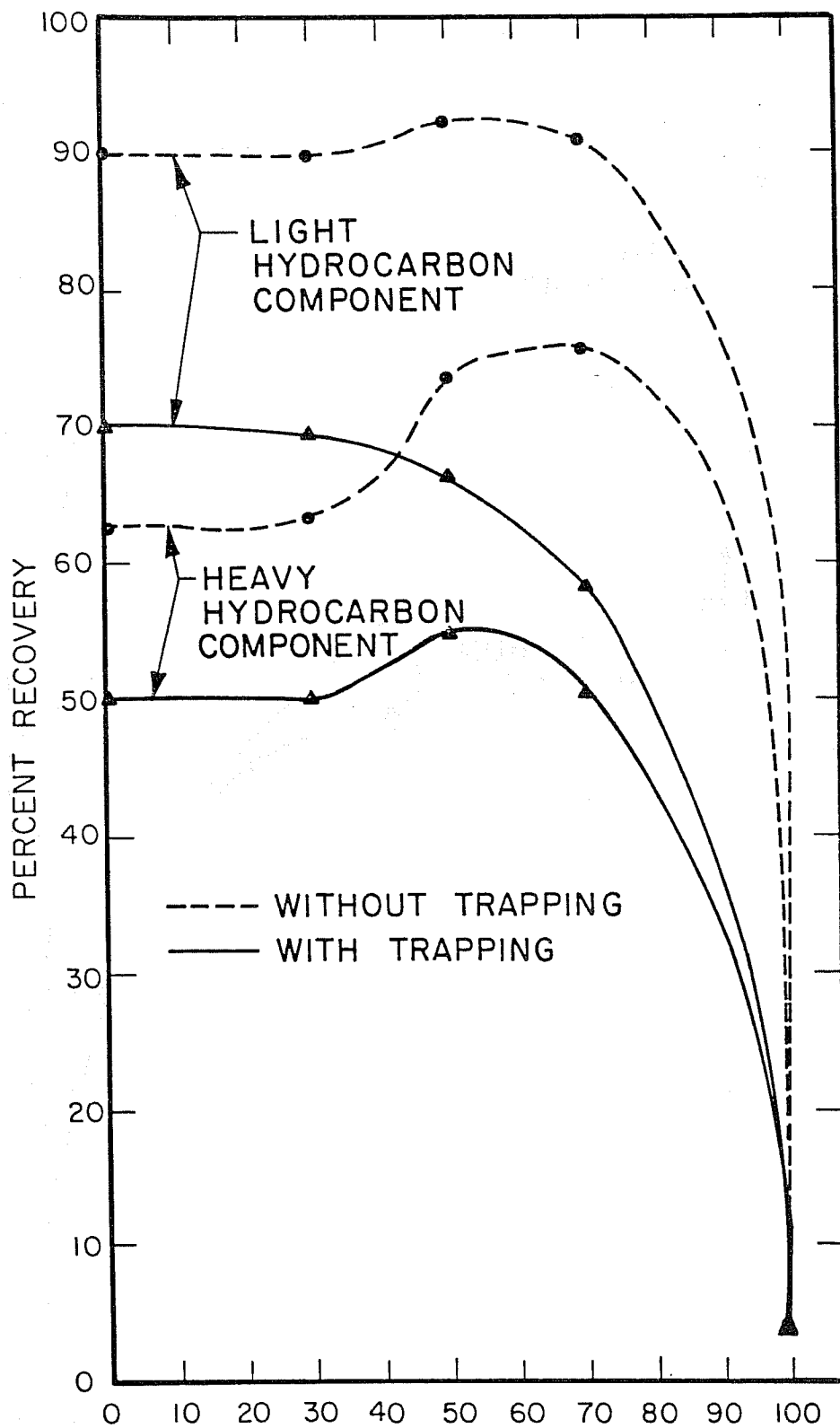


Fig. 4.8 Secondary oil ( $S_{wi} = 0.312$ ) recovered by alternate injection of CO<sub>2</sub> and water.



PERCENT WATER IN TOTAL INJECTED PORE VOLUME

Fig. 4.9 Tertiary oil ( $S_{wi} = 0.814$ ) recovered by simultaneous injection of CO<sub>2</sub> and water.



PERCENT WATER IN TOTAL INJECTED PORE VOLUME

Fig. 4.10 Tertiary oil ( $S_{wi} = 0.814$ ) recovered by alternate injection of CO<sub>2</sub> and water.

than would be obtained in two or three dimensions. The low viscosity (high mobility) of the CO<sub>2</sub> phase does reduce the recovery, however, because it produces a high fractional flow for the CO<sub>2</sub> phase, which leads, in turn to early CO<sub>2</sub> breakthrough, just as early water breakthrough occurs in a Buckley-Leverett calculation when low viscosity water displaces high viscosity oil. Thus, while the results shown in Fig. 4.7 illustrate the adverse effects of trapping, they do not provide a quantitative assessment of the trade-off between mobility control and trapping.

Results of simulations of alternate water and CO<sub>2</sub> injection are shown in Fig. 4.8. Injection cycles of 0.2 PV were divided into CO<sub>2</sub> and water slugs. For the case considered here, there was little difference between simultaneous and alternate injection, though there was a slightly larger range of injection ratios for which improved recoveries were observed. Again, the effect of trapping was to reduce the recovery slightly.

The effects of trapping were much larger, however, in the tertiary displacements, results of which are shown in Fig. 4.9 for simultaneous injection and in Fig. 4.10 for alternate injection. Continuous CO<sub>2</sub> injection without trapping recovered 90% of the light component and 63% of the heavy hydrocarbon. With trapping, those recoveries were reduced to 70 and 50%. Without trapping, simultaneous injection improved recovery of both components; with trapping present, recovery declined as the volume fraction of water in the injected fluid increased. The injection of water clearly increased substantially the amount of oil which was inaccessible to CO<sub>2</sub>. As in the secondary cases, there was little difference between simultaneous and alternate injection schemes (Fig. 4.10).

The results presented here, though limited by the fact that the calculations were one-dimensional, illustrate the potential impact of a trapped oil saturation. When oil saturation is high, as in the secondary cases, little oil is trapped, mixing of CO<sub>2</sub> and oil is efficient and oil recovery is high. When the oil saturation is low, much of it is trapped, mixing of oil and CO<sub>2</sub> is less efficient and recovery is lower. What is needed to establish quantitative effects of trapping is a set of multidimensional simulations based on measurements of the amount of oil trapped at a given water saturation in reservoir cores.

### 4.3 Conclusions

The simulation results presented here indicate that:

- (1) Displacement of oil by CO<sub>2</sub> in a slim tube is efficient when extraction of hydrocarbons by a CO<sub>2</sub>-rich phase is efficient.
- (2) Efficient extraction accounts for the high oil recovery observed in slim tube displacements. Increases in the density and viscosity of CO<sub>2</sub> with increasing pressure in the absence of extraction do not.

- (3) Quantitative predictions of slim tube performance can be obtained based on simple representations of phase composition and density data obtained from the continuous multiple contact experiment.
- (4) Isolation (or trapping) of oil by water causes lower recovery of oil by CO<sub>2</sub> injection.
- (5) The adverse effect of trapping partly offsets the benefits of mobility control when CO<sub>2</sub> and water are injected simultaneously or alternately.
- (6) Effects of trapping are much more important in tertiary CO<sub>2</sub> floods than in secondary displacements.

## 5. SUMMARY

This report describes progress in three research areas:

- (1) Development of experimental displacement techniques to study effects of pore structure and high water saturations on miscible displacement efficiency.
- (2) Measurement of phase behavior and fluid properties of CO<sub>2</sub>-crude oil mixtures.
- (3) Interpretation of the effects of individual parts of the process mechanism on the performance of laboratory and field scale CO<sub>2</sub> floods.

In the first area, equipment being used to study displacement behavior in cores and in glass models is described. Results of flow visualization experiments indicate that the CO<sub>2</sub> can displace very effectively that oil which it contacts, a fact which has long been known from slim tube displacements. When water is present, however, CO<sub>2</sub> no longer mixes freely with all of the oil. Some oil is isolated by water and can be reached only by CO<sub>2</sub> which diffuses through the water to the oil. Direct observation of swelling of trapped oil blobs suggests that the solubility of CO<sub>2</sub> in the water may have a positive impact on the mobilization of trapped oil. Those observations also indicate that in displacements at high water saturations, a substantial portion of the oil that is recovered diffuses into a flowing stream from oil ganglia surrounded on most sides by water. Preliminary results of core displacements with simple miscible fluids indicate that similar effects occur in rock samples.

In the second area, results of a variety of measurements of CO<sub>2</sub>-hydrocarbon phase behavior are reported. Pressure composition phase diagrams for nine oils are presented which indicate clearly the effects of changing system temperature and adding solution gas to an oil. Because different oil fields have been subjected to widely varying pressure histories and because amounts of gas present initially vary widely, gas-oil ratios for fields to be CO<sub>2</sub> flooded will also vary widely. The results given here outline effects of a change in the gas-oil ratio for oils similar in composition. Also given is a simple physical explanation for the temperature dependence of empirical minimum miscibility correlations.

Also given as part of research area (2) is a detailed description of the recent progress in the development of the continuous multiple contact experiment, which can be used to measure equilibrium phase compositions and densities rapidly. The experimental apparatus has been modified so that most operations and data acquisitions are controlled by a small computer. In addition, results of experiments to investigate the effect of oil composition on component partitioning in mixtures with CO<sub>2</sub> are given.

In the third area, modifications to a one-dimensional simulator to model

the effects of volume change on mixing are described. The new simulator was used to make quantitative predictions of the performance of slim tube displacements from completely independent phase behavior data obtained in the continuous multiple contact experiment. Prediction and experiment agreed well, which suggests that the behavior of stable one-dimensional displacements is well understood despite the complexity of CO<sub>2</sub>-crude oil phase behavior. In addition, preliminary results of a computational investigation of the effects of an isolated oil saturation on secondary and tertiary displacements are reported. While it is clear that isolation of some of the oil by water reduces displacement efficiency, quantitative assessment of the magnitude of the effect must await additional measurements of the trapped oil saturation in reservoir rocks.

Thus, the research program reviewed here continues to concentrate on the mechanisms which act and interact to determine displacement efficiency in a CO<sub>2</sub> flood. The combination of experimental work and analysis is aimed, therefore, at development of better tools for prediction of CO<sub>2</sub> flood performance on a field scale.

#### ACKNOWLEDGEMENT

This report was compiled with a lot of help from a lot of people. R.E. Bretz, M.K. Silva, M.T. Mayer, K.K. Dai, and J.C. Franklin all wrote sections of the text, and, of course, did large portions of the work reported. Bob Bretz supervised the core flood work, with assistance from Mike Mayer, who made a variety of improvements to the equipment and ran many of the displacements. The continuous oil-water separator was Bob Bretz's idea; as usual, Mickey Pelletier had a hand in building it and making it work. Matthew Silva continued the development of the continuous multiple contact experiment with considerable assistance from Mickey Pelletier who built crystal holders and numerous data interfaces, and Joe Franklin, who wrote a lot of microcomputer code. Chris Lien oversaw the analytical effort which supports all the experiments. Claire Jensen ran the PVT experiments. Bruce Campbell designed, built and operated the flow visualization experiment. Kar-Keung Dai modified the one-dimensional simulator to include effects of trapped oil, finding in the process a bug or two installed by the original author. Bob Specter continued his examination of the reservoir rock samples. Final editing, figure preparation, and production of this report was the work of Paula Bradley, Lorraine Valencia, Jessica McKinnis, and Kathy Grattan.

Many people not associated formally with the project also contributed to its progress. John Heller, Norman Morrow and Dave Martin, as well as members of their research groups, helped us wrestle with the usual problems of experimental life and participated in endless discussions of the interpretation of the results. Roger Card of American Cyanamid helped us take a fresh look at partitioning in CO<sub>2</sub> systems. Bill Shreve of Hewlett-Packard had crystals made for us and helped us get started in the oscillating crystal work. Without support from the U.S. Department of Energy and the New Mexico Energy Research and Development Institute (NMERDI), this work would not have been undertaken. Royal Watts, Leo Noll of the U.S. DOE and George Vavra of NMERDI deserve thanks for their continued interest and encouragement.

## REFERENCES

- Baker, L. E. 1977, "Effects of Dispersion and Dead-End Pore Volume in Miscible Flooding," Soc. Pet. Eng. J. 17, 219-227.
- Batycky, J. P., Maini, B. B., and Fisher, D. B. 1982, "Simulation of Miscible Displacement in Full Diameter Carbonate Cores," Soc. Pet. Eng. J. (October) 647-657.
- Brigham, W. E., Reed, P. W., and Dew, J. N. 1961, "Experiments on Mixing During Miscible Displacement in Porous Media," Soc. Pet. Eng. J. (March) 1-8.
- Campbell, B. T. 1983, "Flow Visualization of CO<sub>2</sub>-Crude Oil Mixtures," M.Sc. Thesis, New Mexico Institute of Mining and Technology, Socorro (May).
- Campbell, B. T. 1983, "Photofabrication of Porous Networks in Two-Dimensional Glass Plate Micromodels" PRRC Report 83-3, Petroleum Recovery Research Center (January).
- Chatzis, I. 1982, "Photofabrication Technique of 2-D Glass Micromodels," PRRC Report 82-12, Petroleum Recovery Research Center (March).
- Collings, A. F. and McLaughlin, E. 1971, "Torsional Crystal Technique for the Measurement of Viscosities of Liquids at High Pressure," Trans. Faraday Soc. 67, 340-352.
- Corey, A. T., Rathjens, C. H., Henderson, J. H., and Wyllie, M. R. J. 1956, "Three-Phase Relative Permeability," Trans. AIME 207, 349.
- Deans, H. A. 1963, "A Mathematical Model for Dispersion in the Direction of Flow in Porous Media," Soc. Pet. Eng. J. 3, 49.
- De Bock, A., Grevendonk, W., and Awouters, H. 1967, "Pressure Dependence of the Viscosity of Liquid Argon and Liquid Oxygen, Measured by Means of a Torsionally Vibrating Quartz Crystal," Physica 34, 49-52.
- Diller, D. E. 1980, "Measurements of the Viscosity of Compressed Gaseous and Liquid Methane," Physica 104A, 417-426.
- Francis, A. W. 1954, "Ternary Systems of Liquid Carbon Dioxide," J. Phys. Chem. 58, 1099-1114.
- Gardner, J. W., Orr, F. M., Jr., and Patel, P. D. 1981, "The Effect of Phase Behavior on CO<sub>2</sub> Flood Displacement Efficiency," J. Pet. Tech. 33 (November) 2067-2081.
- Gardner, J. W. and Ypma, J. G. J. 1982, "An Investigation of Phase Behavior-Macroscopic Bypassing in CO<sub>2</sub> Flooding," SPE/DOE 10686, presented at SPE/DOE Third Joint Symposium on Enhanced Oil Recovery, Tulsa, April 4-7.

- Haynes, W. M. 1973, "Viscosity of Gaseous and Liquid Argon," Physica 67, 440-470.
- Helfferich, F. G. 1981, "Theory of Multicomponent, Multi-Phase Displacement in Porous Media," Soc. Pet. Eng. J. 21 (February) 51-62.
- Holm, L. W. and Josendal, V. A. 1982, "Effect of Oil Composition on Miscible-Type Displacement by Carbon Dioxide," Soc. Pet. Eng. J. 22, 87-98.
- Lantz, R. B. 1971, "Quantitative Evaluation of Numerical Diffusion (Truncation Error)," Soc. Pet. Eng. J. (September) 315.
- Mason, W. P. 1947, "Measurement of the Viscosity and Shear Elasticity of Liquids by Means of a Torsionally Vibrating Crystal," Trans. A.S.M.E. (May) 359-370.
- McCain, W. D., Jr. 1973, "The Properties of Petroleum Fluids," Petroleum Publishing Company, Tulsa, Oklahoma.
- Meldrum, A. H. and Nielsen, R. F. 1955, "A Study of Three-Phase Equilibria for Carbon Dioxide-Hydrocarbon Mixtures," Prod. Monthly (August) 22-35.
- Michels, A., Botzen, A., and Schuurman, W. 1957, "The Viscosity of Carbon Dioxide Between 0°C and 75°C at Pressures up to 2000 Atmospheres," Physica 23, 95-102.
- Naar, J., Wygal, R. J., and Henderson, J. H. 1962, "Imbibition Relative Permeability in Unconsolidated Porous Media," Soc. Pet. Eng. J. 2, 13-17.
- Newitt, D. M., Pai, M. U., Kuloor, N. R., and Huggill, J. A. 1956, "Carbon Dioxide" in Thermodynamic Functions of Gases, Vol. 1., F. Din, Ed., Butterworths, London, 102-134.
- Orr, F. M., Jr. 1980, "Simulation of One-Dimensional Convection of Four Phase, Four Component Mixtures," Topical Report DOE/ET/12082-8, U.S. Department of Energy, Bartlesville, Oklahoma.
- Orr, F. M., Jr. and Jensen, C. M. 1982, "Interpretation of Pressure-Composition Phase Diagrams for CO<sub>2</sub>-Crude Oil Systems," SPE 11125, presented at 57th Annual Fall Technical Conference and Exhibition of SPE of AIIME, New Orleans, September 26-29.
- Orr, F. M., Jr., Jensen, C. M., and Silva, M. K. 1981, "Effect of Solution Gas on the Phase Behavior of CO<sub>2</sub>-Crude Oil Mixtures," presented at the International Energy Agency Workshop on Enhanced Oil Recovery, Winfrith, U.K., September 24.
- Orr, F. M., Jr., Lien, C. L., and Pelletier, M. T. 1981, "Liquid-Liquid Phase Behavior in CO<sub>2</sub>-Hydrocarbon Systems," Symposium on Chemistry of Enhanced Oil Recovery, American Chemical Society, Atlanta, March 29-April 3.
- Orr, F. M., Jr., Silva, M. K., and Lien, C. L. 1983, "Equilibrium Phase

Compositions of CO<sub>2</sub>-Crude Oil Mixtures: Comparison of Continuous Multiple Contact and Slim Tube Displacement Tests," Soc. Pet. Eng. J., Accepted for publication.

Orr, F. M., Jr., Silva, M. K., Lien, C. L., and Pelletier, M. T. 1982, "Laboratory Experiments to Evaluate Field Prospects for CO<sub>2</sub> Flooding," J. Pet. Tech. 34 (April) 888-898.

Orr, F. M., Jr. and Taber, J. J. 1981, "Displacement of Oil by Carbon Dioxide," Final Report to the U.S. Department of Energy, Report No. DOE/ET/12082-9 (May).

Orr, F. M., Jr. and Taber, J. J. 1982, "Displacement of Oil by Carbon Dioxide," Annual Report to the U.S. Department of Energy, Report No. DOE/BC/10331-4 (April).

Orr, F. M., Jr., Yu, A. D., and Lien, C. L. 1981, "Phase Behavior of CO<sub>2</sub> and Crude Oil in Low Temperature Reservoirs," Soc. Pet. Eng. J. 21 (August) 480-492.

Rosman, A. and Zana, E. 1977, "Experimental Studies of Low IFT Displacement by CO<sub>2</sub> Injection," SPE 6723, presented at SPE 52nd Annual Technical Conference and Exhibition, Denver, October 9-12.

Salter, S. J. and Mohanty, K. K. 1982, "Multiphase Flow in Porous Media: I. Macroscopic Observations and Modelling," SPE 11017, presented at 57th Annual Fall Technical Conference and Exhibition of SPE of AIME, New Orleans, September 26-29.

Silva, M. K., Lien, C. L., Franklin, J. C., and Orr, F. M., Jr. 1982a, "Phase Compositions and Densities of Mixtures of CO<sub>2</sub> with Maljamar Separator Oil at 90°F and 1000 psia," PRRC Report 82-5, Petroleum Recovery Research Center (January).

Silva, M. K., Lien, C. L., Franklin, J. C., and Orr, F. M., Jr. 1982b, "Phase Compositions and Densities of Mixtures of CO<sub>2</sub> with Rock Creek Separator Oil with Aromatic Spikes at 75°F and 1300 psia," PRRC Report 82-27, Petroleum Recovery Research Center (June).

Silva, M. K., Lien, C. L., Franklin, J. C., and Orr, F. M., Jr. 1981a, "Phase Compositions and Densities of Mixtures of CO<sub>2</sub> with Maljamar Separator Oil at 90°F and 1200 psia," PRRC Report 81-53, Petroleum Recovery Research Center (November).

Silva, M. K., Lien, C. L., Franklin, J. C., and Orr, F. M., Jr. 1981b, "Phase Compositions and Densities of Mixtures of CO<sub>2</sub> with Rock Creek Separator Oil at 75°F and 1300 psia," PRRC Report 81-52, Petroleum Recovery Research Center (November).

Silva, M. K., Lien, C. L., Franklin, J. C., and Orr, F. M., Jr. 1981c, "Phase Compositions and Densities of Mixtures of CO<sub>2</sub> with Maljamar Separator Oil at 90°F and 1400 psia," PRRC Report 81-51, Petroleum Recovery Research Center (November).

Silva, M. K., Lien, C. L., Pelletier, M. T., and Orr, F. M., Jr. 1981d, "Phase Compositions for Mixtures of CO<sub>2</sub> with Maljamar Separator Oil at 90°F and 800 psia," PRRC Report 81-30, Petroleum Recovery Research Center (July).

Simon, R. and Schmidt, R. L. 1983, "A System for Determining Fluid Properties Up to 136 MPa and 473 K," Proceedings, Symposium on Supercritical Fluids: Their Chemistry and Application, Faraday Division, Roy. Soc. Chem., Cambridge, England (September) Elsevier.

Spence, A. P. and Watkins, R. W. 1980, "The Effect of Microscopic Core Heterogeneity on Miscible Flood Residual Oil Saturation," SPE 9229, presented at 55th Annual Fall Meeting of SPE of AIME, Dallas, September 21-24.

Stalkup, F. I. 1970, "Displacement of Oil by Solvent at High Water Saturation," Soc. Pet. Eng. J. 10 (December) 337-348.

Stewart, W. C. and Nielson, R. F. 1954, "Phase Equilibria for Mixtures of Carbon Dioxide and Several Normal Saturated Hydrocarbons," Prod. Monthly (January) 27-32.

Taylor, G. I. 1953, "Dispersion of Soluble Matter in Solvent Flowing Slowly Through a Tube," Proc. Royal Soc., London 219, 186.

Thomas, H. C. 1944, "Heterogeneous Ion Exchange in a Flowing Stream," J. Amer. Chem. Soc. 66 (October) 1664-1666.

Webeler, R. W. H. 1961, "Viscosity X Density Measurements for Normal Liquid Hydrogen and Various Ortho-Para Mixtures," Ph.D. Thesis, University of Cincinnati.

Welber, B. 1960, "Damping of a Torsionally Oscillating Cylinder in Liquid Helium at Various Temperatures and Densities," Physical Review 119 No. 6 (September) 1816-1822.

Yellig, W. F. and Metcalfe, R. S. 1980, "Determination and Prediction of CO<sub>2</sub> Minimum Miscibility Pressures," J. Pet. Tech. 32 (January) 160-168.